# MULTI-SCALE SIMULATION OF FILTERED FLOW AND SPECIES TRANSPORT WITH NANO-STRUCTURED MATERIAL

by

XIAOFAN YANG

B.Eng., Tsinghua University, Beijing, China, 2003
M.S., Royal Institute of Technology (KTH), Stockholm, Sweden, 2005

AN ABSTRACT OF A DISSERTATION

submitted in partial fulfillment of the requirements for the degree

DOCTOR OF PHILOSOPHY

Department of Mechanical and Nuclear Engineering
College of Engineering

KANSAS STATE UNIVERSITY
Manhattan, Kansas

2010

# Abstract

A nano-material filter is an efficient device for improving indoor environmental quality (e.g. smoke reduction, air purification in buildings). Studying the effectiveness of nano-materials used in the device by computer simulation is challenging because very different size scales are involved. Therefore, numerical methods have to be developed to accommodate varying magnitudes of scales. In the current study, the simulation has been divided into three scales: macro-, micro- and nano-scale. The numerical schemes at each scale are targeted at a particular scale; however, the relationship of the general transport phenomena, physical mechanisms and properties among different scales are uniquely linked at the same time.

The objective of the macro-scale simulation was to design and study a gas filter constructed with nano-material pellets. The filter was considered a packed-bed tube filled with manufactured nano-material pellets. Commercial computational fluid dynamics (CFD) packages were used along with the embedded programming macros. In the filtration process, we focused on the flow and species transport phenomena through the porous substrate. The mathematical/numerical models were built and tested based on the physical models used in the experimental setups for different materials that were tested. The results from the numerical models were validated and compared well to experimental data obtained from the pressure drop measurements and the adsorption (breakthrough) tests.

In the micro-scale simulation, a modified immersed-boundary method (IBM) with the Zwikker-Kosten (ZK) porous model and the high-order schemes was validated and applied to simulate a representative porous unit that represented a periodic array of solid/porous cylinders. In the periodic unit, the solid cylinder case was used to validate the high-order schemes by

comparing it to the results obtained from the commercial CFD software. The relationship between the pressure gradient and the porosity (Blake-Kozeny equation) was determined from this level and fed back to the macro-scale simulation, which provided a link between the two scales. In the porous cylinder case, both flow field and species transport were investigated with a porous model similar to the one used in the macro-scale. The species concentration change was calculated and found to be nonlinearly related to the adsorption coefficient.

In the nano-scale simulation, a molecular dynamics (MD) simulation and a coupled molecular-continuum scheme were applied to solve the momentum and the mass transport problems at the molecular level at which the traditional continuum theory is no longer applicable. Both schemes were verified from the surface slip behavior study compared to the literature. The scale and shear effects in the Coutte flow were investigated, showing that in the micro-scale and macro-scale, the slip behavior could be neglected since it was only important in much smaller scales. The same hybrid scheme was then applied to a diffusion model with nano-pores constructed in the solid substrate. The adsorptions between various gases and the carbon substrate were simulated. The mass fluxes cross the fluid/solid interfaces were counted and both self-diffusivity and transport diffusivity were estimated and compared to their respective values found in the literature. The transport properties are closely related to the species transport (Fick's law) in the macroscopic simulations. Linear concentration profiles in the channel were obtained based on those transport properties for various gases going through different sizes of nano-pores, which, as a connection to the continuum model, were to be used as boundary conditions in the continuum simulation.

# MULTI-SCALE SIMULATION OF FILTERED FLOW AND SPECIES TRANSPORT WITH NANO-STRUCTURED MATERIAL

by

XIAOFAN YANG

B.Eng., Tsinghua University, Beijing, China, 2003
M.S., Royal Institute of Technology (KTH), Stockholm, Sweden, 2005

A DISSERTATION

submitted in partial fulfillment of the requirements for the degree

DOCTOR OF PHILOSOPHY

Department of Mechanical and Nuclear Engineering
College of Engineering

KANSAS STATE UNIVERSITY
Manhattan, Kansas

2010

Approved by:

Major Professor
Dr. Zhongquan Charlie Zheng

# Abstract

A nano-material filter is an efficient device for improving indoor environmental quality (e.g. smoke reduction, air purification in buildings). Studying the effectiveness of nano-materials used in the device by computer simulation is challenging because very different size scales are involved. Therefore, numerical methods have to be developed to accommodate varying magnitudes of scales. In the current study, the simulation has been divided into three scales: macro-, micro- and nano-scale. The numerical schemes at each scale are targeted at a particular scale; however, the relationship of the general transport phenomena, physical mechanisms and properties among different scales are uniquely linked at the same time.

The objective of the macro-scale simulation was to design and study a gas filter constructed with nano-material pellets. The filter was considered a packed-bed tube filled with manufactured nano-material pellets. Commercial computational fluid dynamics (CFD) packages were used along with the embedded programming macros. In the filtration process, we focused on the flow and species transport phenomena through the porous substrate. The mathematical/numerical models were built and tested based on the physical models used in the experimental setups for different materials that were tested. The results from the numerical models were validated and compared well to experimental data obtained from the pressure drop measurements and the adsorption (breakthrough) tests.

In the micro-scale simulation, a modified immersed-boundary method (IBM) with the Zwikker-Kosten (ZK) porous model and the high-order schemes was validated and applied to simulate a representative porous unit that represented a periodic array of solid/porous cylinders. In the periodic unit, the solid cylinder case was used to validate the high-order schemes by

comparing it to the results obtained from the commercial CFD software. The relationship between the pressure gradient and the porosity (Blake-Kozeny equation) was determined from this level and fed back to the macro-scale simulation, which provided a link between the two scales. In the porous cylinder case, both flow field and species transport were investigated with a porous model similar to the one used in the macro-scale. The species concentration change was calculated and found to be nonlinearly related to the adsorption coefficient.

In the nano-scale simulation, a molecular dynamics (MD) simulation and a coupled molecular-continuum scheme were applied to solve the momentum and the mass transport problems at the molecular level at which the traditional continuum theory is no longer applicable. Both schemes were verified from the surface slip behavior study compared to the literature. The scale and shear effects in the Coutte flow were investigated, showing that in the micro-scale and macro-scale, the slip behavior could be neglected since it was only important in much smaller scales. The same hybrid scheme was then applied to a diffusion model with nano-pores constructed in the solid substrate. The adsorptions between various gases and the carbon substrate were simulated. The mass fluxes cross the fluid/solid interfaces were counted and both self-diffusivity and transport diffusivity were estimated and compared to their respective values found in the literature. The transport properties are closely related to the species transport (Fick's law) in the macroscopic simulations. Linear concentration profiles in the channel were obtained based on those transport properties for various gases going through different sizes of nano-pores, which, as a connection to the continuum model, were to be used as boundary conditions in the continuum simulation.

# Table of Contents

# List of Figures

# List of Tables

# List of Publications

Portions of the material presented here have appeared in the following publications of mine:

***Journal Publications***

1. **Yang, X.**, Zheng, Z. C., 2010, "Nonlinear spacing and frequency effects of an oscillating cylinder in the wake of a stationary cylinder," *Physics of Fluids*, Vol. 22, 043601.
2. **Yang, X.**, Zheng, Z. C., 2010, "Effects of channel scale on slip length of flow in micro/nano-channels," *Journal of Fluids Engineering*, Vol. 132, 061201.
3. **Yang, X.**, Zheng, Z. C., Winecki, S., Eckels, S., 2010, "Numerical simulation of the momentum and mass transport in a nano-material filter," *International Journal of Heat and Mass Transfer*, under review.
4. **Yang, X.**, Zheng, Z. C., Xu. Y., 2010, "A study on flow through a periodic array of porous medium cylinders by immersed-boundary methods," *to be submitted to Journal of Fluids Engineering*.
5. Zheng, Z. C., Zou, X., **Yang, X.**, Wu, X., 2010, "Wind shear over a barchan dune," to be submitted to *Geomorphology*.

***Peer-Reviewed Conference Publications***

6. **Yang, X.**, Zheng, Z. C., Xu. Y., 2010, "A study on flow through a periodic array of porous medium cylinders by immersed-boundary methods" *ASME 3rd Joint US-European Fluids Engineering Division Summer Meeting*, FEDSM2010-30535, August 1-5, Montreal, CA.
7. **Yang, X.**, Zheng, Z. C., 2009, "Effects of channel scale on slip length of flow in micro/nano-channels," *ASME Fluids Engineering Division Summer Meeting*, FEDSM2009-78378, August 2-6, Vail, CO.

8. Zheng, Z. C., **Yang, X.**, and Zhang, N., 2007, "Far-field acoustics and near-field drag and lift fluctuations induced by flow over an oscillating cylinders," *37th AIAA Fluid Dynamics Conference & Exhibit*, AIAA2007-4107, June 25-28, Miami, FL.
9. Zheng, Z. C., **Yang, X.**, and Zhang, N., 2006, "Flow/acoustic characteristics for flow over two tandem cylinders," *Proceedings of 2006 International Mechanical Engineering Congress & Exposition*, IMECE2006-15807, November 5-10, Chicago, IL.

# Acknowledgements

This thesis would not be possible without the support and the contribution made by the following people:

My advisor and mentor, Dr. Zhongquan Charlie Zheng, not only guided me to explore the world of science but also taught me to be a better person. With his knowledge, patience and help, my Ph.D. study at Kansas State University has reached a milestone and become a promising start to my future career. I did not know how to do research when I first came here. Dr. Zheng taught me how to ask the right questions as the first step to be a researcher. His art of teaching has been inspiring me. I only hope that I can repay him by being a successful advisor, just like him.

I was delighted to have Dr. Steve Eckels, Dr. Ronaldo Maghirang, Dr. Terry Beck, Dr. Sameer Madanshetty and Dr. Larry Glasgow on my dissertation committee and Dr. Brett DePaola as the committee chair. I thank them all for helping me with the dissertation and the research work.

I would also appreciate the Targeted Excellence Award Grant from K-State. I felt happy and lucky to join the indoor air quality research team. I enjoyed the fruitful discussions with them and learned a lot from this multi-disciplinary group, which included Dr. Steve Eckels, Dr. Ronaldo Maghirang, Dr. Chris Sorenson, Dr. Ken Klabunde, Dr. Larry Ericsson, Dr. Amit Charkrabatti, Dr. Bruce Law and Dr. Slawomir Winecki from NanoScale.

Dr. Mo Hosni also deserves my special thanks for his support and encouragement.

In addition, my lab buddies in Dr. Zheng's research group made it a fun place to work. They include Dr. Ning Zhang, Dr. Wenhua Li, Dr. Ying Xu, Mr. Zhenglun Wei, Mr. Viet

Nguyen and Dr. Xiaoxu Wu. I thank them for sharing their knowledge and being patient when I was debugging and becoming cranky about it.

My deepest gratitude goes to my family for their love and support throughout my life. I am indebted to my father, Prof. Mingchuan Yang, for his care and love. As a typical father in a Chinese family, he doesn't talk much but was determined to find every way to raise me in the best possible environment. I could not ask for more from my mother, Prof. Ruizhen Cao, as she was always willing to listen and be supportive. My husband, Dr. Fangmao Ye and I met five years ago at K-State. We did not know each other in China and just had to fly a long way to meet and finally get married here in this small college town. We have been through a lot together, learning more than just the differences between chemistry and mechanical engineering. I feel blessed to have had him by my side during the pursuit of my degree and look forward to our future life. Finally, during the five years, I have been challenged and had sleepless nights, just as everyone has. The inspiration of my family made these challenges surmountable. I know no suitable word that can fully describe that love I received from them.

# CHAPTER 1 - Introduction

This introduction discusses the background of the current research, the methods used to meet the objectives and the organization of this thesis.

## 1.1 Research Background

Indoor air environment (IAE) is an important subject that addresses both the health of occupants and their exposure to air pollution. IAE balances the indoor environmental quality (IEQ) and living comfort. The environmental variables affecting IAE are complex and include temperature, humidity, lighting, noise, and source control – air cleaning. The primary influences on IAE are the sources of released hazardous gases and toxic particles. However, identifying and removing these pollutants is very difficult, practically speaking, due to their physical/chemical properties. Thus, ventilation and filtration become critical maintaining IAE. The efficiency of ventilation systems is limited since the energy costs are high and contaminants can not be eliminated only by exchanging indoor and outdoor air. Inadequate filtration can increase indoor pollutant levels by failing to "fresh" the indoor air with contaminants. Several air cleaning devices designed for specific pollutants are available on the market for controlling both particulate and gaseous pollutants. These could be used to improve the overall efficiency of efforts to control IAE. A number of mechanical purification/filtration devices are available that can remove contaminants and make the air clean. However, studies on the effectiveness of such devices in removing gaseous pollutants are not complete and have not been performed systematically. The packed-bed/packed-column filled with materials (such as carbon, fiber, etc) with adsorbing ability is a common experimental setup that can be used to evaluate the

performance of both the sorbents and the devices in a lab environment. The adsorption capability and the breakthrough time are two parameters that can and need to be rated. Also, the following conditions need to be measured and determined:

- The air flow rate through the packed-bed
- The design of the bed, especially the depth
- The concentration of the pollutants
- The physical and chemical characteristics of the pollutants and the sorbent
- The environmental conditions including the temperature, humidity, etc.

In those purifiers/filters, activated carbon has been used traditionally and effectively as the most common filtration material due to its adsorbing ability. Usually it is clustered as pellet, powder or condensed film. It can adsorb some pollutants, mostly hydrocarbons and non-polar gases, both in dry and humid conditions. One of the constraints of this type of adsorbent is that it is not efficient in removing low molecular weight gases and its effective lifetime is relatively short. In most cases, activated carbon is used to remove odor; however, the absence of odor alone does not guarantee good air quality. Because of the recent and rapid development of new nano-materials, those innovative nano-materials with high surface areas are expected to replace activated carbon in the filtration industry. The drawback of using nano-materials, however, comes from the limited knowledge of the materials including their capabilities, how the sorbents and the contaminants react, and the materials' toxicity to humans and environment. Hence, the major objective of the current study was to use nano-materials in air purifiers/filters and test their performance with respect to improving indoor air quality. Figure 1-1 illustrates the concept that

informs this study, which aimed to combine the evaluation of the air filter with an investigation of the properties of the nano-material for the purpose of improving IAE.


**Figure 1-1 Nano-material air filters to improve indoor air environment.**

Computational fluid dynamics (CFD) has developed rapidly in recent decades and can be applied to numerous applications, especially those that cannot be modeled by experimentation. CFD tools and other numerical simulations were used to model filtration processes and transport phenomena as well as material properties so that the designs of filtration devices could be evaluated. CFD can also benefit the laboratory study of such devices. However, some information required by the CFD simulations, such as the model set up and material selection,

need to be obtained from the experiments. The results from the simulation are then calibrated and compared to the experimental data. A complete study needs to examine filter designs and materials in several scale lengths, which may be only accomplished by using computational methods. Finally, computer simulation can supplement laboratory studies with additional information economically. In the process of this study, we used both numerical simulation and experiment results to create a multi-scale platform that is able to cover flow and mass transport at very different scales for the current and future studies.

## 1.2 Research Objectives and Methods

The multi-scale simulation of the flow/species transport in a nano-material filter is a complicated problem that involves several levels of length scales. Also, a complete and successful system of theories to study the nano-material, especially using computer aided simulations, does not exist. In addition, this is a multidisciplinary project that requires backgrounds and experiences in engineering, physics and chemistry. Different computational methods have to be used to accommodate various scales. Hence the objectives for each scale need to differ as well. However, the relationship among different scales and how the information exchanges among them have to be explored. Based on the problem, the simulation was divided into three levels as illustrated in Fig. 1-2.

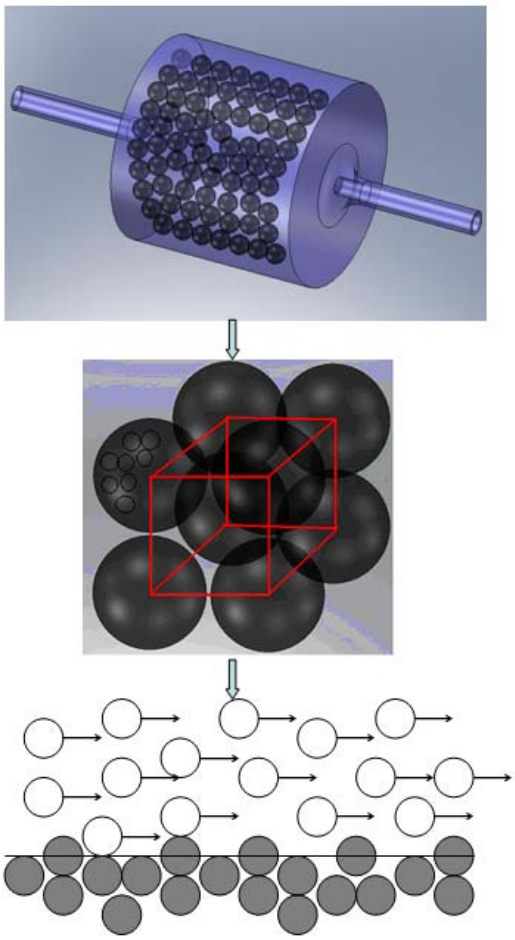

**Figure 1-2 Multi-scale simulation: (from top to bottom) Macro – Micro – Nano.**

The objective for the first scale (macro-scale) was to design and study a gas filter constructed with nano-material pellets. The filter was a packed-bed tube filled with manufactured nano-material pellets. Commercial computational fluid dynamics (CFD) software and packages were used to run the simulation along with the use of the embedded programming macros. In the filtration process, we focused on the flow and species (concentration) transport phenomena through the porous substrate. The mathematical/numerical models were built and

tested based on the physical models that corresponded to the experimental setups. The results were then validated and compared to experimental data. The momentum transport (pressure drop) and the mass transport (breakthrough behavior) were both analyzed.

The second scale (micro-scale) involved investigating the flow/species transport around and inside a group of nano-material pellets. To simplify the problem, we adapted a structural unit, which was a periodic array of circular cylinders, to study the flow field and the concentration change. A modified immersed-boundary method (IBM) along with high-order numerical schemes was used to solve the transport equations including the additional Zwikker-Kosten (ZK) porous models. A tandem cylinder system was studied first to validate the IBM scheme. In the solid/porous structural unit, both fluid/solid interaction (FSI) and fluid/porous interaction (FPI) problems were investigated. The species transport simulation was then carried out based on the flow field. Also, the results obtained from this scale provided information for the macro-scale.

Down to the smallest scale (nano-scale), the diffusion through the nano-pellets surfaces was of interest. The fluid/solid interactions occurred between molecules. By using molecular dynamics (MD) simulation, which is a discrete model that is very different from the continuum theory, we calculated the macroscopic properties from a "nanoscopic" point of view while some mechanisms could only be captured in molecular scales. Also, to improve the efficiency and maintain accuracy, we applied a hybrid molecular-continuum scheme to this problem. The surface slip behavior and the diffusion/adsorption mechanisms were studied and this information was applied to macroscopic investigations.

Based on the results from studying all three scales, we used a series of computational tools (such as immersed-boundary method, molecular dynamics simulation, commercial CFD software and packages) to build up a platform to simulate and test the designated filter

constructed with innovative nano-materials. The data we used, for building this platform, included momentum and mass transport phenomena, surface properties and mechanisms, and fluid/solid interactions. The objectives, numerical methods and the perspective results of three scales are listed in Table 1-1.

| | Objective | Method | Result |
|---|---|---|---|
| Macro-scale | Momentum/mass transport phenomena | Commercial CFD software with programmed macro | Validated and compared with experimental data |
| Micro-scale | Fluid/solid interaction (FSI); Fluid/porous interaction (FPI) | Immersed-boundary method (IBM); Porous model; High-order schemes | Validated and compared with macro-scale results |
| Nano-scale | Slip behavior; Diffusion | Molecular dynamics simulation (MD); Hybrid scheme | Validated and compared with literature and macroscopic results |

**Table 1-1 Summary of the multi-scale simulations.**

## 1.3 Organization of Thesis

The organization of the thesis is shown in Fig. 1-3. Since the objectives and the numerical methods are very different for each scale, each chapter includes an introduction of the modeled problem, the numerical method used, and a discussion of the results and a conclusion.

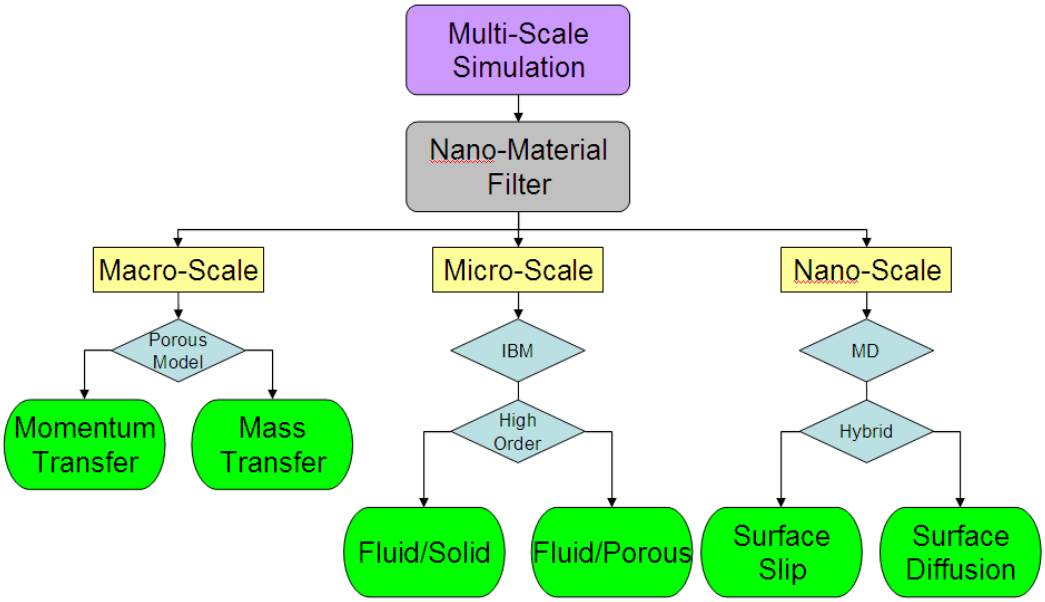


**Figure 1-3 Organization of the thesis.**

Chapter 2 is about the macro-scale simulation, which focuses on the flow and species transport through a packed-bed filter filled with nano-material pellets. Both momentum and mass transport phenomena with specific porous models were studied and explained in this chapter. The numerical model was built and the governing equations solved using commercial CFD software. The pressure drop and the breakthrough behavior were measured and compared to the experimental data, with good agreements achieved.

Chapter 3 investigates the 2D fluid/solid and fluid/porous interactions in a group of nano-material (porous) pellets, which is the micro-scale simulation. The structural arrangement of the pellets we constructed was a unit of a periodic array of solid/porous cylinders. The porous models implemented in a modified immersed-boundary method for the flow and species transport equations were validated and used for computation. Also several high-order numerical

schemes were tested to resolve the interface problems. The macroscopic characteristics were studied from a microscopic point of view and the link between macro- and micro- scales was established.

In Chapter 4, the fluid/solid interactions on the surfaces are examined at the molecular level, for which the nano-scale simulation was carried out. The computational tools used in this level were very different from the other two since the continuum theory is not applicable. Molecular dynamics simulation and a hybrid molecular-continuum scheme were the discrete models we used to study the slip behavior on the solid surface and the diffusion of various gases into the nano-pores in the solid substrate. The collected information was analyzed and fed back to the macroscopic simulations.

Finally our conclusions are discussed in Chapter 5.

# CHAPTER 2 - Macro-Scale Simulation

A computational fluid dynamics (CFD) technique for evaluating the performance of nano-material packed-bed filters was developed. The porous effects of the momentum and mass transport within the filter bed were simulated. For the momentum transport, an Ergun type of porous model was applied and the pressure drop across the packed-bed was simulated and compared with measurement. For the mass transport, a bulk adsorption model was developed to study the adsorption process (breakthrough behavior). Various types of porous materials and gas flows were tested in the filter system where mathematical/numerical models used in the porous substrate were implemented and validated by comparing with experimental data and analytical solutions under similar conditions. Generally good agreement was obtained between experiments and numerical predictions.

## 2.1 Introduction

Packed-bed filters have been used for decades to remove hazardous gases and vapors from contaminated air flows. Because of their relatively simple but robust structure, these filters have been utilized in different manufacturing industries. The purpose of the filtration is to remove the toxic gases by the porous sorbent. The fluid/solid interaction/adsorption is involved in this process. There have been numerous experimental investigations on the adsorption process occurring between the gas flow (e.g. water vapor or ammonia) and the granules (e.g. activated carbon, zeolite compounds) in the packed-bed column, e.g. Mangun et al. (1999), Lee et al. (2005), Park and Kim (2005), Qi et al. (2006), Long et al. (2008) and Ribeiro et al. (2008). The breakthrough behavior, which is the typical mechanism in the adsorption process, has been well

stated in those publications. Also, there exists a theoretical solution (Wheeler-Jonas Equation) that determines the breakthrough time (Jonas and Rehrmann, 1973; Lodewyckx et al. 2004), which could be used to compare with the experimental data.

Numerical simulation is an efficient way to conduct parametric studies due to its low cost and efficiency. However, a complete study using the computational fluid dynamics (CFD) technique of gas filtration is very rare compared with the typical studies of the packed-bed reactors. To investigate the mass and heat transfer in the reactor, Nijemeisland and Dixon (2001, 2004) reviewed the use of CFD as a design tool for fixed bed reactors. Their study presented the relationship between the local flow field and the local wall heat flux in a packed bed of spheres. CFD is used to obtain the detailed velocity and temperature fields. For the filtration problem in the current study, Arturo et al. (2002) used an Eulerian 2-D transient CFD model to describe the space-time evolution of clogging patterns developing in deep-bed filtration of the liquids. A local formulation of the macroscopic logarithmic filtration law is proposed, as well as a geometrical model for the effective specific surface area of momentum exchange. The comparison between the simulations and experiments showed that CFD is useful for the quantitative description of packed-bed clogging. Tung et al. (2004) studied the mechanism of the deep bed filtration for submicron and nano- particles suspension by means of a force analysis on the suspended particles flow path through order-packed granular filter beds. The flow fields through the filter beds were calculated using CFD. There has not been a complete study of both the momentum and mass transport through a packed-bed filter, especially those filled with nano-materials.

Recently, nano-materials (usually made by clustering powders or pellets, e.g. zinc oxide (ZnO), magnesium oxide (MgO)) with high surface areas were proved to be more efficient than the traditional adsorbing filter media (Savage and Diallo, 2005). These materials have the

potential to enhance the present day science and technological applications. Hence, the adsorption process (breakthrough behavior) of these materials becomes an important subject. Existing knowledge of physical adsorption is not sufficient to predict the performance of nano-materials due to their properties. One of the primary applications of this study is to utilize nano-materials in filtration media to enhance indoor environmental quality. However, one of the difficulties of testing nano-materials is the unknown transport properties of the new materials, which require either unique experimental measurements or new theoretical models.

At the present time, a platform that combines a series of experimental equipment and numerical models has been developed. Several test facilities (packed-beds) and related numerical models have been designed to evaluate the performance of novel nano-adsorbent materials for removing gas contamination. The current packed-bed model is capable of monitoring real time effects of concentration in the adsorption column. Various types of porous material (e.g. zirconium, activated carbon, zinc oxide, etc) were used as filter media to test the effectiveness of the system in data replication. Pressure drop measurements have been carried out to validate the function of the packed-bed system. Breakthrough analysis has been done to understand the adsorption kinetics in the filter bed. The results from CFD simulations were in agreement with the experimental data. Thus, the relationships between experiment and numerical simulations can be demonstrated.

This chapter has three following parts: Section 2.2 presents the details of the numerical simulation and the experiment setup; Section 2.3 shows the results comparison and analysis with discussions including the pressure drop estimation and the breakthrough behavior investigation, with conclusions given in Section 2.4.

## 2.2 Model Description

The CFD model has been developed to simulate the filtered flow with species transport in the packed-bed filter. The geometries of the physical models were based on the experimental setup. The transport equations for both flow and species were discretized and solved numerically. In the simulation, we assumed that the flow is incompressible and Newtonian. The packed-bed was filled with porous material pellets with equal size, thus the porous medium was assumed to be isotropic and homogeneous. The reaction between the fluid and the porous material was neglected in the species transport simulation since it is a relatively slow process. The heat generated from the adsorption procedure was not taken into account, either. In the numerical model for this study, new source terms were added to the momentum and mass transport equations in the porous medium to account for the flow resistance and adsorbing effects of the porous medium (see Fig. 2-1). The computational domain was divided into two zones: the fluid zone and the porous zone. The numerical models (with the porous models) were first validated by comparing the experimental results, and then applied to predicting the performance of the filter. Different tests with various filter medium and gas flows have been carried out for momentum and mass transport.

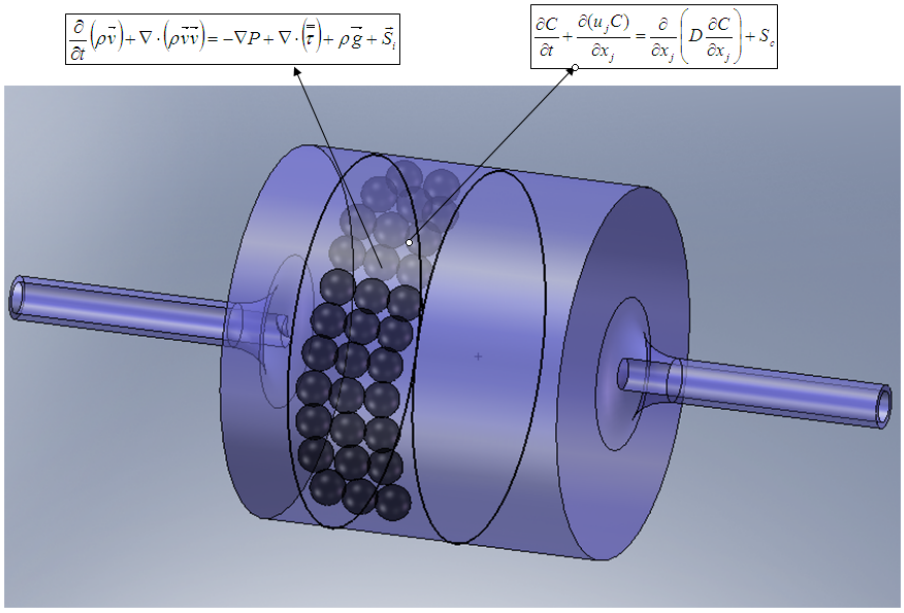


**Figure 2-1 Transport equations used in the porous medium.**

A commercial CFD solver (FLUENT 6.3) is used to solve the equations. The governing equations for the flow are the Navier-Stokes equations for incompressible flow, including the continuity equation (Eq. 2.1) and the momentum equation (Eq. 2.2):

$$\frac{\partial \rho}{\partial t}+\nabla\cdot(\rho\vec{v})=0\ , \tag{2.1}$$

$$\frac{\partial}{\partial t}(\rho\vec{v})+\nabla\cdot(\rho\vec{v}\vec{v})=-\nabla p+\nabla\cdot(\bar{\bar{\tau}})+\rho\vec{g}+\vec{S}\ , \tag{2.2}$$

where $\rho$ is the density of the fluid (constant for homogeneous incompressible flow), $\vec{v}$ is the velocity vector, $t$ is the time, $p$ is the pressure, $\bar{\bar{\tau}}$ is the shear stress, $\vec{g}$ is the gravitational acceleration, and, $\vec{S}$ is the additional source term (to be defined later). Also, the standard k-$\varepsilon$ turbulence model is selected to include the turbulent flow effect.

For the packed-bed investigation, there exists an analytical approximation called the Ergun equation (Bird et al. 2002) to calculate the pressure drop per length and its relationship with the properties of the pellets. The Ergun equation is valid if the packing is statistically uniform and that the equivalent diameter of the pellets is much smaller than the diameter of the bed column ($d_p << D$). In this case, the Reynolds number ($\mathrm{Re} = \rho UD/\mu$) based on the incoming velocity and the diameter of the pipe is in the range of 1000, since low flow rates (which are typical in air filtration systems used in the indoor environment) are applied at the inlet. The general expression for the Ergun equation (Ergun, 1952) is:

$$\frac{\Delta p}{L} = \frac{150\mu}{d_p^2}\frac{(1-\varepsilon)^2}{\varepsilon^3}U_0 + \frac{1.75\rho}{d_p}\frac{(1-\varepsilon)}{\varepsilon^3}U_0{}^2 \quad , \tag{2.3}$$

where $\Delta p$ is the pressure drop between the two ends of the packed bed, $L$ is the depth of the bed, $\mu$ is the viscosity of the flow, $\rho$ is the density of the flow, $U_0$ is the superficial flow velocity (defined as the ratio of the volumetric flow rate of the carrier gas to the cross-sectional area of the empty packed-bed $Q/A_c$), $d_p$ is the equivalent diameter of the pellets, and, $\varepsilon$ is the void fraction of the packed bed (ratio between the volume of the void space and the total volume of the bed, defined as $\varepsilon = 1 - V_{pellets}/V_{bed}$). For spherical pellets, $d_p$ is the diameter of the sphere, and for other shapes, $d_p$ can be calculated as the diameter of a sphere with equal volume. The first term on the right-hand-side of Eq. (2.3) is the Blake-Kozeny equation (Bird et al. 2002) representing pressure drop due to the viscous effect, while the second term is the Forchheimer component representing the inertial effect related to the second-order of velocity. Eq. (2.3) is usually applicable in a wide range of Reynolds numbers covering the flow from laminar to turbulent. To use the Ergun equation as a benchmark solution, it should be noted that the length

of the packed-bed needs to be long enough to avoid the entrance effect of the flow.

The porous effect of an arbitrary packed-bed is simulated by empirically determining flow resistance in the substrate. In the transport equations, the flow resistance is modeled by an added momentum sink term on the right-hand-side of the momentum equations. In this study, we assumed that the porous media is homogeneous and isotropic. And this sink term was based on the extended Darcy's law (Darcy, 1856) and in the format of the Ergun equation (Ergun, 1952):

$$S_i = -\left(C_{R1} u_i + C_{R2} |U| u_i\right), \tag{2.4}$$

where $S_i$ is the component of the sink term, $u_i$ is the flow velocity component, and, $|U|$ is the magnitude of the velocity. $C_{R1}$ and $C_{R2}$ are viscous and inertial loss coefficients, which are functions of flow and pellets properties and can be calculated as:

$$C_{R1} = \frac{\mu}{\alpha}, \tag{2.5}$$

and

$$C_{R2} = \frac{\rho C_2}{2}, \tag{2.6}$$

where $\alpha$ is the permeability and $C_2$ is the inertial resistance factor defined as:

$$\alpha = \frac{d_p^2}{150} \frac{\varepsilon^3}{(1-\varepsilon)^2}, \tag{2.7}$$

and

$$C_2 = \frac{3.5}{d_p} \frac{(1-\varepsilon)}{\varepsilon^3}, \tag{2.8}$$

where $d_p$ (equivalent particle size, calculated from total mass of the pellets divided by their total volume, $m_{pellet}/V_{pellet}$) and $\varepsilon$ (void fraction) can be obtained from the properties of the pellets.

As for the modified species transport equation (Eq. 2.9), the unsteady term, convection term, diffusion term and an additional source term are included. The source term (actually a sink in this case) represents the adsorbing ability of the porous substrate:

$$\frac{\partial C}{\partial t}+\frac{\partial(u_j C)}{\partial x_j}=\frac{\partial}{\partial x_j}\left(D_s\frac{\partial C}{\partial x_j}\right)+S_c, \tag{2.9}$$

where $C$ represents the concentration of the contaminants, which is treated as a passive scalar, $u_j$ is the velocity component obtained from the steady-state solution of the coupled momentum transport equations, $D_s$ is the diffusivity, and, $S_c$ is the adsorbing sink term to be determined. And the linearized sink term is modeled as (Perry and Green, 1997):

$$S_c=-\frac{1}{\varepsilon}S_0 k_f(C-C_{in}), \tag{2.10}$$

where $\varepsilon$ is the void fraction, $S_0$ is the surface area/volume ratio of the pellet (which is $6/d_p$ if the pellet is considered a sphere), $k_f$ is the mass transfer coefficient that depends on the contaminant material and porous material properties, and, $C_{in}$ is the initial concentration (also the final concentration after fully saturated) at the inlet. Combining Eqs. (2.9) and (2.10) and non-dimensionalizing it by dividing $C_{in}$, the species transport equation becomes:

$$\frac{\partial(C/C_{in})}{\partial t}+\frac{\partial(u_j C/C_{in})}{\partial x_j}=\frac{\partial}{\partial x_j}\left(D_s\frac{\partial(C/C_{in})}{\partial x_j}\right)-\frac{1}{\varepsilon}S_0 k_f(C/C_{in}-1). \tag{2.11}$$

Eq. (2.11) is solved simultaneously with Eqs. (2.1) and (2.2), and the discretized

computational scheme is second-order in time and space. The second-order upwind scheme is used for the convection terms, and the second-order central differencing for the diffusion terms. The coupling scheme between the velocity field and the pressure field was the SIMPLE algorithm. The passive scalar transport equation (Eq. 2.11) was implemented by using the programming macros enabled in the commercial solver using user-defined subroutines for the unsteady term, convection term, and the additional sink term.

As with the model used in the momentum transport, the geometry was meshed by unstructured tetrahedral elements. The difference was in the adsorption model, where the porous substrate was arranged in the middle of the empty bed, leaving enough space for flow to be fully developed.

In the numerical model, the computational domain is divided into a bulk fluid zone and a porous zone. The general no-slip condition is applied on all the solid walls. At the inlet, the velocity to be specified is determined based on the volumetric flow rate of the carrier gas and the diameter of the inlet tube. At the outlet vent, the pressure is specified based on the experimental value. For the dimensionless species transport simulation, at the inlet, the incoming boundary condition will be user-defined and explained later.

## 2.3 Results and Discussion

To validate the numerical model, and then perform various tests in the filter, the cases were arranged to study both flow and species transport, which are summarized in Table 2-1.

| | Gas | Pellet | Transport | Objective |
|---|---|---|---|---|
| Pressure Drop Test | Air | Zirconium; Activated Carbon | Flow (momentum) | Pressure drop |
| Adsorption Test | Air w/ $H_2S$ | Zinc Oxide (NanoActive ZnO) | Species (mass) | Breakthrough behavior |

**Table 2-1 Testing setup.**

To validate the momentum transport model, pressure drop measurements were conducted (the pressure drop experiments were conducted by Dr. Steve Eckels' group at Kansas State University), with the pure air flow and two kinds of porous material pellets: spherical shaped zirconium and the cylindrical activated carbon pellets. The surface-averaged pressure drop between the inlet and outlet of the filter was calculated and compared with the data from experiments. For the validation cases using zirconium pellets, the results were also compared with calculated solution from the Ergun equation. The later tests with activated carbon pellets were performed to test the model in a range of packed-beds with different sizes, especially those shorter beds since the porous substrate was only a thin layer in the adsorption test.

For the adsorption tests (to test the behavior of breakthrough), the porous substrate was filled with ZnO (NanoActive) pellets to remove the $H_2S$ from the incoming gas flow. The breakthrough curve was the real time concentration change captured at the measuring point downstream in the filter. The concentration history data recorded at the upstream point from the

experiment was used as the incoming concentration required by the simulation from the beginning. Then, the simulation results were calibrated and compared with available experimental data. The breakthrough process and the saturation time could be estimated

### 2.3.1 Results of the Pressure Drop Measurements

The dry air (at room temperature of 23$^{o}$C) was pumped into a cylindrical packed-bed (length *L* and diameter *D*) filled with porous material pellets including zirconium spheres and activated carbon pellets. For both types of the pellets, similar flow conditions were provided, as shown in Table 2-2. The packed-bed tubes used for zirconium and the activated carbon were not the same. The packed-bed used for zirconium tests was a fixed long tube. However, for the tests using activated carbon pellets, the total amount of mass for filtration was varied; thus, the length of the bed was different (the diameter of the bed was kept the same). The pellet properties used for porous effect estimation ( $d_p$ and $\varepsilon$ ) were calculated based on the mass and the volume mentioned in the last section. A volumetric flow rate meter was used to control the incoming air flow rate, which was in the range of 0.057 – 0.34 m$^3$/min (2 – 12 ft$^3$/hr). Polymer sieves were placed at both ends to prevent loss of bed granules. During the filtration process, the pressure drop ( $\Delta p$ ) between the two ends of the bed was monitored and recorded in real time. The numerical model included the inlet and outlet pipes and the packed-bed tube (porous substrate). The length for each pipe was 1.27 m (50 in) and the diameter was 4 mm. The geometry of the setup was generated and meshed with unstructured tetrahedral elements (the number of cells is around 274,558 after grid-resolution check) by using the grid generation package in the commercial flow solver for this study. Measured results with two pellet materials, zirconium and activated carbon, were compared with numerical simulation.

| | Size of the bed ($D$ (m) x $L$ (m)) | $d_p$ (m) | $\rho_p$ (kg/m$^3$) | $\varepsilon$ | Flow condition |
|---|---|---|---|---|---|
| Zirconium | 0.02 x 0.87 | 0.005 | 6520 | 0.41 | Air, 24$^o$C, 0.023-0.34 m$^3$/min 5 – 12 ft$^3$/hr |
| Activated-Carbon | 0.037 x $L$ (mass dependent) | 0.0047 | 984 | 0.4 | Air, 24$^o$C, 0.057-0.34 m$^3$/min 2 – 12 ft$^3$/hr |

**Table 2-2 Pellet properties and flow parameters in the pressure-drop measurements.**

First, the bed was saturated with air and filled with manufactured spherical zirconium pellets. The length of the packed-bed is around 0.87 m. Since the ratio between the length and the diameter of the bed ($L$/$D$) is very large (the entrance effect of the flow is ignored), the Ergun equation can be used as the benchmark solution. In this test, the total pressure drop (area-averaged pressure difference between the two ends of the bed) was measured and compared with simulation. In Fig. 2-2, the numerical simulation results match the analytical solution from the Ergun equation very well. Also, they are in good agreement with the experimental data though there are some deviations in the low flow-rate cases. The reason is that for such a long bed, smaller pressure drops due to low flow rates are considerably more difficult to detect in the experiments.

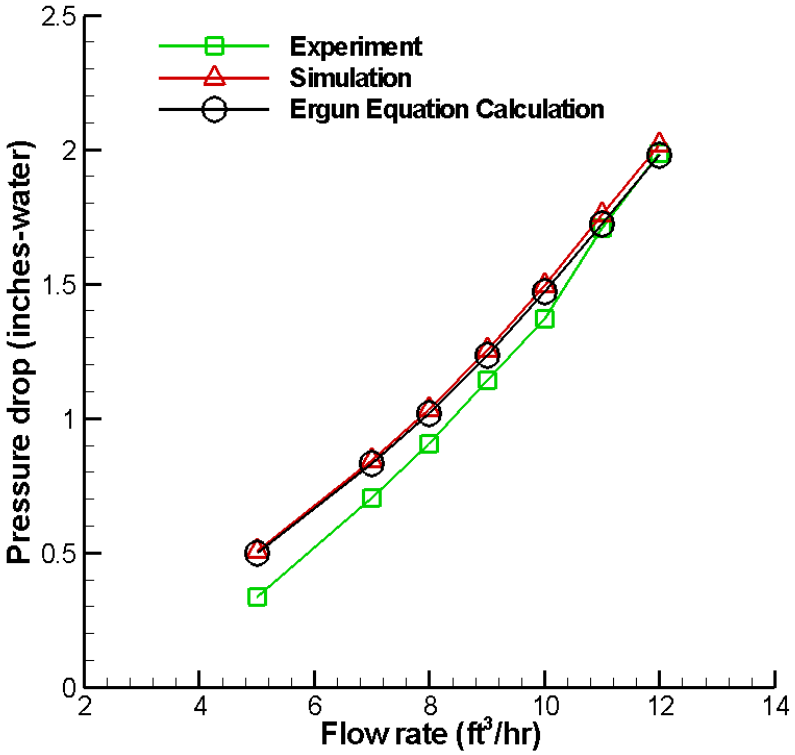


**Figure 2-2 Pressure drop results for spherical zirconium pellets: comparisons between numerical simulation, experiment and analytical solution.**

The tube filter material was then replaced with activated carbon pellets (commonly used as the filtration material in air purifiers) and tested under similar conditions as the zirconium tests, but with different lengths of shorter beds for different amounts of mass of the pellets, as the length of the bed is dependent on the total mass of the pellets. One purpose is to validate the model without having the Ergun equation as a benchmark. Since in a short packed-bed, the entrance effect cannot be neglected. Figure 2-3 shows good results in the pressure drop

compared to the experimental data. Especially, for the 21 mg mass test (more pellets, longer tube), the results from simulation and experiment are almost identical. However, there are some differences in the 4.2 mg mass test (fewer pellets, shorter tube) since the bed used in this test is the shortest; thus, the pressure drop is hard to accurately measure (due to its small value). These comparisons show that the numerical model established here is capable of predicting the filtration results in a wide range.

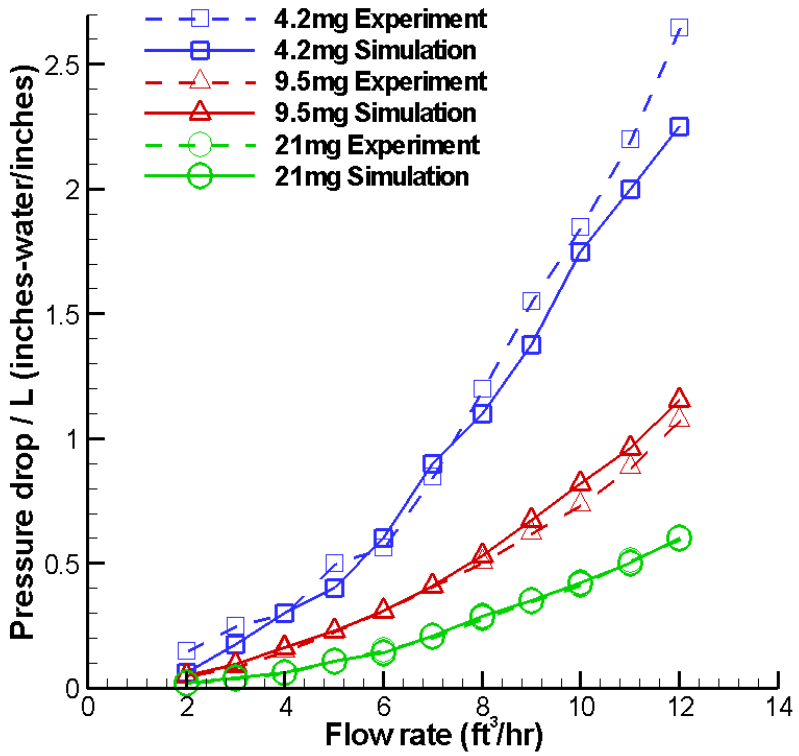


**Figure 2-3 Pressure drop results for activated carbon pellets: comparisons between numerical simulation and the experiment.**

It is apparent, from the comparison between the simulation and the experiment, that the nano-structured materials (the activated carbon pellets) do not show any particular difference from the traditional materials (zirconium beads) in terms of their momentum transport behavior. The material properties of the porous medium that influence momentum transport at the current level are the macroscopic properties that have little to do with the nano-scale properties.

### 2.3.2 Results of the Adsorption Tests

In the adsorption tests, the main purpose was to evaluate the adsorbing ability of the nano-material (the adsorption experiments were conducted by NanoScale, Inc). Hence, only a thin layer (a short bed) of nano-material pellets was tested. Performance of air filtration sorbents is usually evaluated using a breakthrough method. A schematic of a typical breakthrough setup is shown in Fig. 2-4 (a). In this setup, an air stream was conditioned in a dryer and a humidifier to achieve the desired relative humidity level. Then, the air was mixed with a controlled stream of pollutant to reach the needed concentration. A fixed bed of tested material in a granulate form was placed in a test tube that allows for uniform flow distribution that minimizes wall channeling effects. Figure 2-4(b) presents the test tube used by NanoScale, Inc. The test tube was 30 mm in diameter, which for granulated adsorbents used (mesh 16-35, 0.5-1.2 mm) is sufficient to minimize wall effects. Prior to the breakthrough test the test tube was filled with the adsorbent that formed a 10 mm thick bed. This thickness was found to be sufficient to prevent bed channeling and premature pollutant breakthrough for superficial air velocity of 6 cm/s. Air flow through the bed was in the downward direction in order to eliminate bed fluidization.

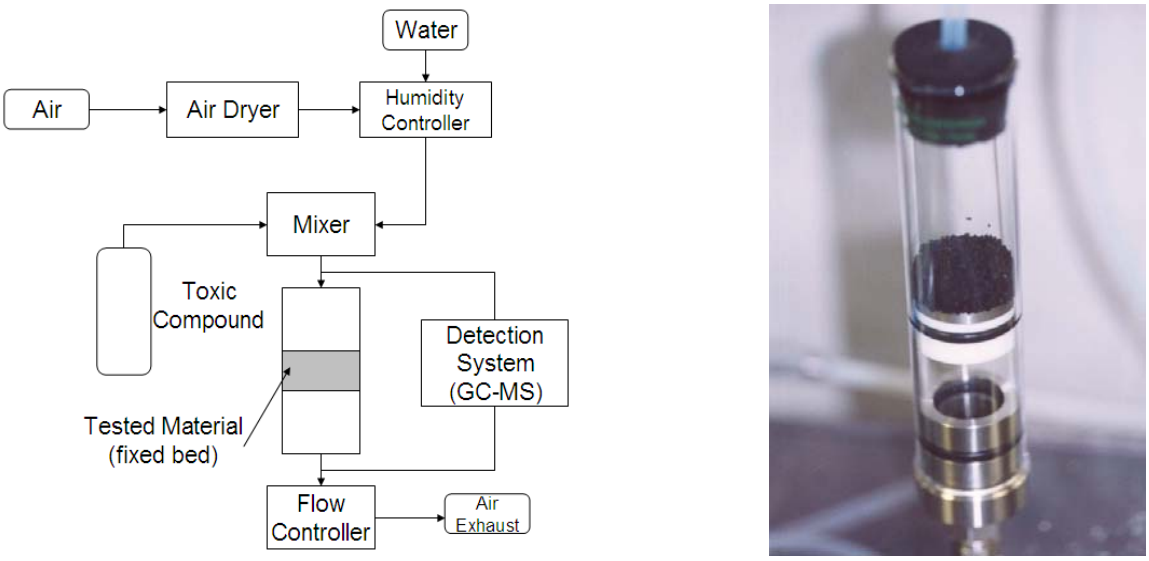


**(a)** **(b)**

**Figure 2-4 (a) Schematic of the air filtration breakthrough apparatus; (b) Test tube used in the experiment.**

Adsorption performance is evaluated by monitoring toxic pollutant concentrations before and after passing through a fixed bed of tested material. NanoScale's breakthrough setup uses a GC-MS spectrometer (HP 5890 Series II gas chromatograph and HP 972 mass spectrometer) equipped with an automatic valve system and PC data acquisition workstation. During the analysis, air upstream and downstream of the adsorbent bed was sampled and periodically (5-10 minutes intervals) analyzed by the GC-MS spectrometer. A typical breakthrough test was conducted over a period of several hours until the toxic pollutant appears downstream of the filter. Performance of tested materials was evaluated based on the overall shape of breakthrough curves (downstream pollutant concentration plotted as a function of time) and breakthrough times. In this study, a set of breakthrough curves were obtained for granulated NanoActive ZnO

sorbent exposed to hydrogen sulfide ($H_2S$).

The numerical model is an exact replica of the experimental conditions for comparison purposes. The geometry, based on the experimental setup and the simplified computational model with the same conditions, is shown in Fig. 2-5. Also, some of the flow and material properties can be found in Fig. 2-5(a). The porous medium (the monomer particles inside the packed-bed) is also assumed to be isotropic and homogenous.

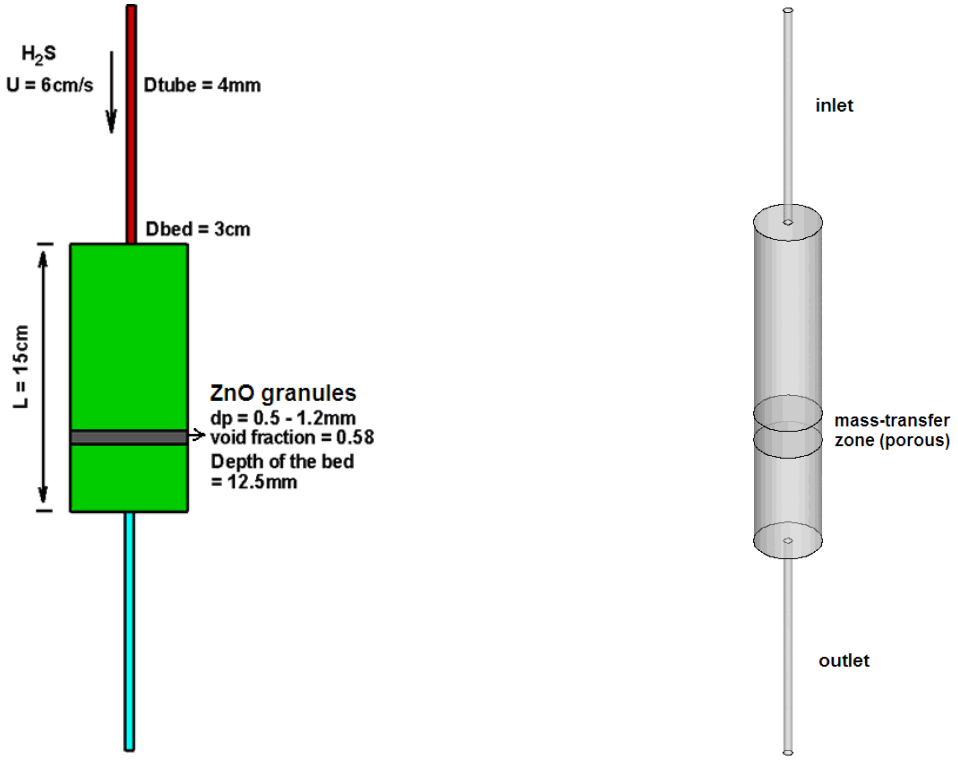


**(a)** **(b)**

**Figure 2-5 Computational model used in the adsorption simulation: (a) physical model with dimension and parameters; (b) computational domain.**

The local concentration of the flow with contaminant is assumed to have a negligible effect on the thermodynamic properties of the air, and hence, no effect on the predicted flow field. This assumption enabled the steady-state flow field solution to be fixed during the transient simulation of the species transport equation. In the simulation, the concentration changes of $H_2S$ in the two locations (upstream and downstream of the porous bed) were recorded and compared with the experimental data.

The value of molecular diffusivity ( $D_s$ ) for $H_2S$ in air was estimated using the models of Chapman-Enskog (Bird et al. 2002) and Wilke-Lee (Wilke and Lee, 1955) in Perry's Chemical Engineering Handbook (Perry and Green, 1997). Both models yielded a value very close to 0.19 $cm^2/s$. The diffusion processes inside the pores of NanoActive ZnO sorbent were evaluated in terms of effective diffusivity and calculated using a random pore model, frequently used to describe solid sorbents or catalysts. The parameters used by the random pore model, mainly densities obtained by direct measurement and pore characteristics measured by the nitrogen adsorption method (Wakao and Smith, 1964; Froment and Bischoff, 1990), are presented in Table 2-3. In the numerical simulation, the mass transfer coefficient, $k_f$ , is 0.0000284 m/s. Those measured material properties were used in the simulations.

| ZnO (NanoActive) Properties | Value |
|---|---|
| Average particle diameter ($d_p$) | 0.5 – 1.2 mm |
| Density ($\rho_p$) | 5.25 g/cm$^3$ |
| Void fraction ($\varepsilon$) | 0.58 |
| Specific surface area to volume ratio ($S_0$) | 7059 |
| Average pore diameter for micro-pores | 10.5 nm |
| Simulated mass transport coefficient ($k_f$) | 0.0000284 m/s |

**Table 2-3 Pellet properties in the adsorption test.**

The model used in the species transport equation was run simultaneously with the momentum transport equations. It was also computed transiently to demonstrate gradual saturation of the filter, which is responsible for the breakthrough, a process also known as percolation.

As mentioned earlier, in the current simulation, the reaction and the heat of adsorption have not been taken into account (since those effects are so small that can be negligible), and a linearized adsorption model was used in the mass transport equation. First, the flow field was simulated. Figure 2-6 (a) illustrates the velocity field in the computational domain. The streamlines predict the direction of the flow and the color represents the magnitude of the velocity. It is apparent that the flow is slowed in the bed and becomes more laminar, especially in the thin porous zone, which is typical.

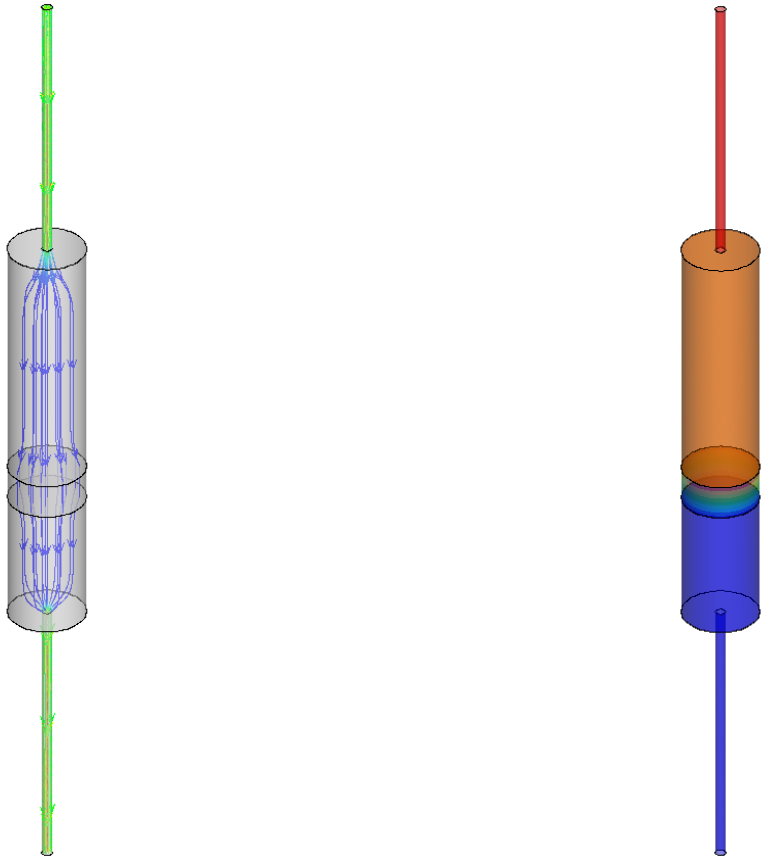

**(a)** **(b)**

**Figure 2-6 Streamline colored by Velocity Magnitude and contour plot of the concentration in the filter.**

The local concentration of the $H_2S$ is assumed to have a negligible effect on the thermodynamic properties of the air, and hence, no effect on the calculated flow field. This assumption enables the steady-state flow field solution to be fixed during the transient (unsteady) simulation for the species transport. So, only species transport is actually solved based on the obtained flow field, which saves the computational time by avoiding the transient simulation for

the velocity field. An intermediate contour plot of the concentration in the filtration process is in Fig. 2-6 (b) where the color represents the magnitude of the concentration. Before entering the porous zone, the concentration stays constant in the inlet tube and the entrance zone of the bed. In the thin porous substrate, due to the adsorption, the concentration of $H_2S$ is gradually reduced. This process continued until the porous sorbent was totally saturated.

The breakthrough curve can be used to monitor this process by measuring the concentration change at two locations: upstream and downstream in the bed. The upstream location records the incoming concentration while the downstream one tracks the adsorption behavior. Figure 2-7 shows the concentration measurements at the above locations by simulation and experiment. It is noticed that the incoming concentration in the experiment is very difficult to be kept as a constant. In Fig. 2-7 (a), the incoming concentration in the simulation is kept as a constant, which is the averaged value from the data history of the experiment. By having the linearized sink term in the species transport equation, the concentration change from the numerical simulation at the downstream location (breakthrough curve) is very close to the experimental data. Initially, the concentration is almost zero since the gas flow has not reached that location yet. After more than an hour (the breakthrough time), the adsorption process begins and the concentration is accumulating until the porous substrate is fully saturated. The downstream concentration reaches the incoming value after 6 hours, which is a very slow process. Since the incoming concentration used in the simulation is lower than that in the experiment after 6 hours, the final concentration deems to be lower than the data captured in the experiment.

To improve the results, the incoming concentration time history was modified by dividing it into three periods based on the experimental data: 1) 0-3 hrs, use a constant value by

averaging; 2) 3-6 hrs, use a linear correlation as a transition; 3) 6-12 hrs, use another constant value by averaging. By implementing this transient incoming concentration profile, the resulting concentration reached the final stage in the experiment (Fig. 2-7b).

Based on the above results of the breakthrough tests, the numerical model is calibrated and validated by comparing with the experimental data. Hence, the CFD technique used in this study is proved to be sufficiently accurate. The porous models and the related numerical simulation treatments can possibly be further applied to modeling of filtration/adsorption processes with other materials and types of packed-bed filters.

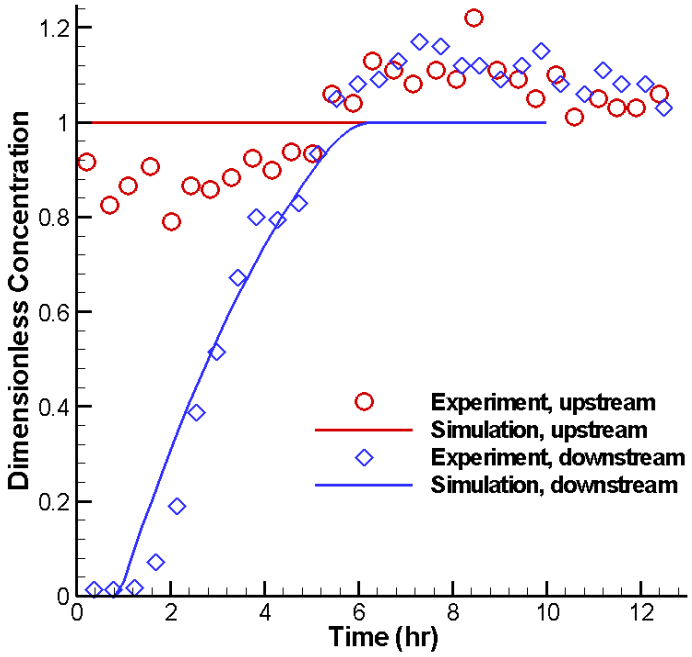


**(a)**

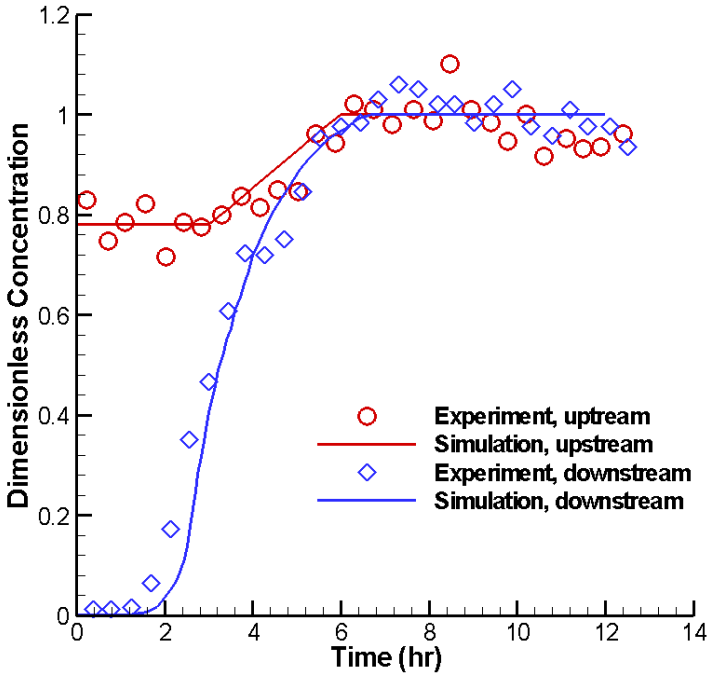


**(b)**

**Figure 2-7 The concentration change along the central line of the setup by using different source terms in the species transport equations.**

## 2.4 Summary of the Macro-Scale Simulation

In this chapter, the flow/species going through a substrate of a packed-bed filter filled with nano-material pellets are simulated, which provides a platform to test and evaluate the design of such devices. Numerical models, which exactly followed the experimental setups, were developed to make use of CFD simulation. To simulate the porous/adsorbing effect, additional source terms were added to the momentum and mass transport equations. Various types of packed-bed and materials have been tested in this study. The numerical models were validated by comparing with both the analytical solution and the experimental data. The linearized sink terms added in the porous substrate were applicable in a range of materials and types of packed-

beds. Good agreement was achieved for both the results of the pressure drop and the breakthrough behavior in the filtration process. Especially, the simulation results from the tests with nano-material pellets as the adsorbent were proved to be efficient and accurate.

# CHAPTER 3 - Micro-Scale Simulation

## 3.1 Flow in Porous Medium

In a nano-material air filter, the air flow will go through the porous substrate. Consequently, the flow mechanisms and the adsorption process become interesting. This, therefore, involves the micro-scale simulation, which requires the momentum and mass transport in the porous medium be studied. In this chapter, the objectives of our study include both multi-body fluid/solid and fluid/porous interactions. An illustration of the problem is shown in Fig. 3-1.

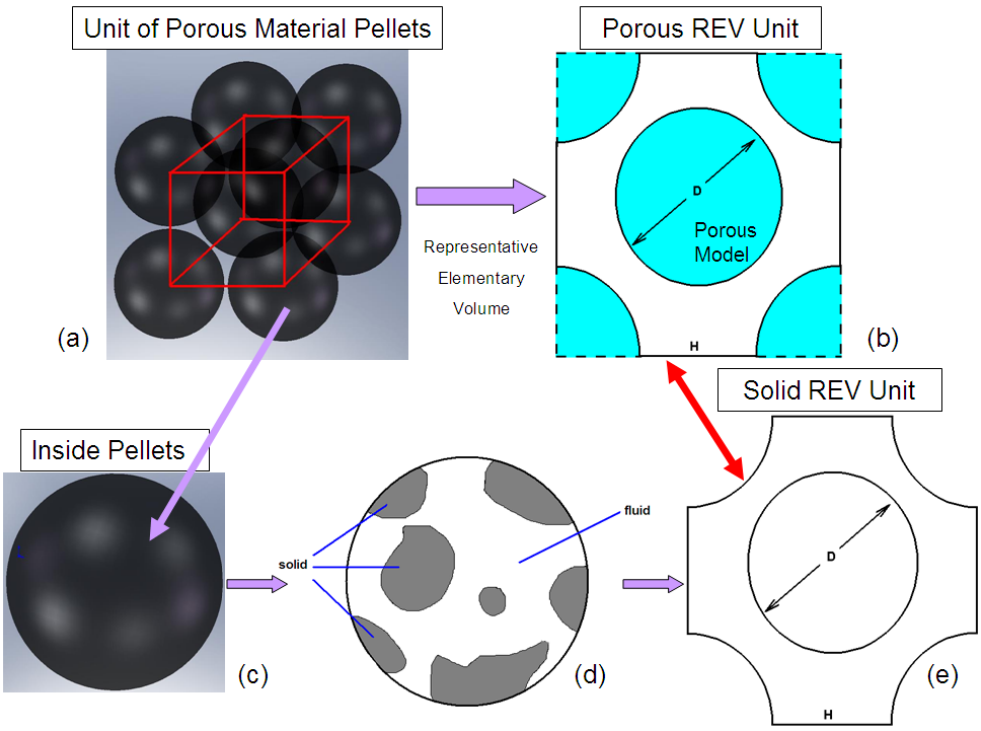


**Figure 3-1 Multi-body fluid/solid and fluid/porous interaction in porous medium: (a) a unit of porous material pellets (b) porous REV unit (c) to study the transport phenomena inside the pellets (d) the inside porous structure (e) solid REV unit.**

As shown in Fig. 3-1, a group of nano-material (porous) pellets was first selected for constructing a unit (Fig. 3-1a). A 2D simplified numerical model (Fig. 3-1b) can be defined based on the concept above. So in this 2D porous unit, the flow and species transport phenomena could be explored with the use of porous models inside the cylinders. To answer the question about the transport in the pores, we looked inside those porous material pellets (Fig. 3-1c) and treated the pores as a Representative Elementary Volume (REV) as shown in Fig. 3-1(d). The gray areas are solid bodies, so the fluid will go though the pores. And this fluid/solid interaction problem could also be simplified as a 2D solid unit as shown in Fig. 3-1(e). Thus, the same geometry/structure with different transport models could represent and solve different scales of mechanisms.

In this chapter, the numerical algorithms used in this scale including the immersed-boundary method (IBM), the porous model (Zwikker-Kosten equation) and the high-order schemes (used on the interface) are explained in Section 3.2. The results and discussion in Section 3.3 are divided into two parts: 1) fluid/solid interactions in a tandem cylinders system as the validation case for the IBM and 2) fluid and species transport in a periodic array of solid/porous cylinders. A conclusion is presented in Section 3.4.

## 3.2 Numerical Scheme and Algorithm

### 3.2.1 Immersed-Boundary Method

The concept of immersed-boundary methods (IBM) involves implementing a defined forcing term in the momentum transport equations in the vicinity of the solid boundary. It has been successfully used to study various fluid-structure interaction (FSI) problems. The advantages of using IBM are: 1) only a simple Cartesian grid is needed, 2) no moving grid is

required to simulate an object in motion, and 3) The shape/arrangement of the objects can be arbitrary. Peskin (1997) introduced this innovative method in his Ph. D. thesis for which the internal blood flow was simulated. Since then, several schemes for IBM have been developed, e.g. Saiki and Biringen (1996), Mohd-Yusof (1996), Yang and Balaras (2006), and Mittal et al. (2008). A review of the IBM was presented by Mittal and Iaccarino (2005). For our current study, a modified IBM with a direct compensation forcing term was used to compute the fluid flow. This computational algorithm was verified using numerous sets of data in the literature on flow over cylinders and spheres (Zhang and Zheng, 2007).

The governing equations for the IBM are the continuity equation and the Navier-Stokes equations for incompressible flow. In our study, for numerical convenience, the equations mentioned above have been characterized with the free stream velocity ($U$), the diameter of the cylinder ($D$) and the density of the flow ($\rho$) to be dimensionless. Thus the time ($t$), the length scale ($\mathbf{x}$), velocity scale ($\mathbf{u}$) and the pressure term ($p$) can be characterized as: $t = \frac{U}{D} t^*$, $\mathbf{x} = \frac{\mathbf{x}^*}{D}$, $\mathbf{u} = \frac{\mathbf{u}^*}{U}$, $p = \frac{p^*}{\rho U^2}$. The non-dimensionalized continuity equation (Eq. 3.1) and the momentum equations (Eq. 3.2) for the current IBM (Zhang and Zheng, 2007) are:

$$\nabla \cdot \mathbf{u} = 0 \tag{3.1}$$

and

$$\frac{\partial \mathbf{u}}{\partial t} + \mathbf{u} \cdot \nabla \mathbf{u} = -\nabla p + \frac{1}{Re} \nabla^2 \mathbf{u} + \mathbf{f} \ , \tag{3.2}$$

where $Re$ is the Reynolds number defined as $\mathrm{Re} = \rho UD / \mu$ ($\mu$ is the dynamics viscosity of the flow), and, $\mathbf{f}$ is the body force representing the virtual boundary.

The external forcing term **f** is updated at each time step to establish the desired boundary velocity (**v**). It should be noted that this force is only applied in an internal layer adjunct to the IB while kept zero elsewhere. This force can be expressed as

$$\mathbf{f} = \mathbf{S} + \nabla p - \frac{1}{\mathrm{Re}}\nabla^2 \mathbf{u} + \frac{1}{\Delta t}(\mathbf{v} - \mathbf{u}^n), \tag{3.3}$$

where the desired boundary velocity is on the internal layer as well. And, **S** is the convection term defined as:

$$\mathbf{S} = (\mathbf{u} \cdot \nabla)\mathbf{u}. \tag{3.4}$$

The direct-forcing IB method used here follows the concept of the scheme explained in Mohd-Yusof (1996). The governing equations, Eqs. (3.1) and (3.2), are discretized using the first order time-marching, with a semi-implicit term for the diffusion terms and the Adams-Bashforth scheme for convection and central differencing for diffusion. An interpolation/extrapolation scheme (Saiki and Biringen, 1996) is used to interpolate the direct force. This force is then extrapolated back on the grid points inside the IB.

The solving scheme involves a two-step, predictor-corrector procedure. The velocity predictor equation is:

$$\mathbf{u}^* = \mathbf{u}^n + \Delta t\left\{-\left(\frac{3}{2}\mathbf{S}^n - \frac{1}{2}\mathbf{S}^{n-1}\right) - \nabla p^* + \frac{1}{2Re}\nabla^2\left(\mathbf{u}^n + \mathbf{u}^*\right) + \mathbf{f}\right\}, \tag{3.5}$$

where the pressure estimation can be derived as:

$$\nabla^2 p^* = -\nabla \cdot \left[(\mathbf{u}^n \cdot \nabla)\mathbf{u}^n - \mathbf{f}\right]. \tag{3.6}$$

Then, with the following correction step, the real time velocity and pressure are given by:

$$\mathbf{u}^{n+1} = \mathbf{u}^* - \nabla\phi, \tag{3.7}$$

and

$$p^{n+1} = p^* + \phi, \tag{3.8}$$

where $\phi$ is the solution of the modified Pressure Poisson Equation (PPE) to satisfy the continuity:

$$\nabla^2 \phi = \nabla \mathbf{u}^*. \tag{3.9}$$

And both Eqs. (3.6) and (3.9) are solved using FISHPACK (Swarztrauber and Sweet, 1979).

The stability condition for a two-dimensional problem is no more restrictive than an explicit scheme for a two-dimensional convection-diffusion equation:

$$\delta t < \min\left[\frac{h^2 Re}{4}, \frac{2}{(u^2 + v^2)Re}\right], \tag{3.10}$$

where *h* is the grid size. The first part in Eq. (3.10) is from diffusion, while the second part (Courant number) is related to convection.

The computational scheme, including the interpolation/extrapolation procedure, is implemented on a staggered grid. Since the forcing is used to enforce the velocity on the boundary, the *x*-direction force is calculated on the *u*-grid and the *y*-direction force is calculated on the *v*-grid. Because the grid points involved in the interpolation/ extrapolation procedure can be applied to either the *u*-grid or the *v*-grid, there would be no discrepancies should exist among the staggered grid used in computing the governing equations and the grid used in the interpolation/extrapolation procedure.

### 3.2.2 Porous Medium Model

Darcy's law has been widely used inside the porous medium to solve fluid mechanics and hydrology problems. This law was first introduced by Henry Darcy based on hydraulic experimental data (Darcy, 1856), which determined the flow rate of water through the filters. Darcy's law is a simple proportional relationship between the instantaneous discharge rate through a porous medium, the viscosity of the fluid and the pressure drop over a given distance:

$$u = -\frac{K}{\mu}\frac{\partial p}{\partial x}, \tag{3.11}$$

where $u$ is the velocity of the flow, $\partial p / \partial x$ is the pressure gradient in the flow direction, and, $\mu$ is the dynamic viscosity of the fluid. The coefficient $K$ is called the permeability, which only depends on the geometry of the medium and describes the penetrating ability. Darcy's law is the most recognized model and has been extended into other models for various perspectives.

In three dimensions, for the case of an isotropic and homogeneous porous medium, Eq. (3.11) can be rewritten as:

$$\nabla p = -\frac{\mu}{K}\mathbf{u}. \tag{3.12}$$

To extend Darcy's law in a more realistic format for the real fluid flow, the unsteady term, convection term and the diffusion term need to be considered in the porous medium. When Eq. (3.12) is combined with the Navier-Stokes (NS) equation and the porous structure in the medium considered, the NS equation can be extended as:

$$\frac{\partial \mathbf{u}}{\partial t} + \frac{1}{\varepsilon}(\mathbf{u}\cdot\nabla)\mathbf{u} = -\frac{\varepsilon}{\rho}\nabla p - \frac{\mu\varepsilon}{\rho K}\mathbf{u}, \tag{3.13}$$

where the porosity $\varepsilon$ is defined as the void fraction of the total volume of the medium that is occupied by the void space.

Several publications have examined the flow past porous bluff bodies. Bhattacharyya et al. (2006) investigated the flow field and solute transport around and through a porous cylinder in a range of Darcy numbers ($D_a$) and Reynolds numbers (Re). The momentum and the mass transport equations for fluid through a porous cylinder are written as:

$$\frac{\partial \mathbf{u}}{\partial t} + \frac{1}{\varepsilon}(\mathbf{u}\cdot\nabla)\mathbf{u} = -\varepsilon\nabla p + \frac{\varepsilon}{\mathrm{Re}}\nabla^2\mathbf{u} - \frac{2\varepsilon}{\mathrm{Re}\,D_a}\mathbf{u} - \frac{1.75|\mathbf{u}|}{150\sqrt{D_a\varepsilon}}\mathbf{u}, \tag{3.14}$$

and

$$\frac{\partial C}{\partial t}+\frac{1}{\varepsilon}(\mathbf{u}\cdot\nabla)C=\frac{2}{\mathrm{Re}\cdot Sc}\nabla^2 C\,. \tag{3.15}$$

Equation (3.14) includes the convection term, the diffusion term, the Darcy term and the Forchheimer term. $C$ represents the dimensionless concentration. The Darcy number is defined as $D_a = K/a^2$ and the Reynolds number as $\mathrm{Re} = 2\rho Ua/\mu$, where $a$ is the characteristic length. The Schmidt number, $S_c$, is the ratio between the kinetic viscosity and the diffusivity. Bhattacharyya et al. (2006) performed a thorough study of this problem and their results compared well with the literature. However, the fluid/porous interface problem was not mentioned in their study.

Chen et al. (2008, 2009) investigated the flow past a porous square/trapezoidal cylinder based on the stress-jump boundary conditions. In their study, the governing equation for flow inside the porous medium, when the viscous and inertial effects are considered, is expressed as:

$$\rho\frac{\partial \mathbf{u}}{\partial t}+\nabla\cdot\left(\frac{\rho\mathbf{u}\mathbf{u}}{\varepsilon}\right)=-\varepsilon\nabla p^{*}+\mu\nabla^2\mathbf{u}-\frac{\mu\varepsilon}{K}\mathbf{u}-\frac{\rho\varepsilon C_F|\mathbf{u}|}{\sqrt{K}}\mathbf{u}\,, \tag{3.16}$$

Eq. (3.16) is called the Darcy-Brinkman-Forchheimer extended model and $C_F$ is the Forchheimer coefficient. Also $p^*$ is the intrinsic average that can be calculated from the Dupuit-Forchheimer relationship ( $p^* = p/\varepsilon$ ). At the interface between the homogeneous fluid and porous medium, the boundary conditions need to be determined to couple the two phases. The stress jump condition (Ochoa-Tapia and Whitaker, 1995 a, b) along with the velocity and stress boundary conditions can be summarized as:

$$\frac{1}{\varepsilon}\frac{\partial U_t}{\partial n}\bigg|_{\text{porous}} - \frac{\partial U_t}{\partial n}\bigg|_{\text{fluid}} = \beta \frac{1}{\sqrt{Da}} U_t\big|_{\text{interface}} + \beta_1 \,\text{Re}\, U_t^2$$
$$\vec{U}\big|_{\text{fluid}} = \vec{U}\big|_{\text{porous}} = \vec{U}\big|_{\text{interface}} \tag{3.17}$$
$$\frac{1}{\varepsilon}\frac{\partial U_n}{\partial n}\bigg|_{\text{porous}} - \frac{1}{\varepsilon}\frac{\partial U_n}{\partial n}\bigg|_{\text{fluid}} = 0$$

where $U_t$ is the tangential velocity component, $U_n$ is the normal velocity component, $\beta$ and $\beta_1$ are the adjustable parameters. Hence, it is clear that this stress-jump boundary condition is strongly problem dependent and parameter dependent. Thus, in this study at the fluid/porous interface, we decided to use the numerically high-order scheme to smooth the discontinuity between the two phases. This will be explained in detail later.

The Zwikker-Kosten (ZK) model (Zwikker and Kosten, 1949) is a linear and phenomenological model used to simulate the porous medium. It has been adapted previously for numerical calculations of linear sound interactions with porous materials (Wilson et al. 2006, 2007; Xu et al. 2010). The original equation of motion for the ZK model in one direction is:

$$-\frac{\partial p}{\partial x} = \frac{\rho k_s}{\varepsilon}\frac{\partial u}{\partial t} + \sigma u\,, \tag{3.18}$$

where $k_s$ is the structure constant and $\sigma$ is the resistance constant. Although Zwikker and Kosten allow these values to depend on frequency, they are normally assumed to be constant in time-domain calculations.

Wilson et al. (2006, 2007) first worked on the application of the ZK equation for time-domain modeling of sound interaction with a porous surface. They also compared the ZK model with other sophisticated models and found good agreement between the rather simple ZK model and other more complex models. In their three-dimension model, for the case of a homogeneous and isotropic porous medium, Eq. (3.18) can be rewritten as:

$$\rho \frac{\partial \mathbf{u}}{\partial t} = -\frac{\varepsilon}{k_s} \nabla p - \sigma_s \mathbf{u} \,. \tag{3.19}$$

For simplification, if we define porosity $\varepsilon$ and structure constant $k_s$ as unity ($\varepsilon = k_s = 1$), then Eq. (3.19) becomes:

$$\rho \frac{\partial \mathbf{u}}{\partial t} = -\nabla p - \sigma_s \mathbf{u} \,. \tag{3.20}$$

Adding the convection term and the diffusion term into Eq. (3.20) and nondimensionlizing it, we obtain the modified ZK equation:

$$\frac{\partial \mathbf{u}}{\partial t} + (\mathbf{u} \cdot \nabla)\mathbf{u} = -\nabla p + \frac{1}{\mathrm{Re}} \nabla^2 \mathbf{u} - \sigma \mathbf{u} \,, \tag{3.21}$$

where $\sigma$ is the dimensionless flow resistivity of the porous medium, non-dimensionalized by $\rho U / D$. The convection term and the diffusion term in Eq. (3.21) are omitted in the original ZK equation (Eq. 3.19) because the velocity is low in the porous medium; however, including them here enables the same Navier-Stokes equation solver to be used for Eq. (3.21). Additionally, we assume the effect of convection automatically becomes small when the velocity is low.

Xu et al. (2010) investigated wind noise reduction by using a screened microphone using the modified ZK equation in Eq. (3.21). They compared their results for a single porous cylinder to the literature and also considered the interface problem by using the high-order scheme for both solid and porous cases. The high-order schemes will be explained in Section 3.2.3. In their study, the ZK equation has been solved and coupled with the immersed-boundary method. The similarity between Eqs. (3.2) and (3.21) is very clear. Thus, in our study, we could later use Eq. (3.2) for the outside fluid flow and use Eq. (3.21) inside the porous medium. The only difference is the additional source (force) term on the right-hand side.

### 3.2.3 High-Order Schemes

Finite-difference methods approximate the solutions to differential equations by replacing derivative expressions with approximately equivalent difference quotients. By using Taylor expansion, different orders of the fixed stencil schemes could be reached. And it is accepted that when the stencil is wider, the scheme will be more accurate. However, in some complex problems with discontinuity, the fixed-stencil type schemes cannot eliminate the numerical oscillation.

To replace the fixed stencil scheme, the adaptive stencil method has been proved to be capable of eliminating the discontinuity. The Essentially Non-Oscillatory (ENO) scheme was the first successful attempt to obtain a self-similar, uniformly high order accurate, yet essentially non-oscillatory, interpolation for piecewise smooth functions. ENO schemes were first introduced by Harten et al. (1987). Improved version of the ENO schemes, called Weighted ENO (WENO) schemes, were developed using a complex combination of all candidate stencils instead of just one as in the original ENO. Both ENO and WENO schemes have been applied successfully to simulate various applications, especially those having interfaces. The idea for both schemes includes a reconstruction procedure based on the local smoothness of the numerical solution to automatically achieve high-order accuracy and determine the non-oscillatory property near discontinuities. The difference is that the ENO uses just one stencil for the reconstruction procedure while the WENO uses a convex combination of all the candidate stencils, each being assigned a nonlinear weight that depends on the local smoothness of the numerical solution based on that stencil. Hence, the WENO improves upon the ENO in robustness, smoothness of fluxes, steady state convergence, provable convergence properties, and the over-all efficiency.

The presence of porous media introduces a discontinuity in some flow variables or their derivatives around the flow/porous interface. Under these circumstances, most conventional finite difference schemes would generate some spurious numerical oscillations around the interface. However, accuracy at the interface between flow and porous media is a key issue in simulating such problems. The most widely used method for overcoming the unphysical oscillations and numerical instability is to apply high-order schemes, including the upwind scheme and the WENO scheme (Harten et al. 1987; Shu and Osher, 1988). High-order schemes have been used in simulation for viscous flow around steady and moving solid bodies (Cho et al. 2007). But still have not been applied to simulating flow field in different media. In Xu et al. (2010), the high-order WENO scheme was adopted at the fluid/porous medium interfaces to compare the wind noise reduction between the unscreened microphone and the screened microphone under different frequencies of incoming wind turbulence. Their study was the first to prove that the WENO scheme efficiently and accurately smoothed the discontinuity between the fluid and the porous phases.

Upwind schemes use an adaptive finite difference stencil to numerically simulate the direction of propagation of information. The 1$^{st}$-order upwind scheme is considered to be too dissipative. Thus, our investigation includes 2$^{nd}$- and 3$^{rd}$-order upwind schemes. To understand the discretization in those schemes, the simplified 1D wave equation is considered as:

$$\frac{\partial u}{\partial t} + a\frac{\partial u}{\partial x} = 0 . \tag{3.22}$$

For the 2$^{nd}$-order upwind scheme, the discretization of the second term in Eq. (8) would be:

$$a\left.\frac{\partial u}{\partial x}\right|_{x=x_i^n} = \max(a,0)\frac{3u_i - 4u_{i-1} + u_{i-2}}{2\Delta x} + \min(a,0)\frac{-u_{i+2} + 4u_{i+1} - 3u_i}{2\Delta x} \quad . \tag{3.23}$$

Similarly, for the skewed 3rd-order upwind scheme, the convective term becomes:

$$a\left.\frac{\partial u}{\partial x}\right|_{x=x_i^n} = \max(a,0)\frac{2u_{i+1} + 3u_i - 6u_{i-1} + u_{i-2}}{6\Delta x} + \min(a,0)\frac{-u_{i+2} + 6u_{i+1} - 3u_i - 2u_{i-1}}{6\Delta x} \quad . \tag{3.24}$$

The WENO schemes were developed using a convex combination of all candidate stencils. The 5th-order WENO scheme has a more complicated structure and considers the same 1D wave equation but in the conservation form:

$$\frac{\partial u}{\partial t} + \frac{\partial q(u)}{\partial x} = 0, \tag{3.25}$$

The derivative of any flux $q$ at location $x_i$ is discretized as:

$$\left.\frac{\partial q}{\partial x}\right|_{x=x_i} = q_{x,i} = \frac{\hat{q}_{i+1/2} - \hat{q}_{i-1/2}}{\Delta x} \quad , \tag{3.26}$$

If $\partial q / \partial u \geq 0$ ,

$$\begin{aligned}\hat{q}^{+}_{i+1/2} = {} & \omega_1\left(\frac{1}{3}q_{i-2} - \frac{7}{6}q_{i-1} + \frac{11}{6}q_i\right) \\ & + \omega_2\left(-\frac{1}{6}q_{i-1} + \frac{5}{6}q_i + \frac{1}{3}q_{i+1}\right) \quad , \\ & + \omega_3\left(\frac{1}{3}q_i + \frac{5}{6}q_{i+1} - \frac{1}{6}q_{i+2}\right)\end{aligned} \tag{3.27}$$

where $\omega_j = \dfrac{\alpha_j}{\sum_{k=1}^{3}\alpha_k}, \quad \alpha_k = \dfrac{d_k}{(\varepsilon + \beta_k)^2}, \quad \varepsilon = 10^{-6},$

$$d_1 = \frac{1}{10}, \qquad d_2 = \frac{3}{5}, \qquad d_3 = \frac{3}{10},$$

$$\beta_1 = \frac{13}{12}(q_{i-2} - 2q_{i-1} + q_i)^2 + \frac{1}{4}(q_{i-2} - 4q_{i-1} + 3q_i)^2,$$

$$\beta_2 = \frac{13}{12}(q_{i-1} - 2q_i + q_{i+1})^2 + \frac{1}{4}(q_{i-1} - 4q_{i+1})^2,$$

$$\beta_3 = \frac{13}{12}(q_i - 2q_{i+1} + q_{i+2})^2 + \frac{1}{4}(3q_i - 4q_{i+1} + q_{i+2})^2.$$

More details about the WENO scheme can be found in Shu and Osher (1988, 1989), Cho et al. (2007) and Xu et al. (2010). In our study, the high-order schemes are adapted to discretize all the convention terms in the momentum and species transport equations to generate a smooth region between the fluid and porous phases.

## 3.3 Results and Discussion

This section includes two parts: 1) multi-body fluid/solid interaction: uniform flow over a tandem cylinders system and 2) multi-body fluid/solid and fluid/porous interaction: uniform flow over a periodic array of circular cylinders. Section 3.3.1 uses the flow over a tandem cylinders system as a validation case for the immersed-boundary method (IBM) applied to multi-body FSI problem. Section 3.3.2 then shows the results of the solid/porous unit with the modified and extended IBM.

### 3.3.1 Flow over a Tandem Cylinder System

#### *3.3.1.1 Introduction*

Wake-structure interactions among tandem cylinders can be found in many engineering applications, such as arrays of tubes in heat exchangers, power lines, and off-shore engineering

structures. It is a complicated problem because the behavior of this nonlinear system depends on the parameter related to the tandem arrangement. This creates many nonlinear physical phenomena that are of interest to those who research fluid dynamics.

The literature concerning flow over two stationary tandem cylinders includes experimental observations presented in Zdravkovich (1985), Zdravkovich (1997), Igarashi (1981), and Tanida et al. (1973) and numerical simulations from Li et al. (1991), Jester and Kallinderis (2003), Sharman et al. (2005), Deng et al. (2006) and Papaioannou et al. (2006, 2008). Physical mechanisms involved in two tandem cylinders are very different from those in a single cylinder because the wakes that are shed from both cylinders are coupled and interact with each other. The vorticity field is significantly affected by the Reynolds number ( $\mathrm{Re} = UD/\upsilon$ ) and the spacing between the two cylinders. As confirmed in the literature (Sharman et al., 2005) and this study, the Strouhal number ( $St = fD/U$ ) of the two tandem cylinders is not the same value as that of the single cylinder for the same Reynolds number. In addition, the Strouhal number is identical for both of the cylinders in the system. Compared with single stationary cylinder cases, which are mostly dominated by Reynolds numbers, the spacing effect of the tandem cylinders is another important factor. It has been found that by changing the distance between the two cylinders wake formation and coupling may vary. Most interestingly, there exists a critical spacing distance ( $S_c$ ) on the border of the vortex formation (VF) and vortex suppression (VS) regimes, which is marked by a sudden jump and discontinuity of the Strouhal number. For low Reynolds number laminar cases (in the range of 100s), the critical spacing is predicted by Li et al. (1991) to be between 3 and 4 and by Sharman et al. (2005) to be between 3.75 and 4.

More details of the immersed-boundary method used for this case are explained in Section 3.3.1.2. In Section 3.3.1.3, the flow patterns of a system of two stationary cylinders at different spacing and the related Strouhal number effect are described. And the conclusions are made in Section 3.3.1.4.

### *3.3.1.2 Numerical Simulation*

Direct numerical simulations based on an improved immersed-boundary method (IBM) with direct-forcing (Zhang and Zheng, 2007) are carried out to simulate the flow system. The non-dimensionalized governing equations and the numerical schemes of the IBM can be found in Section 3.2.1.

When the immersed-boundary method is used, arbitrary shapes and motions of solid bodies can be effectively simulated by a proper construction of the boundary forcing term so that a simple, non-moving Cartesian grid can be used. The domain size selected for this study is $38.4 \times 25.6$ (non-dimensionalized by the cylinder diameter $D$), as shown in Fig. 3-2. The upstream cylinder is located at 8, sufficiently away from the inlet boundary to eliminate the inlet effect. The distance between the two cylinders is defined as $S$ (also non-dimensionalized by the cylinder diameter $D$). The outlet boundary is also far enough from the downstream cylinder to allow the vortex street to develop fully. The grid-size independence check (Zhang and Zheng, 2007) determined that a grid size with $\Delta x = \Delta y = 0.025$ provides an acceptable grid resolution for all the computational cases at $\mathrm{Re} = 100$. The boundary conditions are also shown in Fig. 3-2. For a stationary cylinder, the velocity on the surface is zero.

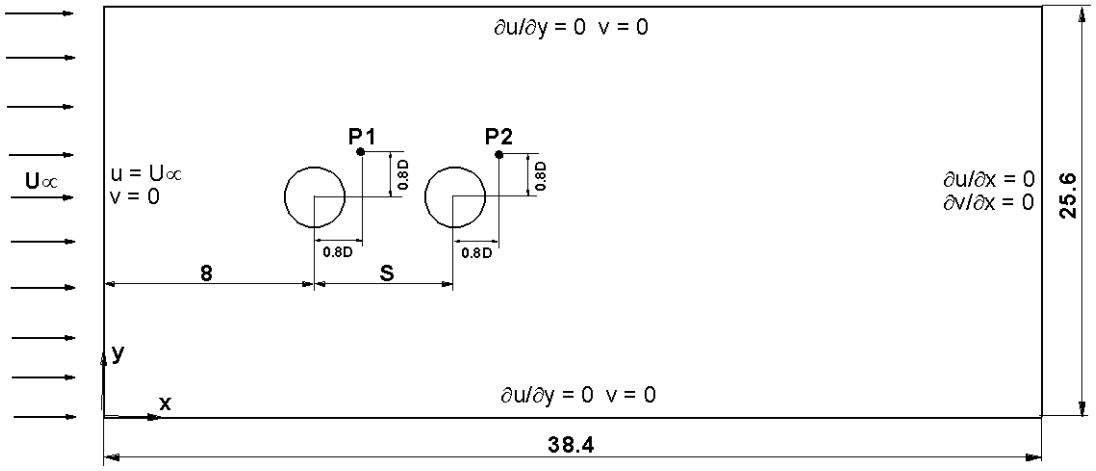


**Figure 3-2 Computational domain of the tandem cylinders system.**

The computational scheme has been verified with numerous experimental and computational data (Zhang and Zheng, 2007). For example, for flow over a single oscillating cylinder, the computational results at various forcing frequencies were shown in Zheng and Zhang (2008), where both frequency lock-in and non-lock-in cases were identified using time histories and power spectra of lift and drag. Good agreements were achieved in comparison with Guilmineau and Queutey (2002), Ongoren and Rockwell (1988) and Williamson (1988), and Krishnasmoothy (2001).These examples have provided sufficient validations for the computational scheme used in our study.

In order to justify the two-dimensional flow assumption in this study, we have tested a three-dimensional simulation at $\mathrm{Re} = 100$ with a periodic boundary condition in the cylinder axial direction. We have found that the flow remains two-dimensional. We also increased the Reynolds number to 160, which is a case that was treated as two-dimensional tandem cylinders

in Papaioannou et al. (2006), and the three-dimensionality started to show. Oscillation of the downstream cylinder does not enhance the three-dimensional effect much. Therefore, it is expected that the Reynolds number for flow to become three-dimensional could be lower in a tandem cylinder system than that in a single cylinder system (where Re = 188.5, according to Williamson. 1996, with a possibility that oscillation could further reduce that Reynolds number. Considering the stabilizing and destabilizing effect of the downstream cylinder (Papaioannou et al. 2006), this Reynolds number may also vary with the separation distance between the two cylinders. Although for the purpose of this study we do not intend to determine this Reynolds number, based on our simulation this Reynolds number can possibly be below 160. And the case we study here at $\mathrm{Re} = 100$ is still within a safe range for flow to be two-dimensional, hence formation due to instability in the axial direction is not considered. However, it would be interesting to explore the difference between the 2D and 3D simulations for either a single or a tandem cylinder system for higher Reynolds number using the current scheme but in 3D version.

#### *3.3.1.3 Results and Discussion*

Complicated flow patterns in a stationary tandem cylinder system have been demonstrated in the literature, e.g., Zdravkovich (1985), Zdravkovich (1997), Tanida et al. (1973) and Sharman et al. (2005). Basically, the flow patterns can be divided into two regimes by a "critical spacing" ($S_c$). In the case of $\mathrm{Re} = 100$, the value of $S_c$ is between 3.75 and 4, according to Sharman et al. (2005). The different types of vortex streets are shown in the vorticity contours for $\mathrm{Re} = 100$ in Fig. 3-3. When $S < S_c$ ($S = 2$ in Fig. 3- 3a), the flow is in a regime called the "vortex suppression regime" (VS), in which the wakes behind both cylinders are rather weak, and there is almost no vortex shedding, neither in-between nor behind the cylinders other than a low-frequency wavy flow pattern in the wake. The downstream cylinder is

so close to the upstream one that formation of vortices is hindered. The shear layer from the upstream cylinder does not have sufficient room to form shed vortices, although there is no precise relation between the vortex formation length in the wake of a single cylinder and the critical spacing of a tandem cylinder system (Papaioannou et al. 2006). The stabilized wake (in the sense of a Hopf bifurcation (Williamson, 1996) from the upstream cylinder, due to the closeness of the downstream cylinder, further stabilizes the wake from the second cylinder so that there is no clear vortex shedding even in the wake after the downstream cylinder. When approaching the critical spacing, the vortex shedding upstream to the second cylinder (shedding between two cylinders) is intermittent. After a transient period, at $S = S_c$ ($S = 4$ in Fig. 3- 3b), a synchronized vortex street is formed eventually behind the downstream cylinder, and a sudden jump in the Strouhal number ($S_t = fD/U$) for the cylinder system occurs, although there is still no clear vortex shedding between the cylinders. It should be noted that this Strouhal number is for the entire tandem cylinder system and includes interference effects among the two cylinders and their wakes, which is not the same as that for a single cylinder. This sudden jump is indicative that the spacing is reaching the critical spacing. When $S > S_c$ ($S = 6$ in Fig. 3- 3c), the flow is in the ``vortex formation regime'' (VF), in which synchronized vortex shedding occurs and well developed vortices are shed from the upstream cylinder and re-attach themselves to the downstream one. The shedding vortices behind the first cylinder join those from the downstream cylinder to form a coupled vortex street in the wake of the tandem cylinder system.

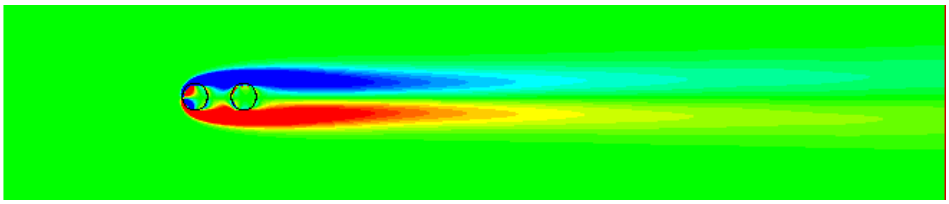

**(a)**

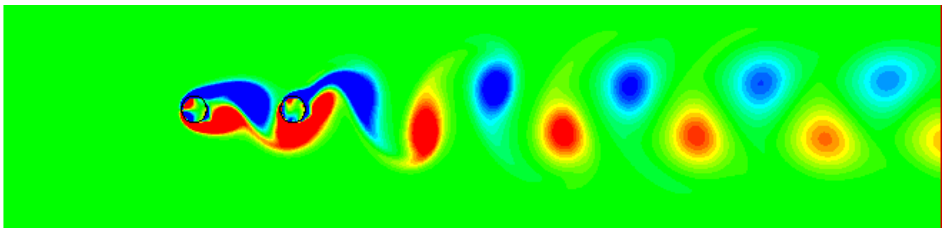

**(b)**

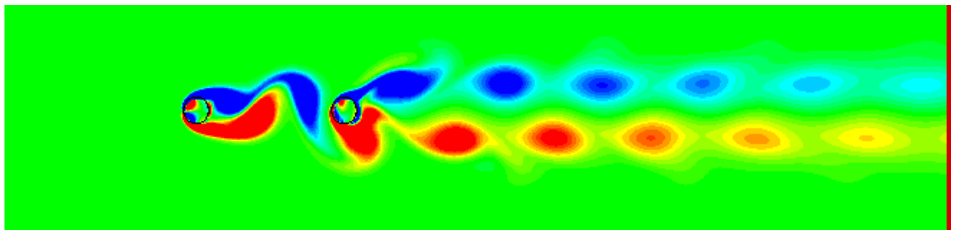

**(c)**

**Figure 3-3 Vorticity contour plot for the stationary tandem cylinders system with different spacings: (a) $S$ = 2; (b) $S$ = 4; (c) $S$ = 6.**

Figure 3-4 shows the computed Strouhal number versus the spacing distance at $\mathrm{Re} = 100$ and two other Reynolds numbers at 80 and 160 for comparison, which is used as the validation cases for the current numerical scheme. The reason to end at $\mathrm{Re} = 160$ is because of three-dimensionality at high Reynolds number flow stated in the previous section. On the other hand, at further lower Reynolds numbers, such as $\mathrm{Re} = 50$ as we tested, the flow is on the verge of being a steady state with a long wake formation length for a single cylinder case. The possible

stabilizing effect of the downstream cylinder can make the flow even more stable and therefore the VF regime is large and no vortex shedding is shown in this regime. In our computation, the Strouhal number is calculated after the periodic vortex streets are formed and the solution converges to a state that shows periodic oscillations. The average surface pressure coefficient history, during the periods after a converged solution (80 or 160 depending on the frequency resolution needed) is established, is then used for spectral analysis to determine the Strouhal number. Our $S_t$ values at $\mathrm{Re} = 100$ fit between those reported by Sharman et al. (2005) and Li et al. (1991). The sudden jump of the Strouhal number occurs at $S = 4$ in all of the three data sets. For another Reynolds number of 80, we also repeated the same procedure and obtained the critical spacing around 5.5 as shown in Fig. 3-3, which agrees well with the result by Tanida et al. (1973), but is different from the value of 3.7 reported by Li et al. (1992). One of the reasons could be the resolutions of the grid mesh. As for the single cylinder case with $\mathrm{Re} = 100$, a relatively coarse mesh was used by Li et al. (1992) that gave the value of $S_t$ as 0.166, a bit lower than the usual value of 0.17 reported in the literature. Another reason could be due to different definitions of the critical spacing. There are several different ways of determining the critical spacing in the literature. We define the critical spacing by observing the sudden increase in the Strouhal number, which is the same definition as what used by Sharman et al. (2005). In Li et al. (1992) the wake length change as an indicator of separate flow regimes was used, while in Tanida et al. (1973) the interference drag was used as the criterion.

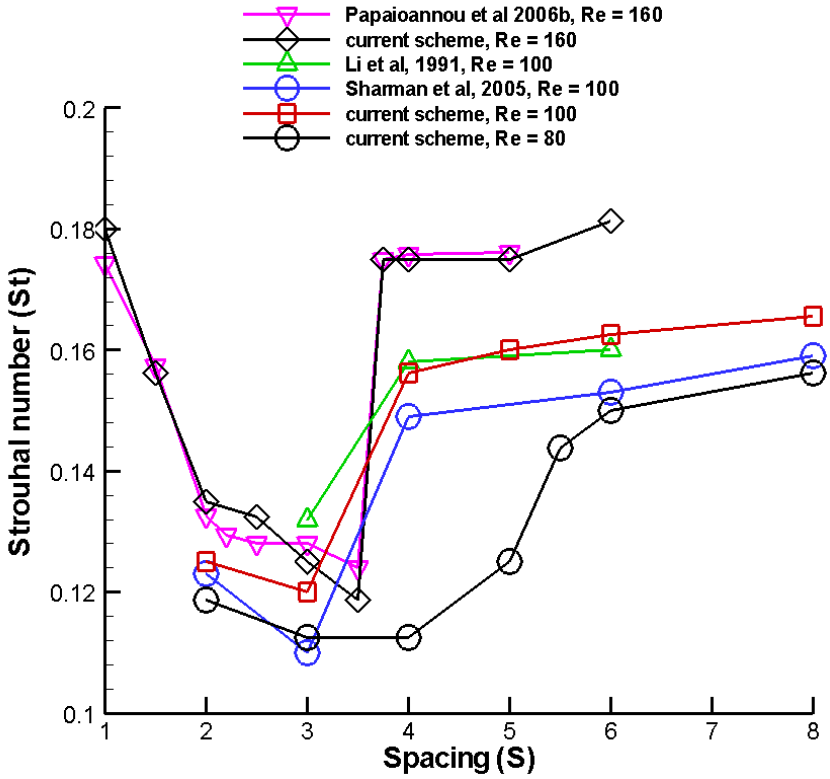


**Figure 3-4 Strouhal number comparisons for different Reynolds numbers with literatures: Re = 80, 100 and 160.**

### *3.3.1.4 Summary*

In Section 3.3.1, a modified immersed-boundary method has been applied to simulate flow over a stationary tandem cylinder system. Three flow regimes occur according to the wake development stage behind the upstream cylinder: VS, critical and VF. Each depends on the spacing distance between the two cylinders. By comparing a series of calculated Strouhal number with the cited values in the literature, the numerical scheme was validated. And it will be applied to the multi-body fluid/solid interaction problem in the following section.

### 3.3.2 Flow over a Multi-Cylinder System

Numerical simulations with an immersed-boundary method are presented for the incompressible flow past a periodic array of porous-medium cylinders. Fluid/porous-medium interactions are greatly influenced by the accuracy on the interface between the surface of the porous cylinder and the flow around it, because of the sudden change in the governing equations for the fluid and for the porous material. In order to retain the smoothness on the interface, momentum fluxes near the interface are discretized using several schemes, including the $2^{nd}$- and $3^{rd}$-order upwind schemes and the $5^{th}$-order Weighted Essentially Non-Oscillatory (WENO) scheme. These schemes are combined with a direct-forcing immersed-boundary method to remove the discontinuity between the fluid and the porous material, and thus accuracy near the interface can be improved. Low and moderate Reynolds number flows, both outside and inside the porous cylinders, are computed simultaneously by solving a combined governing equation set for incompressible flow. The simulation is first validated using flow over an array of impermeable cylinders. The advantage of high-order schemes is then investigated by looking at the flow parameters near the interfaces between the porous cylinders and the outside flow. Species transport in flow with the porous-cylinder-array configuration is also studied.

#### *3.3.2.1 Introduction*

Flow past cylinders has been extensively investigated for decades. This fundamental problem can be applied to various industrial structures, such as off-shore constructions, heat exchangers, etc. Both experimental and numerical methods were used to study this problem. Different flow Reynolds numbers and cylinder shapes and their arrangements have been tested for various objectives. The reviews of flow over a single circular cylinder can be found in Williamson (1996) and Zdravkovich (1997). To study multi-body fluid/solid interactions, tandem

cylinder configurations have been studied (e.g. Papaioannou 2006a, 2006b, and Yang and Zheng, 2010). Staggered cylinder bundles draw some attentions in recent years, as the complicated structures are challenging to simulate fluid/structure interactions (FSI). Rollet-Miet et al. (1999) used Large Eddy Simulation (LES) to study turbulent flow past a cylinder bank. The instantaneous flow field and Reynolds stress components were calculated. For fluid flowing through porous materials, multiple-cylinder structures can be viewed as a Representative Elementary Volume (REV) to study the fluid flow in micro-scales. In Kuwahara et al. (1998, 2006), a square cylinder REV was used to study the macroscopic fluid transport phenomena from the microscopic approach in a range of Reynolds numbers and porosities. LES was also applied for high Reynolds number cases in that study. The correlation between the pressure gradient and the porous properties was analyzed and compared to the macroscopic analytical solution. The good agreement in the comparison proved the validity of using the REV approach to study flow in porous media. Other works in the literature studied the cylinder bundle problem for either heat exchangers or porous media, including Pedras et al. (2001), Roychowdhury et al. (2002), Nakayama et al. (2004), Moulinec et al. (2004), Liang and Papadakis (2007) and Teruel et al. (2007, 2009 a, b, c).

While the staggered cylinder array has been confirmed to be an acceptable REV structure to study flow through porous media in the literature, the cylinders in their study were impermeable and treated as solid bodies. To simulate porous materials composed pellets, the porous effect in even smaller scales need to be included. For that purpose, in this study, we further model the cylinders as a porous medium with smaller pores. This concept of using the same REV with and without the porous model is illustrated in Fig. 3-1. The Darcy or extended Darcy type models can be used as the governing equations in the porous area. In the literature,

even the list of studies of flow past a single porous cylinder is much shorter than that for a solid cylinder. For example, Bhattacharyya et al. (2006) investigated numerically the flow through and around a porous cylinder, and compared the drag coefficient with the experimental data in flow of a low Reynolds number range ($Re$ = 1 - 40). Another example is Chen et al. (2008, 2009) who studied the flow past a porous square/trapezoidal cylinder with different Reynolds numbers, Darcy numbers, and porosities. Wilson et al. (2006, 2007) applied a simplified and modified porous model, the Zwikker-Kosten (ZK) equation (Zwikker and Kosten, 1949), for time-domain modeling of sound propagation with a porous surface. Recently Xu et al. (2010) used the immersed-boundary (IB) method and the ZK equation to study the effect on wind noise reduction of porous windscreens of measurement microphones under different frequencies of incoming wind turbulence. In the current study, we extended the application of the ZK equation to a periodic array of porous cylinders to study momentum transport. We also developed a porous-medium model to calculate mass transport through the array.

The presence of porous media introduces a sudden change (or a discontinuity due to the phase change from bulk fluid to porous media) at the fluid/porous interface and also affects the numerical stability. Under these circumstances, most conventional finite difference schemes are challenged when used around the interfaces. The accuracy at the interface between the fluid flow and the porous medium is a key issue in simulating such problems (James and Davis, 2001; Goyeau et al. 2003). There have been two types of methods to overcome this discontinuity. One is to apply a stress-jump condition between the two media (Ochoa-Tapia and Whitaker, 1995 a, b). In this method, the adjustable parameters that account for the stress jump are critical and problem dependent. Another effective way is to apply higher-order schemes including the 2$^{nd}$- and 3$^{rd}$-order upwind schemes and the 5$^{th}$-order Weighted Essentially Non-Oscillatory (WENO)

scheme (Harten et al. 1987; Shu and Osher, 1988, 1989). High-order schemes have been used in simulation for viscous flow around steady and moving solid bodies (Cho et al. 2007). Also in Xu et al. (2010), several high-order schemes were applied on the interfaces between the screened microphone and the outside flow and achieved very promising results.

In the following sections, first, the computational schemes were validated by using the solid cylinder REV cases in comparison with the results from a commercial flow solver. Second, flow in the same REV but with the porous model for permeable cylinders is simulated. Different numerical schemes are tested on the fluid/porous interfaces. Then, species transport in the porous medium is studied; and finally conclusions are made.

#### *3.3.2.2 Numerical Schemes*

The geometry for both solid and porous REV is shown in Fig. 3-5 with a periodic array of circular cylinders. In the solid unit, all the cylinders are considered to be impermeable, while in the porous unit, the cylinders are porous. The geometry is determined by two lengths of the unit: the diameter of the cylinder (*D*) and the distance (*H*) between the adjacent centers of two cylinders. With this REV unit, the computational domain, including all the related boundary conditions, ensures the periodicity of flow in both the x- and y-directions. Under most circumstances of interest, flow inside porous media is of low speed, therefore laminar, low Reynolds number flows are considered in this study, where $\mathrm{Re} = \rho UD/\mu$, is based on the fluid density $\rho$, viscosity $\mu$, cylinder diameter *D*, and the incoming stream velocity *U*. For the arrangement of the REV in this study, the porosity for the large structure (not inside the cylinder), defined as $\phi = 1-(D/H)^2$, is selected as 0.61.

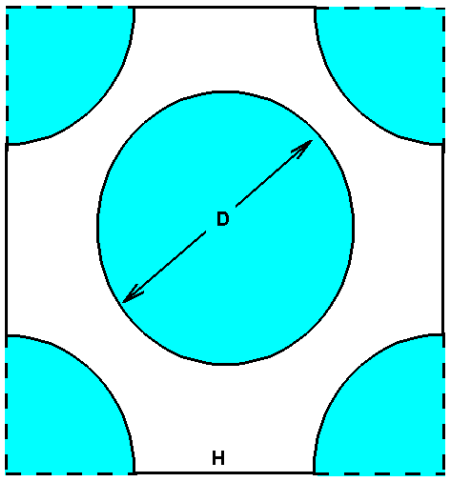


**Figure 3-5 Computational domain of the unit structure.**

The concept of immersed-boundary method (IBM) is to implement a defined forcing term in the momentum transport equations in the vicinity of the solid boundary. It has been successfully used to study various fluid-structure interaction (FSI) problems. The advantages of using IB methods are primarily: 1) only simple Cartesian grid is needed; 2) no moving grid is required to simulate an object in motion; and 3) the shape/arrangement of the objects can be arbitrary. A review of the IB methods can be found in Mittal and Iaccarino (2005). In the current study, a modified immersed-boundary method with a direct compensation forcing term is used to compute the fluid flow. This computational algorithm has been verified using numerous sets of data in the literature on flow over cylinders and spheres (Zhang and Zheng, 2007). The non-dimensional governing equations for the mass and momentum conservations (characterized by the incoming fluid velocity $U$ and the density $\rho$) for incompressible flow are expressed as:

$$\nabla \cdot \mathbf{u} = 0\,, \tag{3.28}$$

and

$$\frac{\partial \mathbf{u}}{\partial t} + \mathbf{u} \cdot \nabla \mathbf{u} = -\nabla p + \frac{1}{Re} \nabla^2 \mathbf{u} + \mathbf{f} \ , \tag{3.29}$$

where *Re* is the Reynolds number and **f** is the body force representing the virtual boundary or the porous medium effect, which will be defined later.

To include the porous medium effect, Darcy's law has been widely used to simulate the pressure loss ($\nabla p$) in the porous medium. Assuming an isotropic medium, Darcy's equation can be written as:

$$\nabla p = -\frac{\mu}{K} \mathbf{u} \, , \tag{3.30}$$

where $\mu$ is the viscosity and *K* is the permeability.

There are several extended formats of Eq. (3.30). The Zwikker-Kosten (ZK) model has been used previously for numerical calculations of linear sound propagations in porous media (Wilson et al. 2006; Xu et al. 2010). A modified version of the ZK equation can be written as:

$$\frac{\partial \mathbf{u}}{\partial t} + \mathbf{u} \cdot \nabla \mathbf{u} = -\nabla p + \frac{1}{\mathrm{Re}} \nabla^2 \mathbf{u} - \sigma \mathbf{u} \, , \tag{3.31}$$

where $\sigma$ is the dimensionless flow resistivity of the porous medium (non-dimensionalized by $\rho U/D$).

It is obvious that Eqs. (3.29) and (3.31) have similar format except for the additional source terms on the right-hand side. Hence in this study, inside the porous medium, a ZK type of source term is applied as the replacement of the forcing term in Eq. (3.29). The forcing term in the two equations can thus be combined as:

$$\mathbf{f} = \begin{cases} 0 & \text{outside porous medium} \\ -\sigma \mathbf{u} & \text{inside porous medium} \end{cases} . \tag{3.32}$$

After a periodically stable flow field has been obtained, a species transport equation for a passive scalar is solved. Similar to the momentum equation in a porous medium, a sink term is added in the species transport equation representing the adsorptive effect of the porous cylinders. Thus the species transport equation can be expressed as:

$$\frac{\partial C}{\partial t} + \mathbf{u} \cdot \nabla C = D_c \nabla^2 C + S_c \,, \tag{3.33}$$

where $C$ is the specie concentration, $D_c$ is the species diffusion coefficient, and, $S_c$ the additional sink term.

The simple linearized sink term can be modeled as:

$$S_c = \begin{cases} 0 & \text{outside the porous medium} \\ -\alpha(C - C_{in}) & \text{inside the porous medium} \end{cases}, \tag{3.34}$$

where $\alpha$ is the adsorption coefficient and $C_{in}$ is the final saturated concentration value of the species.

The momentum and species transport equations are solved using finite difference schemes on a staggered Cartesian grid. A semi-implicit scheme with 2nd-order spatial differencing is used for the diffusion terms, with the normal direction diffusion terms using the Crank-Nicholson scheme. The convection terms in both momentum and species transport equations will be discussed later using different orders of schemes. The incompressibility condition is satisfied by solving a Poisson equation for pressure correction using FISHPACK (Swarztrauber and Sweet, 1979). The overall accuracy of the scheme is able to reach the second order in space. More detailed explanations on the IB solver can be found in Zhang and Zheng (2007).

As shown in Fig. 3-5, there are multiple fluid/porous interfaces in the REV unit. As stated previously, the sudden change between the fluid and the porous medium decreases simulation accuracy. To improve the accuracy near the interfaces, higher-order finite difference schemes are considered. The schemes tested here include the 2nd- and 3rd-order upwind schemes and the 5th-order WENO scheme.

Upwind schemes use an adaptive finite difference stencil to numerically simulate the direction of propagation of information. The 1st-order upwind scheme is too dissipative. Thus, our investigation includes 2nd-order upwind scheme, 3rd-order upwind scheme and 5th-order WENO scheme. The numerical details and the discretizations of those schemes can be found in Section 3.2.3.

To produce the periodicity in this unit with a length $L$, periodic boundary conditions have to be enforced in both streamwise and spanwise directions (Patankar et al. 1977) respectively as:

$$u(0, j) = u(L, j), \quad v(0, j) = v(L, j), \quad p(0, j) = p(L, j) + \Delta p, \tag{3.35}$$

and

$$u(i,0) = u(i, L), \quad v(i,0) = v(i, L), \quad p(i,0) = p(i, L). \tag{3.36}$$

For the species transport, the boundary condition at the inlet is chosen to be uniform. The top and bottom boundaries are symmetry, and at the outlet the normal derivatives are zero.

After the grid-size independence check, the grid size, with $dx = dy = 0.00625$, has been chosen for a uniform Cartesian grid. The stability criterion is no more restrictive than that of an explicit scheme for a two-dimensional convection-diffusion equation as stated in Eq. (3.10).

#### *3.3.2.3 Results and Discussion*

We test several different orders of numerical schemes, and the final selection will go to the scheme which shows the best results among all the cases. We first validate the high-order schemes by comparing the solid cylinder bundle results with the ones calculated using a commercial solver. Second, the porous cylinder unit cases are presented to emphasize the importance of using higher-order schemes. Finally, the results from the species transport will be discussed.

For the solid cylinder cases, the fluid/solid interaction problem in this unique structure is already interesting and is selected to be the validation case before the porous model is involved. By using a commercial CFD solver, the boundary conditions are kept the same as in the IBM simulation, including the periodicity and the pressure drop in the streamwise direction. Also the grid resolution is the same between the two simulations. The $2^{nd}$-order upwind scheme is used to discretize the convection terms in the commercial solver. The results in Fig. 3-6(a) and Fig. 3-6(b) visually show that the velocity field obtained from the IBM simulation using the $5^{th}$–order WENO scheme and that from the commercial solver look very similar to each other (as the contour scale and levels are kept the same). Higher velocity appears in the narrow channel-like space between the neighbor cylinders. The periodic flow pattern is well represented. Although not shown here, the plots from other schemes look the same as the two shown here.

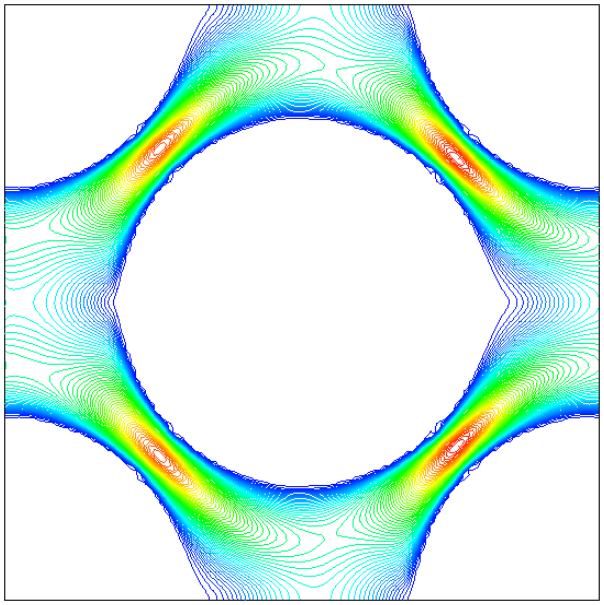

**(a)**

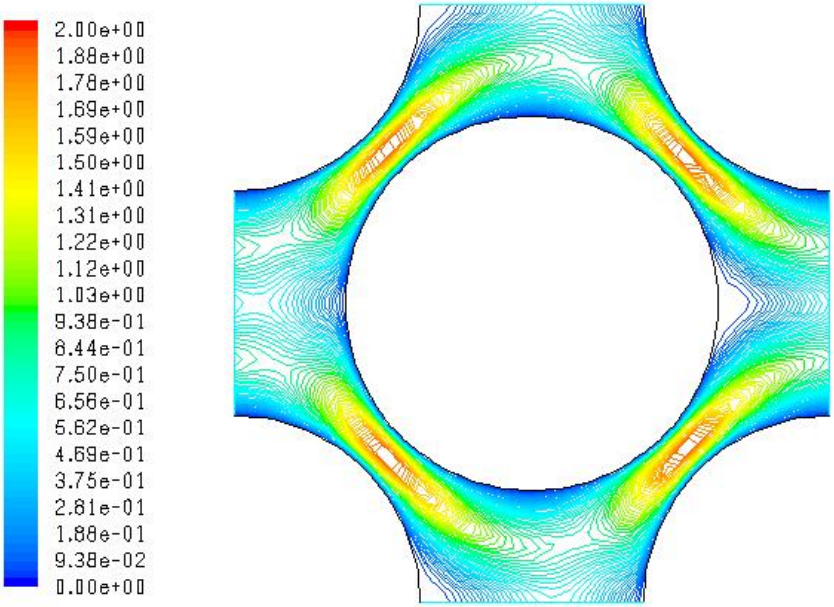


**(b)**

**Figure 3-6 Solid cylinders unit: velocity magnitude contour plot (a) 5$^{th}$-order WENO scheme in IBM; (b) FLUENT simulation (the color range and levels are the same for both cases).**

To obtain more strict quantitative comparisons for the results, we select three locations for velocity profile comparisons: the outlet boundary, the top boundary, and along a line in the x-direction which is 1/4 D distance from the bottom of the domain. Results from different schemes are displayed in Fig. 3-7 and compared with the commercial solver results. In all the locations, the results from 3rd-order upwind scheme and the 5th-order WENO scheme are very close to the commercial solver results, while the results from the two 2nd-order schemes are not. The 2nd-order central difference scheme seems to be the least accurate. We thus decide that the 2nd-order schemes are not the right option even for the solid cylinder case. The 3rd-order upwind and the 5th-order WENO schemes can be the candidates, with the latter showing the best result.

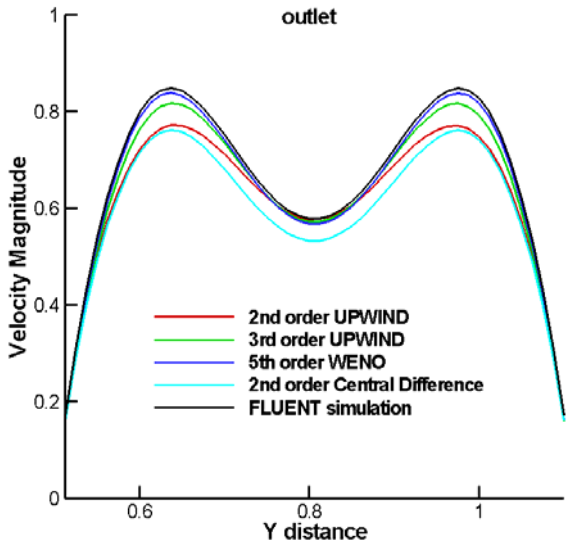


**(a) outlet**

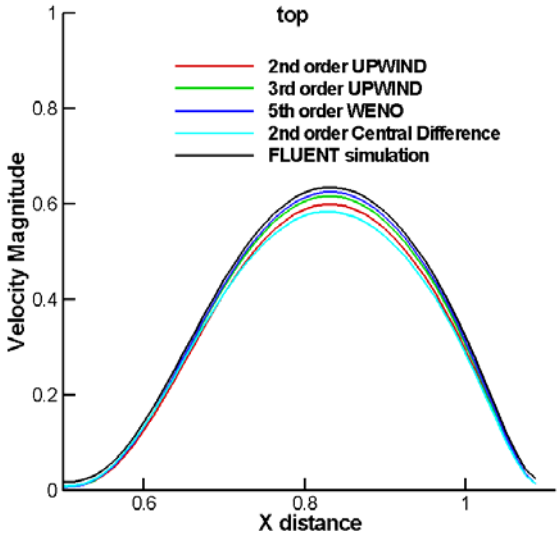


**(b) top**

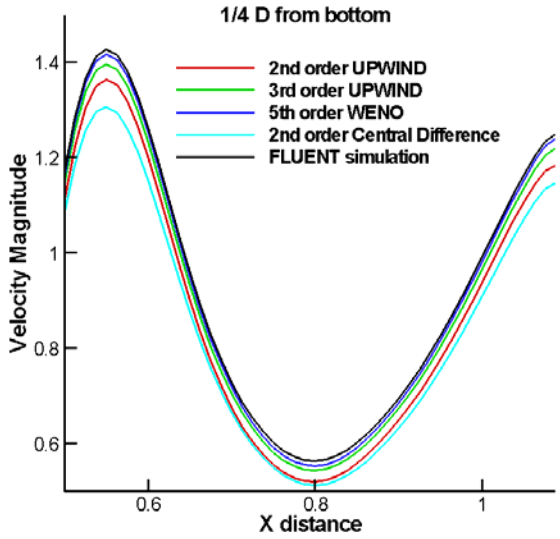


**(c) bottom**

**Figure 3-7 Solid cylinders unit: velocity profiles comparison between high-order schemes in IBM and FLUENT simulation at three different locations (a) at the outlet; (b) at the top boundary; (c) 1/4 D from the bottom boundary.**

As mentioned in Section 3.3.2.1, the periodic array of solid cylinders is viewed as a representative elementary volume (REV) in a porous medium. The simulation of the flow passing the REV can be used as a microscopic representation of flow in the porous medium in order to estimate the macroscopic properties of the porous medium flow. In a macroscopic (or bulk) simulation, the pressure drop is frequently used as the parameter indicating the porous medium behavior. There is the Blake-Kozeny equation (Bird et al. 2002) which relates the pressure drop to the bulk porous medium properties, such as pore size and void fraction. This relationship should also be valid in the micro-scale REV. To demonstrate that point, a series of numerical simulations are performed for a range of porosities ($\phi$). We then process the microscopic numerical results to compare with the Ergun equation.

The porosity is ranging from 0.5 to 0.8 approximately. Thus the arrangement will be different for each porosity case and the flow field will be changed (see Fig. 3-8). Since in this study, we concentrate on the low Reynolds number flow in the porous medium, the modified Darcy's law for the laminar flow regime (in the streamwise direction) is in the following format (without the Forchheimer term for turbulent flow, recalled from Eq. 3.30):

$$\frac{dp}{dx} = -\frac{\mu}{K}u\,, \tag{3.37}$$

where $\mu$ is the flow viscosity (0.01 in this case for $\mathrm{Re} = 100$, $\rho = 1$) and $K$ is the permeability, which needs to be determined.

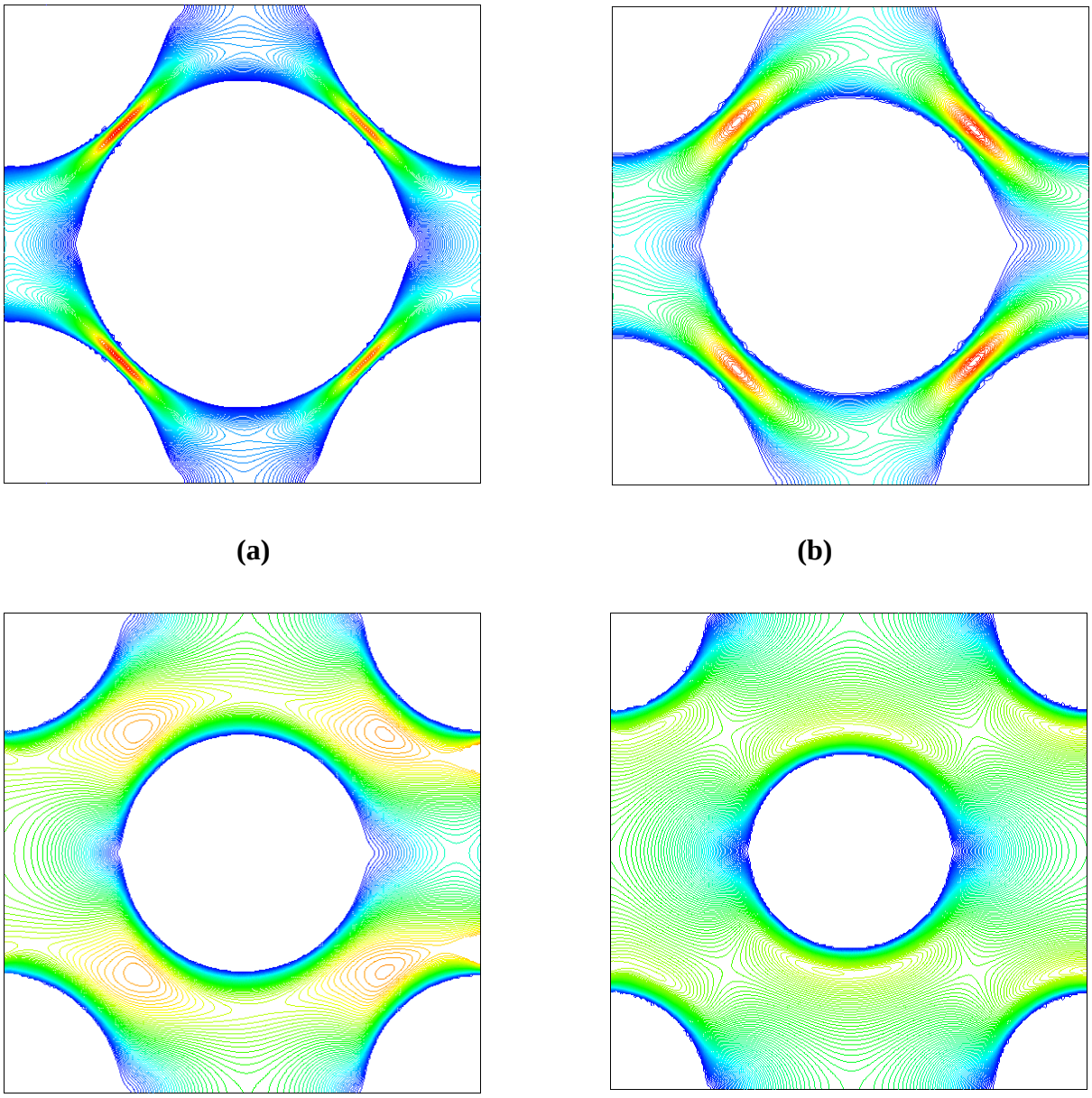

**(a)** **(b)**

**(c)** **(d)**

**Figure 3-8 Solid cylinders unit with different porosities $\phi$ (arrangements): (a) $\phi = 0.54$; (b) $\phi = 0.61$; (c) $\phi = 0.75$; (d) $\phi = 0.83$.**

To determine the pressure drop (pressure gradient) in this study, the dimensionless pressure difference between the inlet and the outlet could be calculated as (Kuwahara et al. 1998):

$$\frac{dp}{dx} = -\frac{1}{H-D}\int_{D/2}^{H-D/2}(p|_{x=0} - p|_{x=H})dy \quad . \tag{3.38}$$

The porosities and related pressure gradient calculation results are summarized in Table 3-1.

| $\phi$ | $(1-\phi)^2/\phi^3$ | $-dp/dx$ |
|---|---|---|
| 0.54 | 1.3 | 1.82 |
| 0.61 | 0.67 | 1.04 |
| 0.75 | 0.15 | 0.21 |
| 0.83 | 0.054 | 0.051 |

**Table 3-1 The relationship between the porosity and the pressure gradient.**

A coefficient of the correlation from current simulations between the dimensionless pressure gradient and $(1-\phi)^2/\phi^3$ is around 142.8 (1.428/0.01, 0.01 is the viscosity $\mu$ since Re = 100), which is very close to 144 for circular rods in Kuwahara et al. (1998). Therefore, for laminar flow going through this solid structural unit (a periodic array of impermeable cylinders), the pressure drop can be correlated with the porosity as:

$$-\frac{dp}{dx} = \frac{142.8\mu(1-\phi)^2}{\phi^3 D^2}u \, . \tag{3.39}$$

This relationship is plotted in Fig. 3-9. Equation (3.39) is very close to the empirical expression of the Blake-Kozeny equation (Bird et al. 2002), which is:

$$-\frac{dp}{dx} = \frac{150\mu(1-\phi)^2}{\phi^3 D^2}u \,. \tag{3.40}$$

The only difference is the coefficient. Also this coefficient is dependent on the shape of the solid obstacle in the unit.

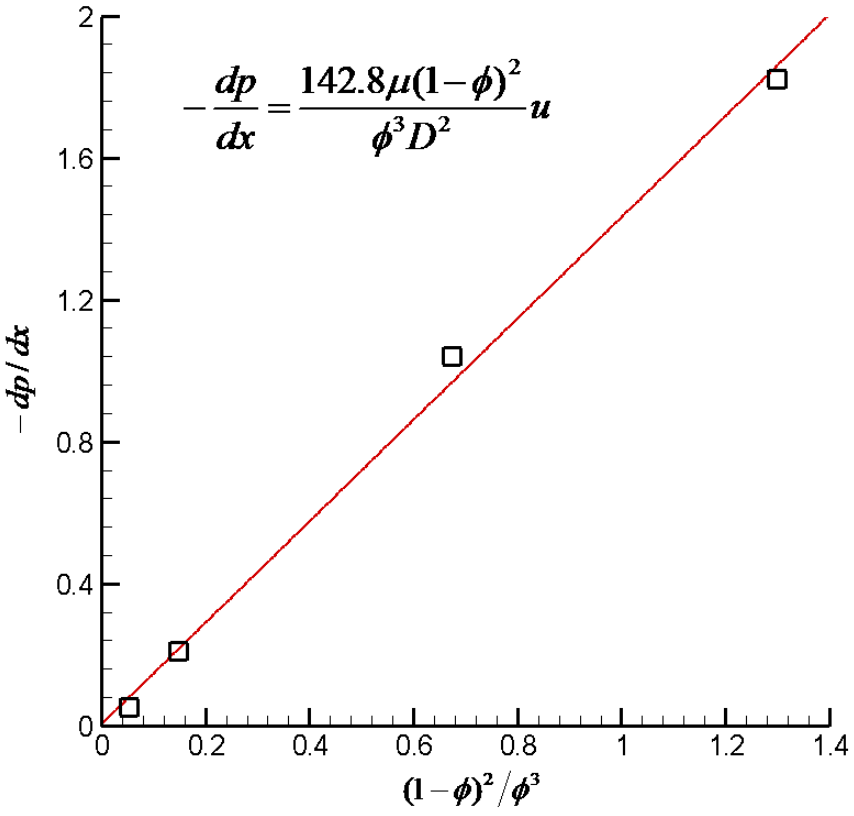


**Figure 3-9 Effect of porosity on pressure gradient.**

By using the modified ZK equation (Eq. 3.31) inside the cylinders, flow through porous cylinders can be simulated. A range of flow resistivity values, $\sigma$, have been chosen from 0.01 to 10000 indicating different levels of the porous effect. When the flow resistivity is small, the cylinders are very permeable, and when it is big, they can be treated almost like solid bodies. Hence, if the resistivity is 10000, the flow field should be similar to that of the solid case. This can be demonstrated in Fig. 3-10 where velocity magnitudes in three locations are plotted by using different orders of schemes. The results from the solid case are used as a benchmark solution for comparisons. The results of the 2nd–order upwind scheme appear to be a lot different from the results by using other schemes, especially in the bottom location where there are wiggles near the inlet, indicating highly unstable numerical results. The results obtained from 3rd-order upwind scheme and the 5th-order WENO schemes are close to each other. The high resistivity results show again that the 2nd-order upwind scheme should not be used. Since the interface behavior is the key issue in the fluid/porous interaction study, the surface pressure coefficient ($C_p$) distribution is used as the parameter for comparison.

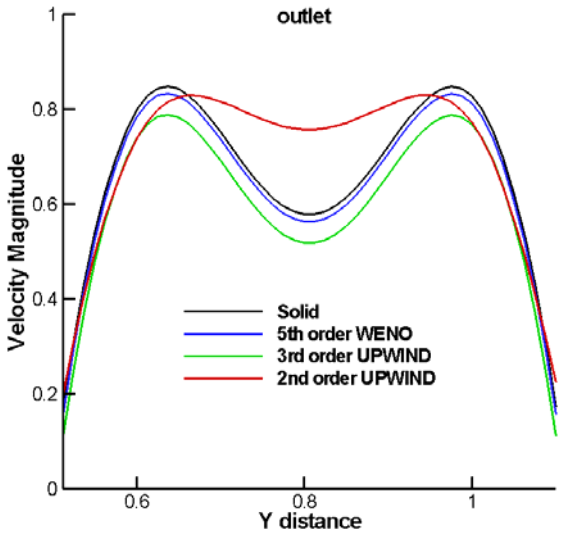


**(a) outlet**

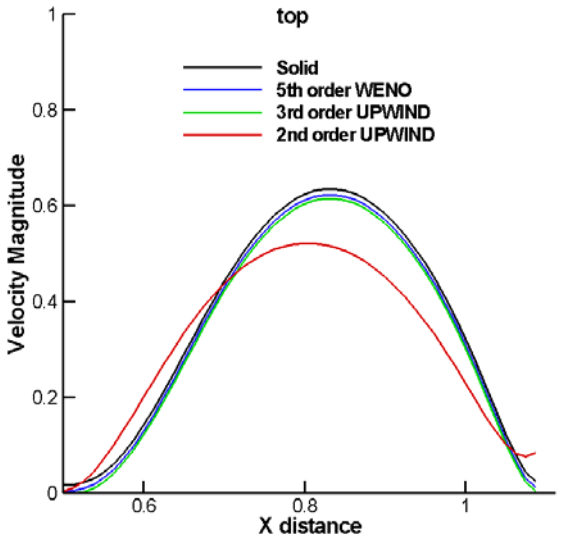


**(b) top**

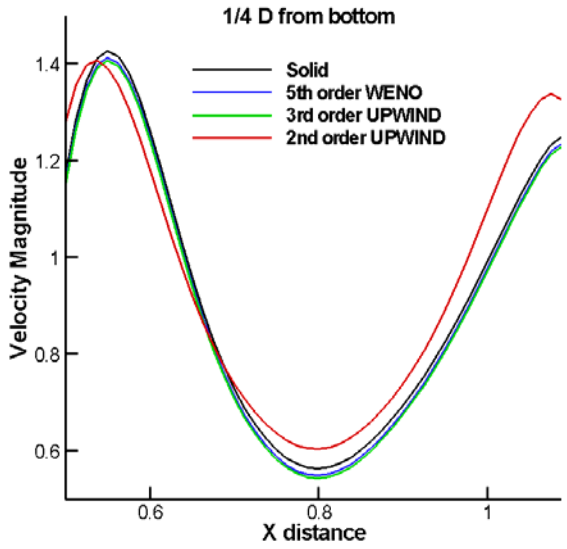


**(c) bottom**

**Figure 3-10 Porous cylinders unit: $\sigma = 10000$, velocity profiles comparison between different schemes at three locations (a) at the outlet; (b) at the top boundary; (c) 1/4 D from the bottom boundary.**

Figure 3-11 compares the $C_p$ for the high-resistivity case around the center cylinder using different schemes along the solid cylinder case. The same conclusion is obtained from the results as that for the velocity profiles in Fig. 3-10 as discussed above.

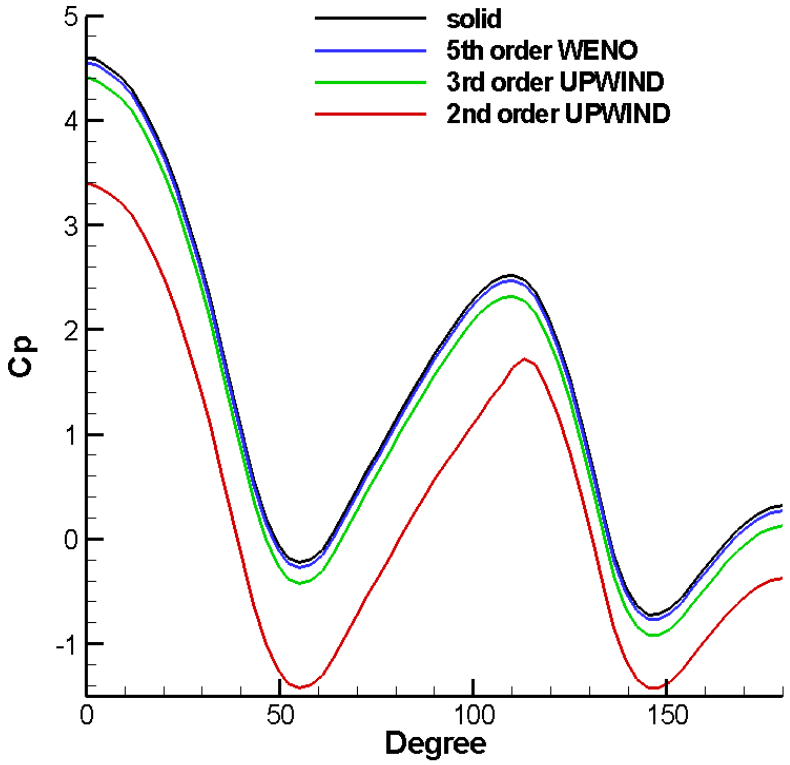


**Figure 3-11 Porous cylinders unit: $\sigma = 10000$, pressure coefficient comparison on the surface of the central cylinder.**

In the porous cylinder cases, when the flow resistivity is getting smaller, which means that the cylinders become more permeable, the differences between high-order schemes are more easily distinguished. In Fig. 3-12, the resistivity is 0.1, much smaller than the almost-solid case with $\sigma = 10000$. In the results from the 3$^{rd}$–order upwind scheme, due to the numerical errors around the fluid/porous interfaces, the structures of the cylinders are almost indiscernible (Fig. 3-12a), which means the accuracy on the fluid/porous interfaces is not sufficient to resolve the

boundaries. On the other hand, in Fig. 3-12(b) for the results of the 5$^{th}$–order WENO scheme, the interfaces between the fluid and the porous cylinders are clearly shown, and the periodicity of the flow is well captured. Therefore, after all those tests, the 5$^{th}$-order WENO scheme has been proved to be the one with the most accurate result. The above mentioned tests are summarized in Table 3-2.

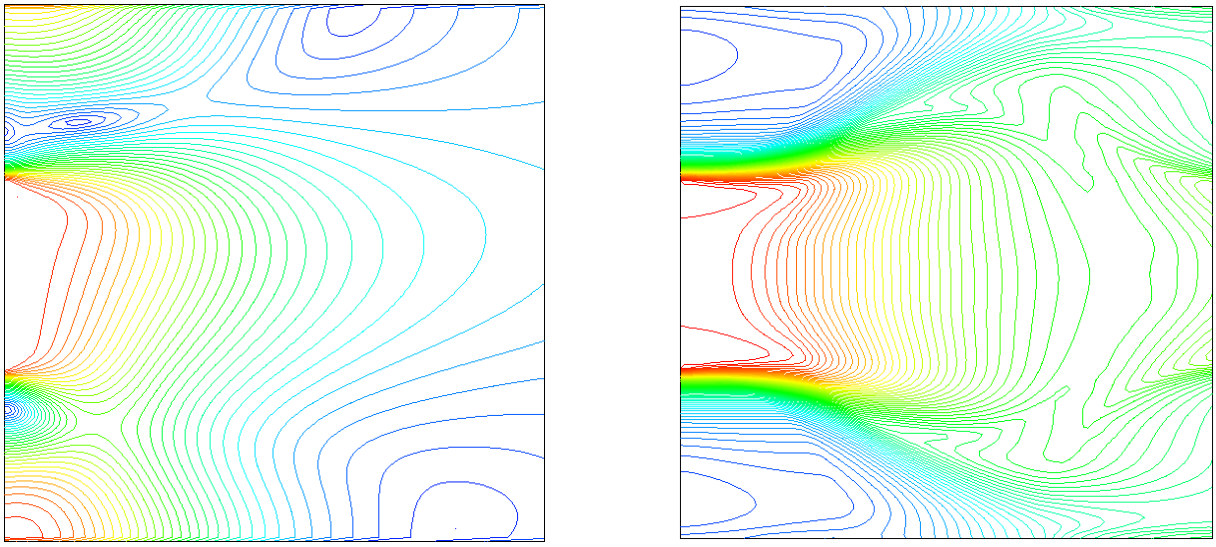

**(a)** **(b)**

**Figure 3-12 Porous cylinders unit: $\sigma = 0.1$, velocity magnitude contour plot: (a) 3$^{rd}$-order upwind scheme; (b) 5$^{th}$-order WENO scheme.**

| | **Solid** | $\sigma = 10000$ | $\sigma = 0.1$ |
|---|---|---|---|
| **2nd-order central difference** | **X** | **X** | **X** |
| **2nd-order upwind** | √ | **X** | **X** |
| **3rd-order upwind** | √ | √ | **X** |
| **5th-order WENO** | √ | √ | √ |

**Table 3-2 Summary of the numerical schemes used for testing (X – not good; √ -- good).**

Since 5th-order WENO scheme has been proved to be the most accurate scheme for both the solid and the porous cases, a complete series of cases with different flow resistivities is shown in Fig. 3-13. It is apparent that with smaller resistivities, it becomes easier for the flow to penetrate the fluid/porous interfaces, which is physically reasonable. On the other hand, for very high resistivities, it turns to be very close to be impermeable. Also by looking at those interfaces, no wiggles or highly dissipative results are noticed indicating the stability of the numerical scheme, which has been confirmed with the quantitative results previously.

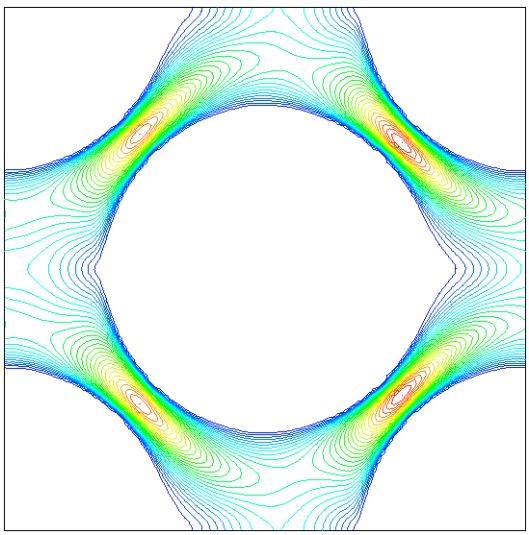

**(a)**

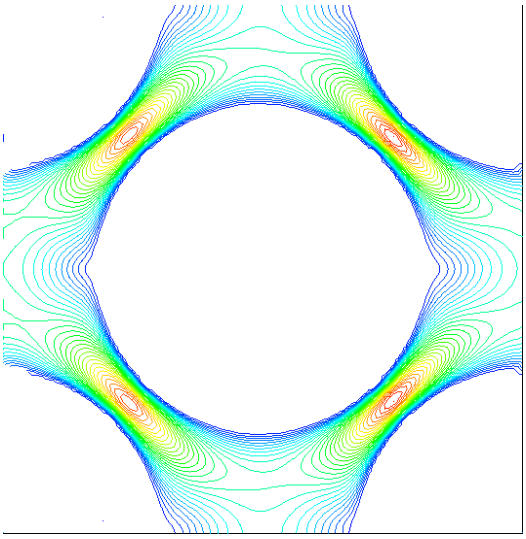

**(b)**

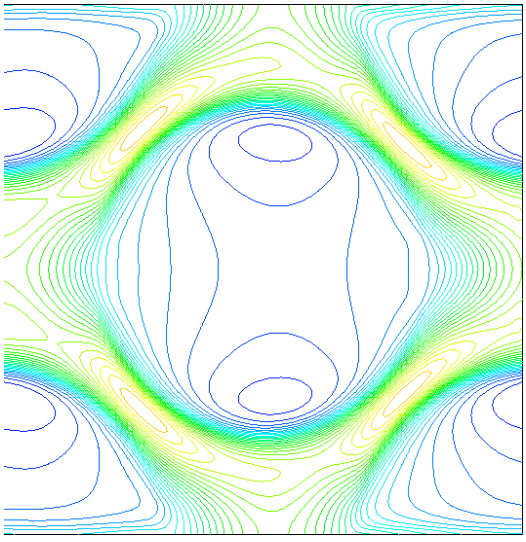

**(c)**

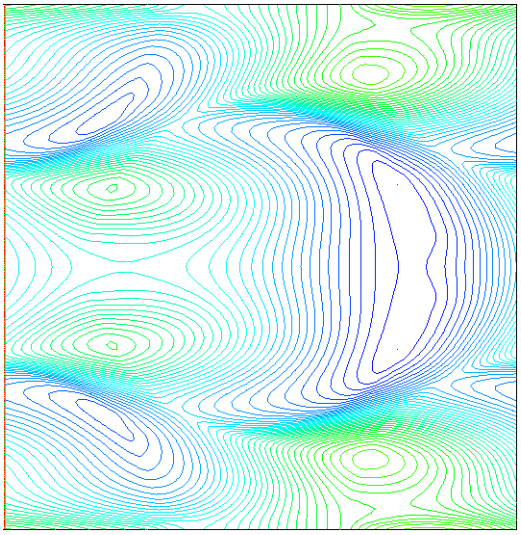

**(d)**

**Figure 3-13 The solid/porous cylinder units simulated by using 5$^{th}$-order WENO scheme with different flow resistivities: (a) solid; (b) $\sigma = 10000$; (c) $\sigma = 10$; (d) $\sigma = 0.01$.**

After obtaining good results from the flow field for both solid and porous cylinder arrays, the species transport equation is then solved with the 5th-order WENO scheme using the solved flow field. As in Eq. (3.34), the porous model for the species sink term is only applied inside the porous cylinders. In the species transport equation, Eq. (3.33), the species diffusion coefficient, $D_C$, is selected as 0.001 for testing purposes. For the porous model in Eq. (3.34), the adsorption coefficient varies from 0.01 to 10000 to test its effect on species transport. In Fig. 3-14, contours of species concentration are displayed with different adsorption coefficient values. It shows for higher adsorption coefficient, the species concentration in between cylinders is higher, while for lower adsorption coefficient, the surface diffusion is more significant and there exist higher concentrations of species inside the cylinders.

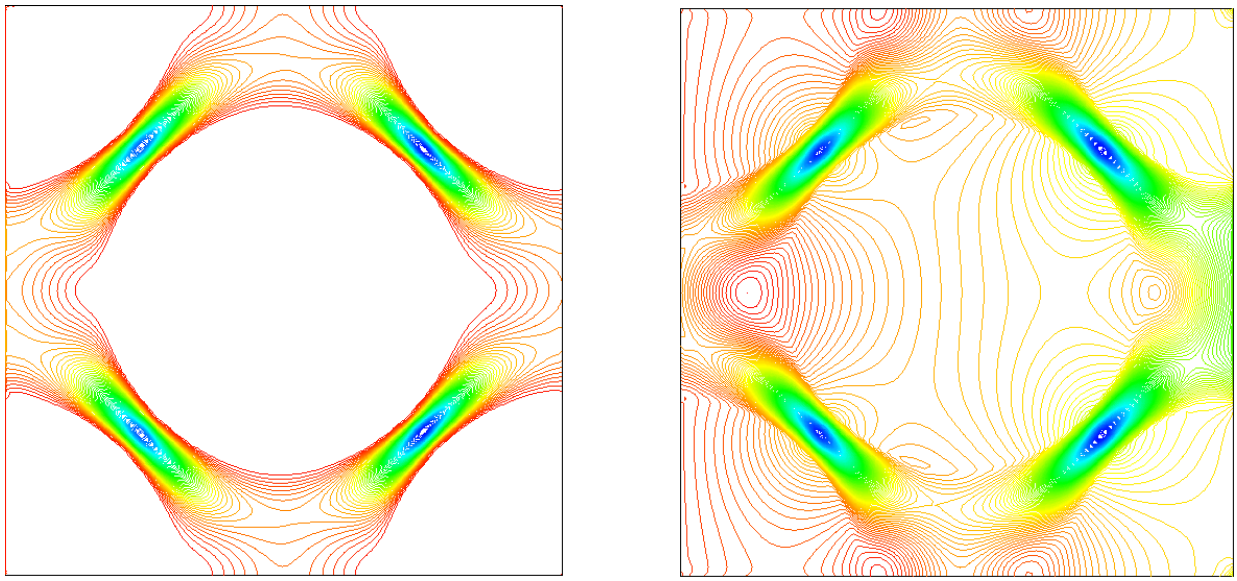

**(a)** **(b)**

**Figure 3-14 Species transport in the porous cylinder array with different adsorption coefficients: (a)** $\alpha = 10000$**; (b)** $\alpha = 1$**.**

In a similar way that we found the correlation between the porosity ($\phi$) and the pressure gradient ($dp/dx$) in the solid cylinder bundle system, in the porous case, a relationship between the adsorption coefficient ($\alpha$) and the concentration change between the inlet and outlet ($\Delta C$) is also anticipated. However, there has not been any empirical correlation for this problem like the Blake-Kozeny equation for the momentum transport. To calculate the concentration change along the flow direction, an analogy of Eq. (3.38) is expressed as:

$$\Delta C = -\frac{1}{H-D}\int_{D/2}^{H-D/2}(C\big|_{x=0} - C\big|_{x=H})dy\,. \tag{3.41}$$

To test the adsorption coefficient effect, a series of simulations of different $\alpha$ (0.01, 0.1, 1, 10, 100, 10000) are carried out with the same porous cylinder REV at $\phi = 0.609375$. Figure 3-15 plots the calculated concentration change correlated with adsorption coefficient. When the adsorption coefficient increases, the concentration change becomes less since there is less mass adsorbed into the porous cylinders. However, the decrease of the concentration change does not linearly change with the adsorption coefficient.

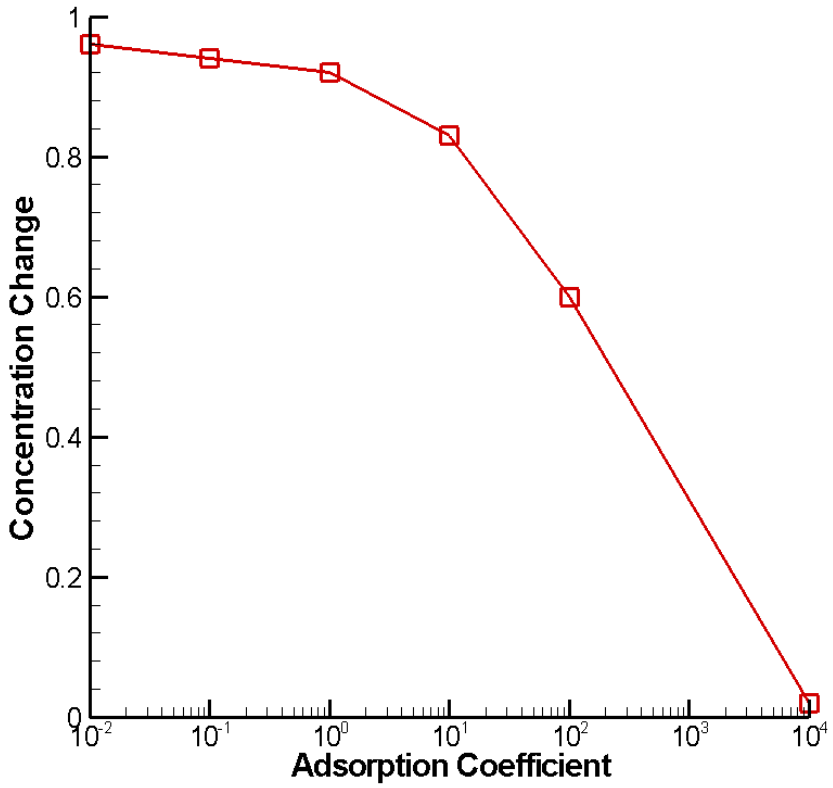


**Figure 3-15 Effect of adsorption coefficient on concentration change.**

### *3.3.2.4 Summary*

Section 3.3.2 presented a series of results from the numerical simulations for flow past a periodic array of both solid and porous cylinders. To maintain numerical accuracy on the interfaces between fluid and solid or porous cylinders, different orders of numerical schemes have been tested to discretize the momentum flux including the 2$^{nd}$- and 3$^{rd}$- order upwind schemes and the 5$^{th}$-order WENO scheme. By using an REV representing an array of impermeable solid cylinders, the present models with different high-order schemes are validated showing the 5$^{th}$-order WENO schemes is the most accurate scheme. The solid-cylinder REV

results are used to compare with the Blake-Kozeny equation for the bulk porous medium behavior. The results from the porous cylinders arrays with a range of flow resistivities showed that the $5^{th}$-order WENO scheme behaves the best from all the tests. The WENO scheme is then used to calculate the species transport with porous cylinder arrays. The results show that for the same geometric arrangement of the cylinder array and same species, the concentration distribution of the species is influenced by the adsorption coefficient of the porous cylinders. The concentration change between the inlet and outlet decreases with the increase of the adsorption coefficient.

## 3.4 Summary of the Micro-Scale Simulation

In the micro-scale simulation, the flow/species transport through a group of porous material pellets was investigated. The fluid/solid and fluid/porous interactions were the most interesting problems. A modified immersed-boundary method along with a Zwikker-Kosten porous model and several high-order discretization schemes were applied to different cases and setups. The simulation results from our investigation have led to the following conclusions:

1. For the multi-body fluid/solid interaction study: uniform flow passing a tandem cylinder system
    - A modified direct-forcing immersed-boundary method was successfully applied to a tandem-cylinder system for low Reynolds number.
    - When the calculated values of the Strouhal number is compared to the experimental values in the literature, the agreement between the values exists for a range of Reynolds numbers. Thus, the numerical scheme has been validated.
    - The spacing between the tandem cylinders was found to play an important role in formatting the vortex shedding patterns and the flow regimes.

2. For the multi-body fluid/solid and fluid/porous interaction study: uniform flow passing a periodic array of circular cylinders

    - A modified immersed-boundary method was applied to simulate flow/species passing a periodic array of solid/porous cylinders.
    - The high-order schemes include $2^{nd}$-order upwind, $3^{rd}$-order upwind and $5^{th}$-order WENO schemes that have been tested on the interfaces of fluid/solid and fluid/porous phases to smooth the discontinuity. In the porous cases, the $5^{th}$-order WENO scheme was found to be the most accurate.
    - In the solid cylinders array, the numerical scheme was validated when the results for velocity profiles at different locations were compared to the ones obtained from commercial CFD software.
    - In the solid cylinders array, the macroscopic pressure-porosity relationship (Blake-Kozeny equation) was studied in this microscopic structure and the results were very promising. These results link macro-scale simulations to the micro-scale simulations.
    - In the porous cylinders array, the modified Zwikker-Kosten equation was used as the porous model inside the cylinders.
    - In the porous cylinders array, when the $5^{th}$-order WENO scheme was used on the interface, the species transport simulation with porous model was carried out as well. The relationship between the concentration change and the adsorption coefficient was established and found to be not linear.

# CHAPTER 4 - Nano-Scale Simulation

Why can porous material remove toxic gases? Why does surface diffusion occur? These two questions, which have been investigated in the previous two scales, lead to postulating one cause: molecular motion and interaction. As with other questions examined in macroscopic research, using smaller scales provides a more detailed understanding of the causes of the above phenomena. In this chapter, discrete models and numerical simulations are used to examine the surface slip and diffusion mechanisms in the molecular level. The fluid/solid interactions (FSI) reach their final stages, which is the interaction of different types of molecules (see Fig. 4-1).

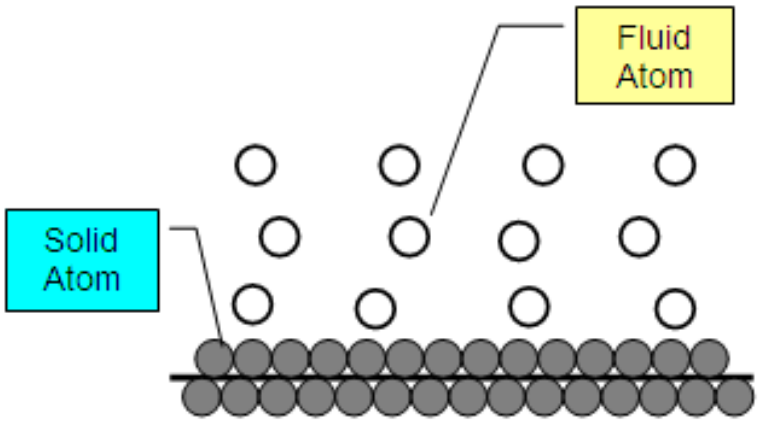


**Figure 4-1 Fluid/solid interaction (FSI) in the molecular level.**

In this chapter, Section 4.1 explains the specific characteristics of the simulation in this smallest scale, which is very different from the other two scales. The slip behavior on the solid surface is examined in Section 4.2 and the surface diffusion (adsorption) in Section 4.3. Section 4.4 presents our conclusions.

## 4.1 Nano-Scale: "Is Everything Different or Just Smaller?"

Flow through micro- and nano-scale structures is of fundamental interest to those designing biological and engineering devices and systems, such as micro-fabricated integrated circuits, carbon nanotubes and bio-sensors. Significant progress has been achieved in understanding flow on this scale and various applications have been developed based on that understanding (Gad-el-Hak, 2004; Squires and Quake, 2005). However, due to the limited knowledge of the microfluidics, many interesting phenomena that have puzzled researchers for a long time are still not understood. Numerical simulation of such a physical system is a preferable approach, because such simulation not only validates the experimental results but also provides information that goes beyond the limits of the experimental observation. Thus, Herwig (2002) posed this question: is everything different or just smaller?

Actually in many micro-/nano- devices, the molecules are not far from the surfaces. The fluid molecules are attracted by the dense solid molecule clusters and can not move freely due to the interaction between fluid and solid. In addition, many physical properties, such as density and viscosity, would deviate from the bulk fluid properties. And surface mechanisms dominate in this regime, which leads to this principal problem: the continuum hypothesis breaks down at the nano-scale and simple no-slip boundary condition treatment is no longer applicable. The Navier-Stokes (NS) equations are based on the continuum approximation and the assumption of thermodynamic equilibrium, both of which rely on the formulation of local flow properties as an average of the fluid elements. Until the equilibrium is achieved, the gradients of those properties are in a linear relationship with the volumes. Thus, the stress varies linearly with strain and the heat flux is linearly related to the temperature gradient. A parameter called the Knudsen number, $K_n = \lambda/L$, where $\lambda$ is the mean-free path and $L$ is a characteristic macroscopic length (e.g.

the radius of a body in a fluid), can be used to categorize different regimes. When this parameter is used, the flow regime can be divided using this parameter as:

a) $K_n < 0.01$, continuum regime. NS equations and no-slip boundary conditions can be used well.

b) $0.01 < K_n < 0.1$, slip-flow regime. NS equations can still be used while the slip condition has to be applied on the boundary.

c) $0.1 < K_n < 10$, transient regime. The stress tensor tends to be substituted with the higher-order model and higher-order slip models at the boundary are needed.

d) $K_n > 10$, atomistic regime. The continuum assumption fails.

In this project, to study the surface mechanisms and properties within the thin layer adjacent to the boundary, we considered $K_n$ to be greater than 10 (even though in the bulk fluid it is still small). So for the continuum region, we kept the NS equations, but at the boundary, we had to use a smaller scale simulation to capture the surface mechanisms. This project had two major aims: First, the slip behavior on the solid surface would be investigated by using the traditional molecular dynamics (MD) simulation and an innovative hybrid scheme in the molecular level. Second, the gas/solid interaction and diffusion aspect would be explored by using the same methods as well. The channel flow problem (Couette flow), without consideration for the surface roughness and curvature, was chosen for both studies.

Since the macro-scale description through the NS equations is not adequate, MD simulation serving as a discrete model could be used in its place. MD simulations are used to model fluids (gas, liquid) characterized by the time and length scales of molecular motion (Frenkel and Smit, 1996). They compute the trajectories of particles interacting through classical

force fields. Koplik and Banavar (1995) reviewed MD methods on their use in this regard. Although MD simulation is able to provide accurate information in the surface-dominant nano-scale region, it is computationally prohibitive for those problems with realistic sizes since nano-scale flows are often part of larger-scale systems. In fact, full MD computing is too expensive for the whole domain in this multi-scale problem; however, only the region near the boundary needs to be simulated. The rest of the domain can be described using the continuum theories less costly. This means that the macro-scale flows determine the external conditions that influence the nano-scale system, which in turn influences the larger scales by modifying its boundary conditions. In this way, we can not only obtain an accurate description from MD, but also utilize the efficiency of the continuum field, which is briefly illustrated in Fig. 4-2.

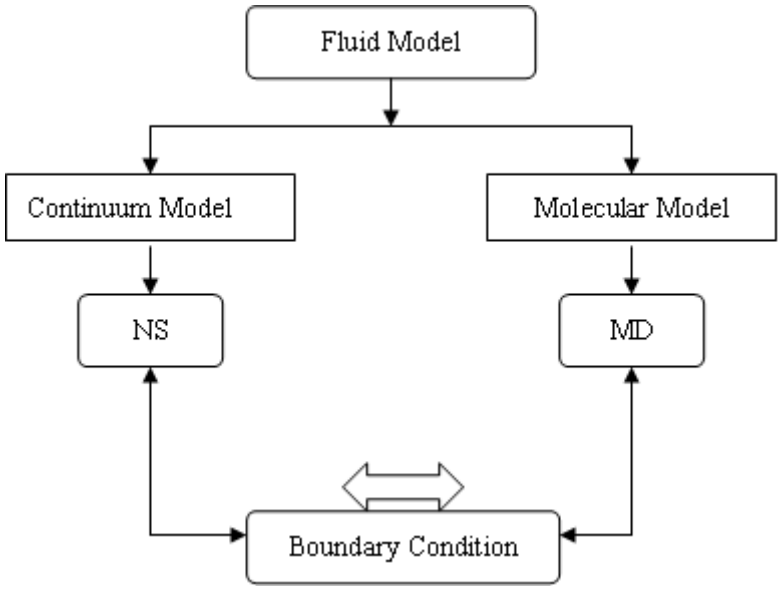


**Figure 4-2 Concept of the coupling scheme.**

The slip behavior is one of the surface properties that are important in micro-/nano-fluidic devices. Figure 4-3 introduces the concept of the slip length in the nano-regime. In the

continuum regime, the common no-slip boundary condition is widely used for solid surfaces while this theory breaks down in smaller scales. Due to the molecular motion, a certain amount of slip exists on the surface, and this feature is characterized as slip length ( $L_s$ ). Hence in this study, we explored the slip behavior by using MD simulation and a hybrid molecular-continuum scheme. Both numerical schemes have been validated by comparing the results with literature. By changing the height of the channel in the Couette flow and the moving velocity on the wall, we varied the shearing conditions; thus, the effect on the slip length could be summarized.

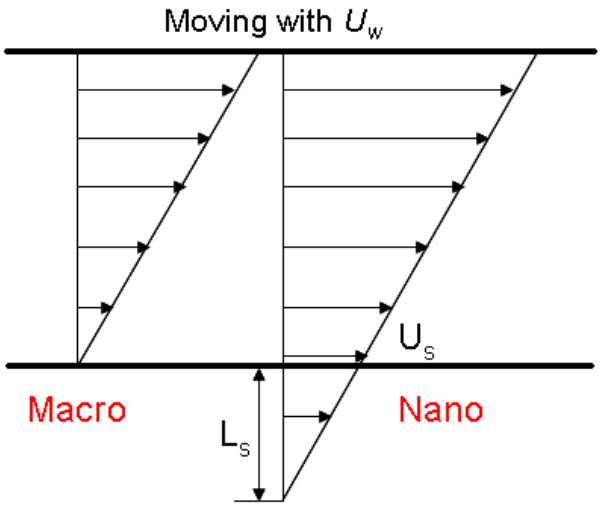


**Figure 4-3 No-slip and slip boundary conditions.**

In the macro- and micro- scales, we simulated the flow/species transport in the nano-material by using porous models to determine how the flow/species could penetrate the fluid/porous interface. The surface diffusion is an important problem that needs to be addressed to understand the transport phenomena and the surface mechanisms. Studying the diffusion into the micro-/nano-pores becomes an interesting topic, which could shed insight into the transport mechanisms involved in this smallest scale. As mentioned previously, the classical continuum

theory based on NS equations assumes that state variables do not vary appreciably on a length scale comparable to the molecular mean free path. However, significant fluctuations in fluid density have been observed in the direction normal to the solid wall both in experiments and in numerical simulations. Consequently, the effectiveness of the classical NS approach should also break down in the diffusion problem. Therefore, the objective of this study was to simulate Couette flow going through the constructed nano-pores on the solid surfaces (Fig. 4-4). Unlike the solid walls in the slip behavior study, several nano-pores are constructed by the molecules, leaving adequate space for the flow developed inside the pores. The transport diffusivity and the flux are calculated based on this simulation. The information would be useful in transport investigations and developing the porous models in the other two larger scales.

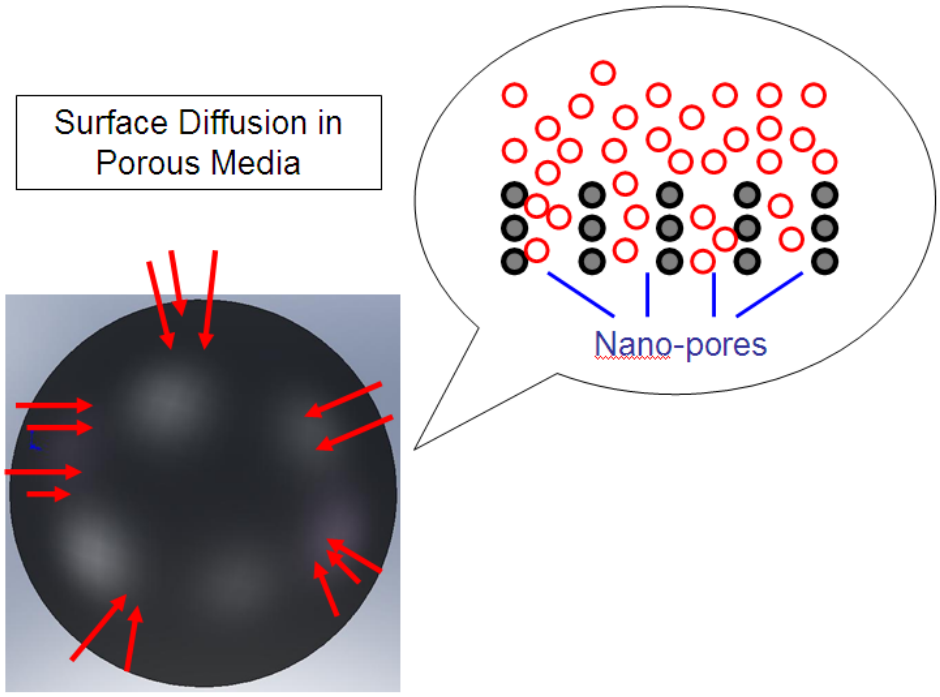


**Figure 4-4 Surface diffusion in nano-scale.**

## 4.2 Slip Behavior on the Solid Surface

The concept of slip length, related to surface velocity and shear rate, is often used to analyze the slip surface property for flow in micro- or nano-channels. In this study, a hybrid scheme that couples molecular dynamics simulation (used near the solid boundary to include the surface effect) and a continuum solution (to study the fluid mechanics) is validated and used for the study of slip length behavior in the Couette flow problem. By varying the height of the channel across multiple length scales, we investigate the effect of channel scale on surface slip length. In addition, by changing the velocity of the moving-solid wall, the influence of shear rate on the slip length in a certain range of the channel height is studied.

The results show that within a certain range of the channel heights (size of the channel), the slip length is size-dependent. This upper bound of the channel height can vary with the shear rate. Under different magnitudes of moving velocities and channel heights, a relative slip length can be introduced which changes with channel height following an exponential function.

### 4.2.1 Introduction

Flow through micro- and nano-scale structures has fundamental applications in many engineering devices, such as micro-integrated circuits, carbon nano-tubes and bio-sensors. In many micro-fluidics devices, the fluid molecules are within a thin layer away from the solid surfaces. The surface properties in this region do not fall into the continuum hypothesis and the simple no-slip boundary condition for flow is no longer applicable. Instead, molecular dynamics (MD) simulations can be used as discrete simulation models in place of the Navier-Stokes (NS) simulation. MD simulations are used to model fluids (including gas and liquid) characterized by the time and length scales of molecular motion (Frenkel and Smit, 1996). They compute the Lagrangian trajectories of particles under the forcing fields calculated by Newton's $2^{nd}$-law. The

review of MD simulation used for fluid mechanics problems can be found in Koplik and Banavar (1995) and Koumoutsakos (2005).

Although MD simulation is sufficient to provide accurate information near the solid surfaces in nano-scale, it is computationally expensive for problems in realistic sizes since the surface mechanisms are part of a macro-scale system. In fact, only in the region very close to the boundary is MD simulations needed. The rest of the domain can still be simulated less costly by traditional continuum solvers. Therefore, a hybrid scheme that allows the two-way interactions between the MD and the continuum simulation can be very useful. The interactions between the two models are facilitated as that the macro-scale flow model determines the external forcing field that influences the nano-scale molecular behavior, while the boundary conditions needed by the continuum simulations can be obtained from the MD computation results. This hybrid molecular-continuum method has become an attractive topic for decades, e.g., the studies in Koumoutsakos (2005), Werder et al. (2005), O'Connell and Thompson (1995), Hadjiconstantinou and Patera (1997), Li et al. (1998), Flekkoy et al. (2000), Nie et al. (2004), Ren and E (2005), Cui et al. (2006) and Wang and He (2007).

The model problem used in the current study is a multi-scale Couette flow problem that has an exact analytical solution in the continuum regime. The purpose is to investigate the slip properties on the solid surfaces within different channel scales and under different shearing conditions. The liquid/solid interface mechanisms have been intensively studied in, for example, Thompson and Robbins (1990), Koplik et al. (1989), Cieplak et al. (2001), Lichter et al. (2004, 2007) and Martini et al. 2008 (a, b). The general boundary conditions (slip and no-slip) on the solid interfaces in the nano-scale were summarized in Thompson and Troian (1997). In the above literature, the concept of slip length was well established and developed. Recently, Xu and Li

(2007) and Yen et al. (2007) studied the channel size effect using hybrid schemes from various points of view. Xu and Li (2007) calculated the slip lengths under the same shear rate by fixing the size of the MD domain in the hybrid scheme. In Yen et al. (2007), they considered the relative slip lengths.

In the current study, we investigate a wide range of cases of the channel flow problem by using either pure MD simulation or the hybrid molecular-continuum scheme. We focus on the influence of shear rate on the slip length that has not been investigated by previous research. The channel scale effect on slip length is investigated under different shear rates.

In the following sections, we use a problem that has a simple analytical solution in the continuum regime, the Couette flow, as a model problem, so that there is no uncertainty in the continuum solution. We then carefully verify our MD solution in comparison with the MD solutions in the literature, although limited to no-thermal energy exchange between the fluid and the solid wall (Martini et al., 2008b). After that, we verify our hybrid method with the full MD simulation and with the literature data, where a detailed description of our hybrid method is provided, giving the parameter selections used in the algorithm, such as sizes of overlapped region and exchange layers, and iteration time steps within each iterative cycle. We also address the time-saving feature of the hybrid method in contrast to full MD simulation. Finally, we used this hybrid method for a wide range of velocity and channel height combinations to systematically study the effects of velocity, size, and shear rate that influence the behaviors of both absolute and relative slip length. The size-scale range reaches all the way to when the continuum assumption can be applicable. A logarithmic correlation between the relative slip length and channel size is sought based on the simulation results.

### 4.2.2 Numerical Schemes

To investigate the slip properties on the fluid/solid interface, both MD simulation and a molecular-continuum coupling method were used. In this section, the numerical schemes of both methods will be explained in detail.

#### *4.2.2.1 Molecular Dynamics Simulation*

Molecular Dynamics (MD) simulation is a technique to compute the equilibrium and transport properties of a particle system, which can be used for a wide range of materials without considering the quantum effects. The theory of this method is: First a certain number of particles are prepared as samples. Then the governing equations follow Newton's 2nd-law. Until the macro properties of the system reach steady, statistic calculation can be carried out. The flow chart of a typical MD program can be concluded as in Fig. 4-5.

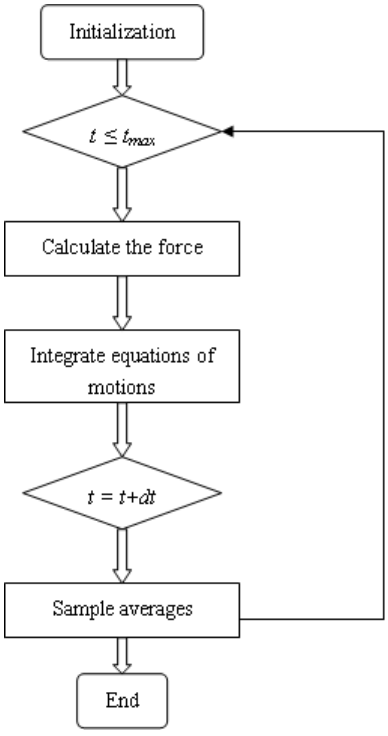


**Figure 4-5 Flow chart of a typical MD simulation process.**

Since the Couette problem in the continuum regime has a linear velocity profile that is an analytical solution, we use it as a model problem for this study. In addition, in a region very close to a wall surface, very often the velocity can be considered a linear distribution, such as that of a viscous sublayer in the continuum regime. Even when the slip occurs, the statistically averaged velocity profile still follows the linear distribution. Furthermore, as the region of interest is in such a close vicinity of a solid wall that molecular behaviors need to be considered, the surface curvature effect in a macroscopic sense can be neglected and the flow there is justifiably assumed to be that over an infinite, flat plate. Therefore, the Couette flow model (Fig. 4-6) is typical for near surface flow and has been commonly used as a model problem in the literature (Thompson and Troian, 1990; Nie et al. 2004; Cui et al. 2006; Wang and He, 2007; Xu and Li, 2007 and Yen et al. 2007).

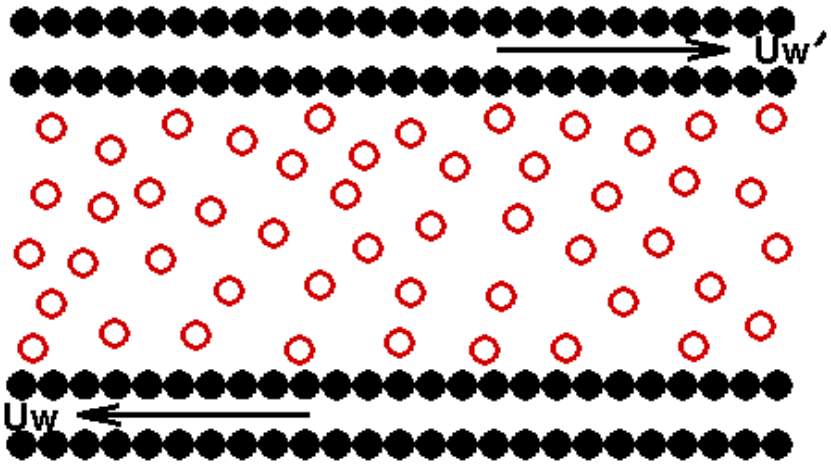


**Figure 4-6 Computational domain of Couette flow by MD: the filled circles represent solid molecules of the wall material; the hollow circles are fluid molecules ($U_w$ and $U_w$' are the moving velocities of the solid walls).**

The computational domain for a pure MD simulation of the Couette problem is in Fig. 4-6. A general computation procedure of the MD simulation has been explained in Allen and Tieldsley (1989), Frenkel and Smit (1996) and Rapaport (2004). The truncated Lennard-Jones (LJ) intermolecular potential that calculates the interaction between molecules is used to compute the force. It is given by:

$$\phi(r) = 4\varepsilon\left[\left(\frac{\sigma}{r}\right)^{12} - \left(\frac{\sigma}{r}\right)^{6} - \left(\frac{\sigma}{r_c}\right)^{12} + \left(\frac{\sigma}{r_c}\right)^{6}\right], \tag{4.1}$$

where $r$ is the distance between two molecules, $\varepsilon$ is the characteristic molecular energy scale, $\sigma$ is the characteristic molecular length scale, and, $r_c$ is the cut-off length, equal to $2.2\sigma$. The distance-dependent LJ potential includes both short-range repulsive forces and longer-range attractive forces. The parameters $\sigma$ and $\varepsilon$ are related to the stable equilibrium length and the maximum depth of the potential well. The liquid we select in this study is argon (due to its simple one-atom structure) with mass per molecule ($m$) as $6.69\times10^{-24}\,g$. The density ($\rho$) is $0.942\,g/cm^3$. The values of the characteristic parameters are: $\sigma = 3.4\times10^{-8}\,cm$, $\varepsilon = 1.656\times10^{-14}\,erg/atom$ ($1erg = 10^{-7}\,J$). The characteristic time scale is calculated as:

$$\tau = \sqrt{m\sigma^2/\varepsilon} = 2.161\times10^{-12}\,s. \tag{4.2}$$

The viscosity of liquid argon can then be determined as:

$$\mu = 2.14\varepsilon\tau\sigma^{-3} = 1.9485\times10^{-4}\,kg/m\cdot s. \tag{4.3}$$

Consequently, from the Newton's 2nd-law, the expression of the acceleration of each molecule is:

$$m\frac{d^2\mathbf{r}_{ij}}{dt^2} = \sum_{i=1,i\neq j}^{N}\frac{\partial\phi}{\partial r_{ij}}\frac{\mathbf{r}_{ij}}{r_{ij}}, \tag{4.4}$$

where the right-hand side includes interactions between one molecule with all the other molecules, both fluid and solid molecules.

In the channel flow problem, there are three kinds of interactions: fluid/fluid, solid/solid, fluid/solid. For fluid molecules, we use liquid argon in this study. The solid molecules compose two layers of FCC (Face-Centered Cubic) lattice to represent the wall of the channel. Equation (4.1) is valid for both solid and fluid molecules, except that different values are specified for related solid or fluid molecules. The solid molecule parameters are: density $\rho_w$, and two LJ parameters, $\sigma_w$ and $\varepsilon_w$. The combinations of these parameters in the LJ potentials near the wall region indicate the effect of surface properties, which will be explained later.

The Gear Predictor-Corrector algorithm is used in the current code for numerically updating the positions, velocities and accelerations of the molecules and the details can be found in Rapaport (2004). The position $r(t+\delta t)$, velocity $u(t+\delta t)$, and forces are evaluated at the end of each time step, $t+\delta t$. Then the predictions are corrected using a combination of the current and previous values for positions and velocities. The size of time step is determined as $\delta t = 0.005\tau$, which is much smaller than the time scale in a usual continuum simulation.

Initially, a random velocity distribution for all the fluid molecules is applied. As the upper wall is moving with a constant speed, the viscous shear stress drives the flow. Periodic boundary conditions are applied in the streamwise and spanwise directions. Since the temperature increases during the simulation due to the viscous effect from its initial value $T = 1.2\varepsilon / k_B$, where $k_B$ is the Boltzmann constant, a velocity scale method is used (Allen and Tildesley, 1989) at every time step to maintain a constant temperature, which can also be used as a stability check for the computational scheme. The velocity scale method can be expressed as:

$$\eta = \left(T / T'\right)^{1/2}, \tag{4.5}$$

$$T' = \frac{1}{2N}\sum_{i=1}^{N}\left|\mathbf{u}_i\right|^2, \tag{4.6}$$

$$\mathbf{u}(t+\frac{1}{2}\delta t) = (2\eta - 1)\mathbf{u}(t-\frac{1}{2}\delta t) + \eta \mathbf{a}t, \tag{4.7}$$

where $T'$ is the actual temperature calculated from the real-time velocities, $\eta$ is the ratio between desired and actual temperatures, and, $\mathbf{a}$ is the acceleration. We have tested other thermostat methods, including those by Andersen (1980), Berendsen et al. (1984), Nose-Hoover (Frenkel and Smit, 1996; Delgado-Buscalioni and Coveney, 2003; Lichter et al. 2007), and the Langevin method (Thompson and Troian, 1990; Cui et al. 2006; Wang and He, 2007; Xu and Li 2007; Yen et al. 2007). After testing all these methods, very close results were obtained for both velocity profiles and slip lengths, as to what were obtained using the velocity scale method expressed in Eqs. (4.5–4.7). Although a conclusion that the velocity profile and slip length can be totally independent of the thermostat method used in the computation may need a more careful check when extended generally to other types of flow, it appears to be true at least for the Couette problem we study here.

#### *4.2.2.2 The Hybrid Scheme*

Figure 4-7 shows the schematic of the hybrid model. The continuum description (C) is used in the shadowed region that is homogeneous and has small velocity gradients and the atomistic description (P) is used in the dotted region around interface. In C → P, continuum solutions (obtained from NS equations) provide boundary conditions for MD simulations. Vice versa, in P → C, atomistic solutions provide boundary conditions for continuum simulations.

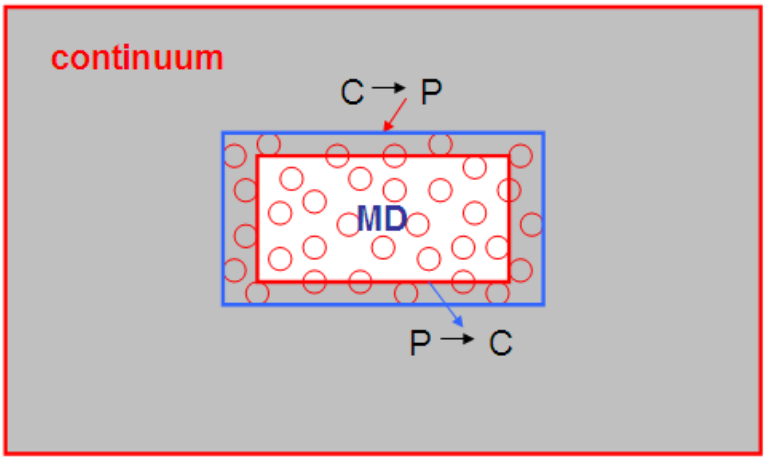


**Figure 4-7 Regimes of the hybrid scheme.**

The major difficulties are to keep the consistencies at the MD-NS interfaces. The two descriptions in the overlapped region are coupled and must be consistent, i.e. the physical quantities, including density, momentum and energy, and their fluxes, must be continuous. The boundary conditions needed for the NS equations can be obtained straightforwardly by averaging the corresponding quantities from the particles over the chosen units and time intervals. However, the reverse problem, generating microscopic particle configurations from known macroscopic quantities, is non-trivial and must be non-unique. Specifically, when there is flux of particles going through the continuum and discrete interface, the problem is magnified. Finally, the time scale coupling is another problem since the time step for continuum simulation is usually several orders of magnitude larger than that in the MD simulation.

Recently, several coupling schemes referring to the exchange of the information between the atomic domain and the continuum domain have been developed. Two main strategies are typically used to handle this process: 1) state-based coupling that involves the transfer of state

variables (e.g. density, temperature) (O'Connell and Thompson, 1995; Hadjiconstantinou and Patera, 1997; Hadjiconstantinou 1999; Li et al. 1998; Nie et al. 2004; Werder et al. 2005; Cui et al. 2006; Wang and He, 2007) 2) flux-based coupling that involves the transfer of the flux of mass, momentum and energy (Flekkoy et al, 2000; Delgado-Buscalioni and Coveney 2003). And there are other types of coupling schemes (Ren and E, 2005) as well.

In this study, since the Couette flow has been chosen as the objective problem; the analytical solution, which is the linear velocity profile, can be easily obtained without actually solving the NS equations. The concept of the hybrid molecular-continuum scheme used in this study is illustrated in Fig. 4-8, which is similar to the method used in Xu and Li (2007). The domain, which is half of the whole channel divided by a symmetry line (it is symmetric since both walls are moving with the same speed but in opposite directions), is separated into three regions: MD (P) region, continuum (C) region and an overlapped region for information exchange between P and C. In the P region, the MD simulation is conducted and in the C region the analytical solution of the Couette flow is used. There exists an overlapped region between the two regions. In addition, there are two layers marked as P $\rightarrow$ C and C $\rightarrow$ P, in which the momentum and mass fluxes are exchanged to maintain conservation of momentum and mass of the whole system (which also requires putting the escaping fluid molecules back into P region). The thickness of the two layers is $4\sigma$. The height of the P region ($H_{cp}$) is $20\sigma$ while the total height of the channel ($2H$) varies from $120\sigma$ to $3200\sigma$ to investigate the influence of the height on the boundary condition. The overlapped region is $10\sigma$, which is half of the height of the P region and sufficiently large for the information exchange between the C and P regions. If this height was reduced, there would not be enough space for performing statistical averaging and exchanging momentum between the two regions. For large channels, this size of the

overlapped region is very small so that only a small amount of computational overhead is spent there. In the stream wise direction, the length of the domain ( $L$ ) is $20\sigma$ , and the width is $5\sigma$ ( $W$ ) in the span wise direction.

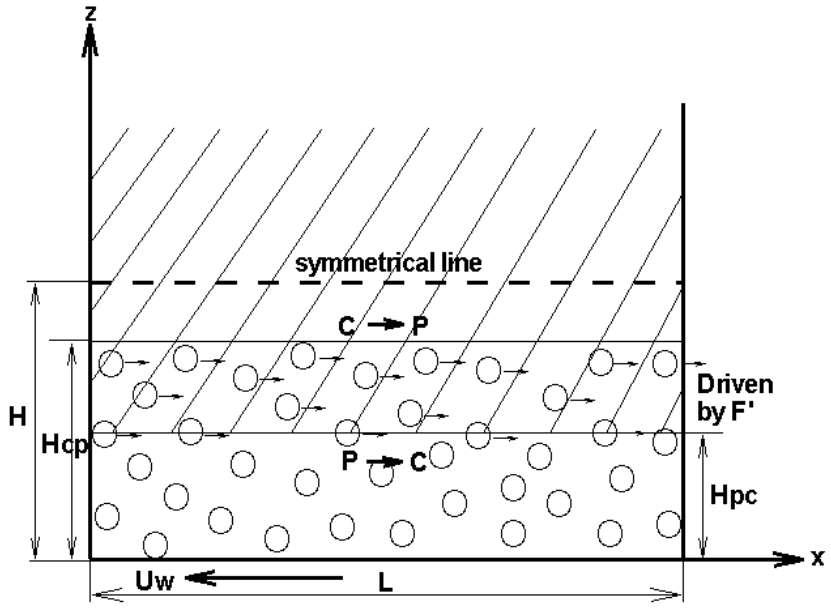


**Figure 4-8 Computational domain and scheme of the hybrid method: the dashed-line area is the continuum region (*C*) and the circled-molecule area is the MD region (*P*). The overlapped region is bounded within two interfaces. And the molecules inside this region are driven by the external forcing field from Eq. (4.11)**

On the interface of P → C, firstly the MD simulation is run in the P region (including the overlapped part) for all the molecules for a sufficient period of time starting from their initial positions and velocities to a statistically stable state. This time period is usually in the range of $100\tau$ to $200\tau$ , varying in different cases. The statistical stability here means when the simulation time is prolonged further, the temperature maintains a constant and the time averaged values,

such as velocities, remain almost unchanged. The results are then averaged statistically on the interface to provide boundary conditions for the continuum solution. The mean velocity, $u_{pc}$, is obtained at the center of the interface layer, which is used as the boundary condition for the linear analytical solution in the C region:

$$u_{pc} = \frac{1}{N_{pc}} \sum_{i=1}^{N_{pc}} u_i \,, \tag{4.8}$$

where $N_{pc}$ is the number of molecules on the P → C layer. Thus the velocity profile in C region is calculated as:

$$u = \frac{u_{pc}}{H - H_{pc}} (z - H) \,. \tag{4.9}$$

The calculation of $u_{pc}$ also needs to be performed for several iteration loops as explained later.

As the P → C step is relatively straightforward, the trouble lies on the C → P interface. In order to keep the consistency of the transfer between the continuum quantities and molecular quantities in the overlapped region, there are three major issues to be resolved: 1) mass flux consistency, 2) momentum flux consistency, and 3) time marching.

There are molecules escaping from the P domain to the C domain due to the random motion of molecules. This results in mass loss and decrease of the total number of molecules in the P region. In order to maintain mass and energy conservation, at each time step, we reflect the escaping molecules back into the domain at the interface boundary. However, this reflecting boundary condition is not needed on the wall boundary because there is no escaping of molecules through the solid wall. The dense structure of the solid wall molecules generates

sufficiently large repulsive forces that prohibit the liquid molecules from escaping through the solid wall.

The MD simulation carried out in the P domain also needs a boundary condition on the upper boundary to drive the motion of the fluid molecules. This condition can be obtained from the results of the C region. The driving force ($\mathbf{F}_i'$) is treated as an external force on the right-hand-side of Eq. (4.4). Then the Newton's 2nd-law in Eq. (4.4) is modified as:

$$m\frac{d^2\mathbf{r}_{ij}}{dt^2} = \sum_{i=1,i\neq j}^{N}\mathbf{F}_{ij} + \frac{1}{N_{cp}}\sum\mathbf{F}', \tag{4.10}$$

where $N_{cp}$ is the number of molecules on the C → P layer and $\mathbf{F}_i'$ is calculated from the shear stress:

$$\sum\mathbf{F}' = -\mu\frac{u_{pc}\mathbf{i}}{H-H_{pc}}LW \quad , \tag{4.11}$$

where $u_{pc}$ is the same as in the P → C coupling, and, $L$ and $W$ are respectively the length and the width of the channel.

Initially, this force is calculated using the shear rate on the moving wall until there is a slipping velocity on the P → C layer. It should be noted that this external forcing field should only be applied to the molecules in the C → P layer.

The time-marching scheme consists of several steps. First, time marching is carried out for about $100\tau$ to $200\tau$ after the MD simulation reaches a statistically stable state from the initial state, at which the time averaged results for $u_{pc}$ can be obtained on the P → C interface, as explained previously. Then the external forcing field on the C → P interface can be

established using Eq. (4.11). Once $\mathbf{F}_i'$ is calculated, Eq. (4.10) is used again and so is Eq. (4.8) to obtain a new $u_{pc}$. This process needs to go on for several cycles, so that $u_{pc}$ and $\mathbf{F}_i'$ are being updated in each computational cycle. For each cycle (except the first cycle starting from the initial state), the MD simulation using Eq. (4.10) advances $50\tau$, after which the statistic averaging is performed. Then the solution in the C region receives the boundary condition, $u_{pc}$, to be used in Eq. (4.11). Also the external forcing field is updated by using the new shear stress value. This procedure is repeated, until the solution of the C region remains unchanged and the entire (C + P) domain has reached a linear velocity profile. The duration of the procedure is around several thousands of $\tau$, again varying in different cases. During the time marching, the energy level, which is represented by the calculated temperature, is maintained the same by using the velocity scale method in Eqs. (4.5 - 4.7).

### 4.2.3 Results and Discussion

A snapshot of the channel flow problem in the molecular level by using pure MD simulation is shown in Fig. 4-9 using VMD (Visual Molecular Dynamics, visualization software developed by the theoretical and computational physics group in UIUC). In this 3D channel flow case in the atomistic scale, the gray particles are solid molecules while the green ones are fluid molecules. The visualization could help understand the problem directly and explain the physical model very well.

To quantify the results, we first verify our schemes of pure MD computation and the hybrid scheme for the Couette flow problem in Section 4.2.3.1. Second, in Section 4.2.3.2, we present the slip length results (surface slip behavior) on the solid walls for both pure MD computation and the hybrid scheme and discuss the scale effect under different shear rates ($\dot{\gamma}$)

and different wall speeds ($U_w$).

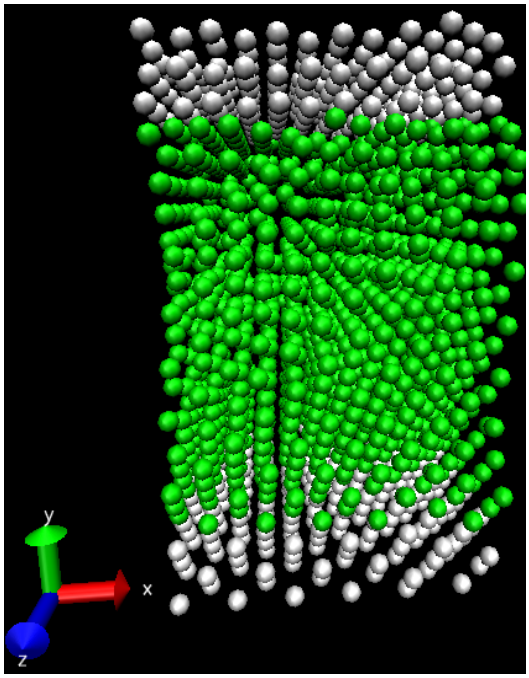


**Figure 4-9 Channel flow simulated by MD and visualized by VMD.**

### *4.2.3.1 Verification of the MD and Hybrid Schemes*

The boundary condition at the interface between the fluid flow and the solid wall depends on several parameters: $\rho$, $\sigma$ and $\varepsilon$ of the fluid and $\rho_w$, $\sigma_w$ and $\varepsilon_w$ of the solid. Thompson and Troian (1997) investigated the relationship between the two groups of parameters and the interface slip properties. For the no-slip boundary condition, the two groups of parameters follow the relation $\rho_w / \rho = 1$, $\sigma_w / \sigma = 1$, $\varepsilon_w / \varepsilon = 0.6$ (Group A). With increased density of the wall (by adding more solid molecules) and decreased characteristic length, $\rho_w / \rho = 4$, $\sigma_w / \sigma = 0.75$, $\varepsilon_w / \varepsilon = 0.6$ (Group B), the slip boundary condition occurs. We simulated these two cases using the pure MD simulation code in a domain of $20\sigma \times 5\sigma \times 25\sigma$ with a stationary bottom wall and a

moving upper wall. The moving speed of the upper wall was $U_w = 1.0\sigma\tau^{-1}$. A perfect agreement to the results of Thompson and Troian (1997), for both Group A and Group B, means that our MD simulation is able to predict the slip properties very well (see Fig. 4-10). In this sense, the verification is achieved by obtaining consistent results with the extensively cited results in Thompson and Troian (1997) and Yen et al. (2007).

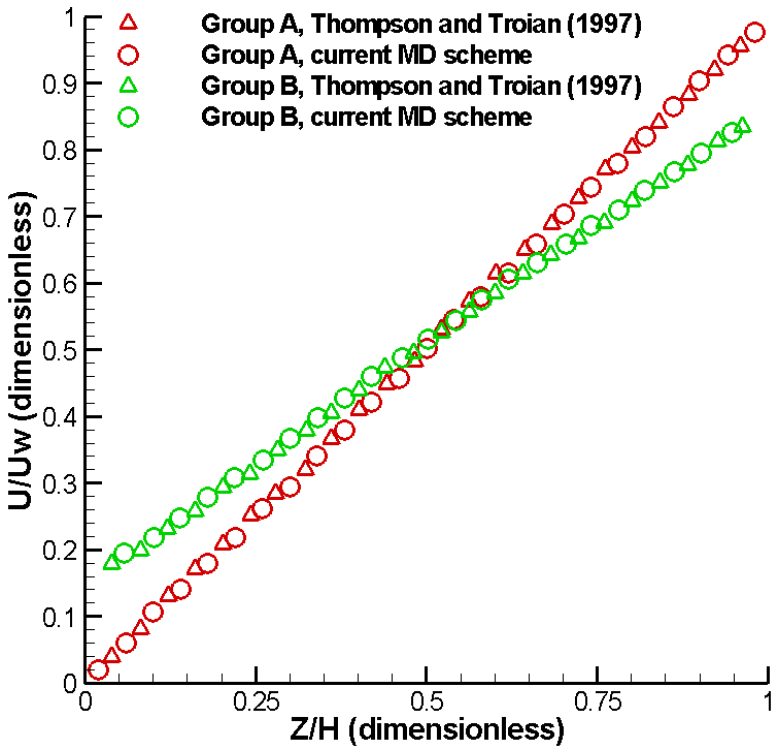


**Figure 4-10 Velocity profile comparisons for Group A (no-slip boundary condition, $\rho_w/\rho = 1$, $\sigma_w/\sigma = 1$, $\varepsilon_w/\varepsilon = 0.6$) and Group B (slip boundary condition, $\rho_w/\rho = 4$, $\sigma_w/\sigma = 0.75$, $\varepsilon_w/\varepsilon = 0.6$) using pure MD simulations.**

For verifying the hybrid scheme, we set up a case in a domain of $20\sigma \times 5\sigma \times 60\sigma$ with the bottom wall moving at $U_w = -1.0\sigma\tau^{-1}$ and the upper wall moving at the same speed in the opposite direction. Both the pure MD simulation and hybrid scheme were run. For the pure MD simulation, the entire channel with the height of $2H$ ($H = 30\sigma$) was simulated, while for the hybrid scheme, only half of the domain (from 0 to $H$) was considered. As shown in Fig. 4-11, using the fluid/solid interaction parameters for both Group A and B, the result from hybrid scheme matches that from the pure MD simulation very well. Also in the hybrid scheme, the overlapped region has identical solution from both the P region solution and the C region solution, which proves that the information exchange between the two regions is successful.

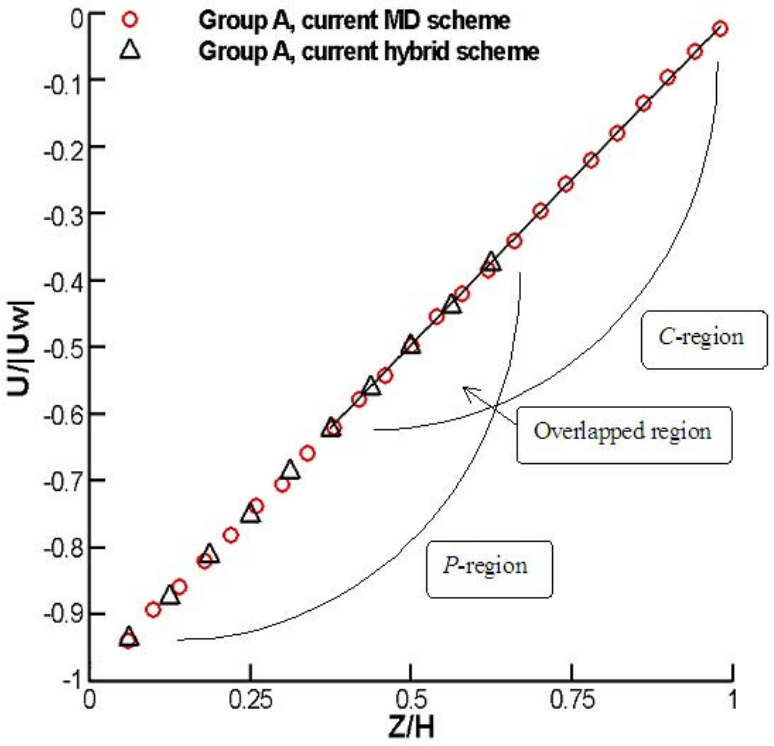


**(a)**

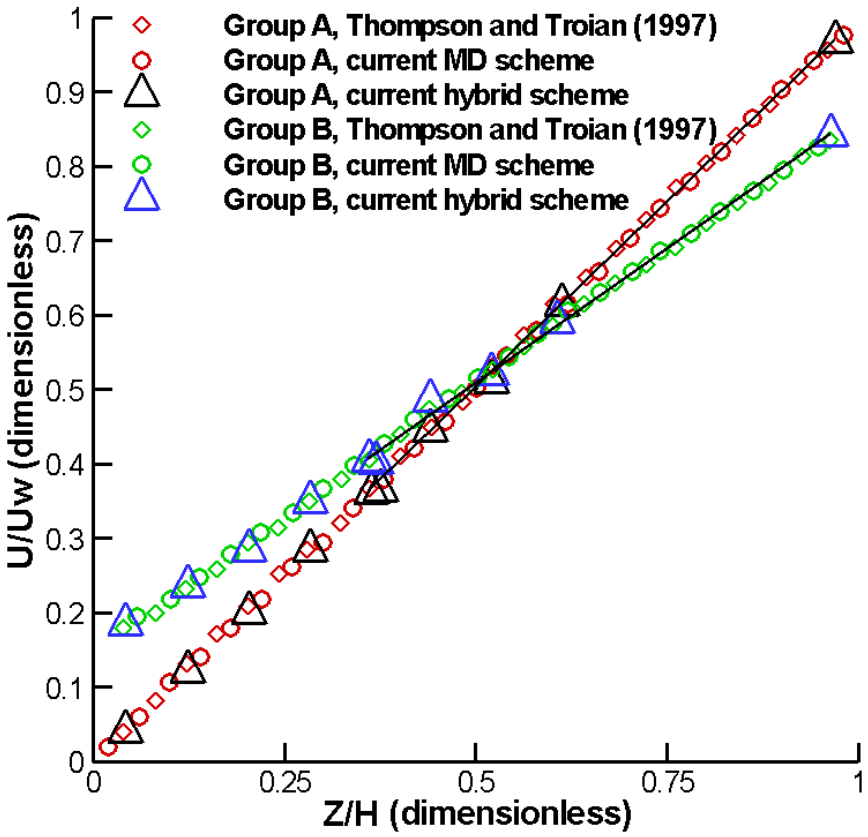


**(b)**

**Figure 4-11 Velocity profiles comparisons under the moving velocity of the bottom wall $U_w = -1.0\sigma\tau^{-1}$: (a) between pure MD simulation and the hybrid scheme for Group A ($\rho_w/\rho = 1$, $\sigma_w/\sigma = 1$, $\varepsilon_w/\varepsilon = 0.6$) (b) between pure MD simulation and the hybrid scheme for both Group A and Group B ($\rho_w/\rho = 4$, $\sigma_w/\sigma = 0.75$, $\varepsilon_w/\varepsilon = 0.6$).**

### *4.2.3.2 Behaviors of Slip Length*

Once we have achieved the solid, though limited, verifications for the MD and hybrid scheme, we use them to investigate the slip length behavior for different channel sizes and shear rates. The hybrid scheme is used for the channel size from tens of $\sigma$ to hundreds of $\sigma$. For small

channel size of several of $\sigma$, only MD simulation is needed. The channel size scale effect is studied in a range that is from $5\sigma$ to $1600\sigma$ (for $H$). We use pure MD simulation between $5\sigma$ to $40\sigma$ and the hybrid scheme for the larger sizes. We selected the parameters of Group B ($\rho_w/\rho = 4$, $\sigma_w/\sigma = 0.75$, $\varepsilon_w/\varepsilon = 0.6$) for fluid/solid potentials for both schemes. Four different velocities of wall motion are studied with the bottom wall of $U_w = -1.0\sigma\tau^{-1}$, $-2.0\sigma\tau^{-1}$, $-4.0\sigma\tau^{-1}$ and $-8.0\sigma\tau^{-1}$.

As the MD scheme was only partially used in the hybrid scheme, computational time was greatly reduced, especially for larger-size channels. For example, for a channel height of $400\sigma$, the time used for the hybrid scheme was about 602s, while for the pure MD simulation, the time was1268s. The time saved is about half. For a channel height of $800\sigma$, the time saved can be as much as two thirds. Therefore, the hybrid scheme is able to save a lot of computational time in simulation for large-size flow systems.

The absolute slip length, $L_s$, is a representative of the wall slip properties. In Martini et al. 2008, it was defined as $L_s = u_s/\dot{\gamma}$, where the shear rate $\dot{\gamma}$ was measured by a fitted curve of the velocity profile and $u_s$ is the slip velocity in the first liquid layer adjacent to the solid wall.

Figure 4.12 shows the absolute slip length versus the channel size with four moving velocities. For the same channel size, different moving velocities give different shear rates. It can be seen that higher shear rates result in larger slip lengths, which also shows in Fig. 2 of Thompson and Troian (1997). Under the same moving velocity, the slip length decreases as the channel height increases and the shear rate decreases (since $\dot{\gamma} = U_w/H$). These trends are only significant when the channel height is small. Above a certain channel height, the slip length almost remains constant around $5\sigma$, even with different shear rates. This asymptotic behavior

agrees with a conclusion of Xu and Li (2007) in which a constant shear rate was maintained. That is, for large $H$, the slip length becomes independent of $H$. However, the threshold channel height for the slip length to asymptotically reach constant increases with the shear rate: $100\sigma$ - $U_w = -1.0\sigma\tau^{-1}$, $200\sigma$ - $U_w = -2.0\sigma\tau^{-1}$, $300\sigma$ - $U_w = -4.0\sigma\tau^{-1}$ and $400\sigma$ - $U_w = -8.0\sigma\tau^{-1}$.

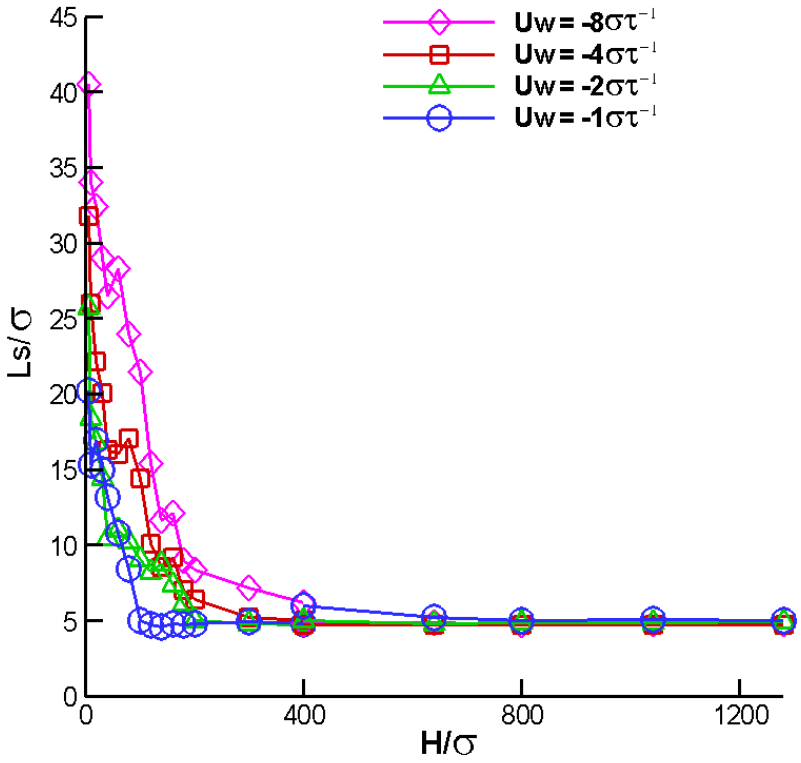


**Figure 4-12 Absolute slip length ($L_s$) for different moving velocities from pure MD simulation and the hybrid scheme.**

This also shows that the effect of slip length is negligible in large-scale channels, because of the relative small value of the slip length (a few number of $\sigma$) in comparison to the large channel size (a few hundreds of $\sigma$). If we use $500\sigma$ as the limit, for the $\sigma$ value considered in

this study, this limit is in the range of a few tenths of micrometers. Although the size and shape of fluid molecules can significantly affect their surface behavior and the limit at which the fluid can be treated as a continuum, the results nevertheless provide evidences that the no-slip assumption can be used in the continuum flow regime, which is usually in the micrometer range or larger.

To explain the relative scale effect, we use the relative slip length when the absolute slip length is re-scaled by the channel height ($H$). The results are plotted in Fig. 4-13 (a), which shows that the four curves in Fig. 4-12 seem to collapse to one curve, with a nominal threshold channel height for the relative slip length to be around $100\sigma$. In the logarithmic plot Fig. 4-13 (b), the four curves of the relative slip length can be approximately fitted, to the channel height up to a few hundreds of $\sigma$, as

$$Log(L_s / H) = -1.447 Log(H / \sigma) + 1.79 . \tag{4.12}$$

For very large $H$, as the slip length asymptotes to a constant value, the slope of the logarithmic line becomes -1 and the second coefficient becomes 0.7:

$$Log(L_s / H) = -Log(H / \sigma) + 0.7 , \tag{4.13}$$

yielding an asymptotic value of $L_s \sim 5\sigma$, the same as obtained before.

An exponential function is used to relate the relative slip length and the channel height in Yen et al. (2007) in the range of channel height from $24\sigma$ to $400\sigma$. In Yen et al. (2007), the solid wall parameters are different from the present simulation. When the exponential function expression in Yen et al. (2007) is converted to a logarithmic expression, it can be expressed as

$$Log(L_s / H) = -1.033 Log(H / \sigma) + 0.79 , \tag{4.14}$$

in which the coefficients are in a close range of those in Eqs. (4.12) and (4.13).

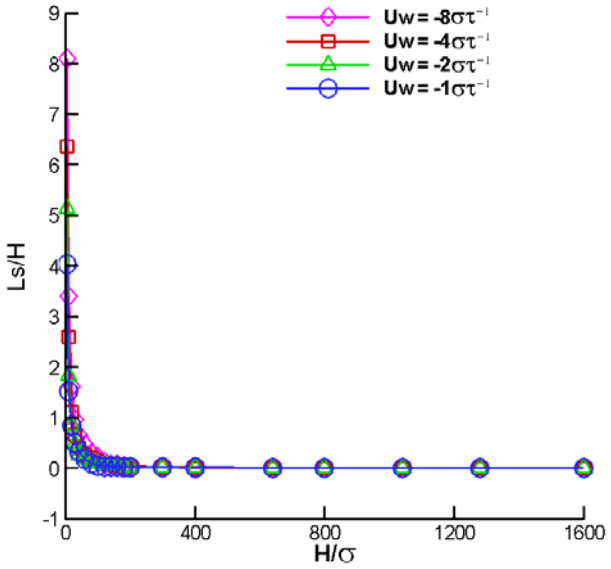


**(a)**

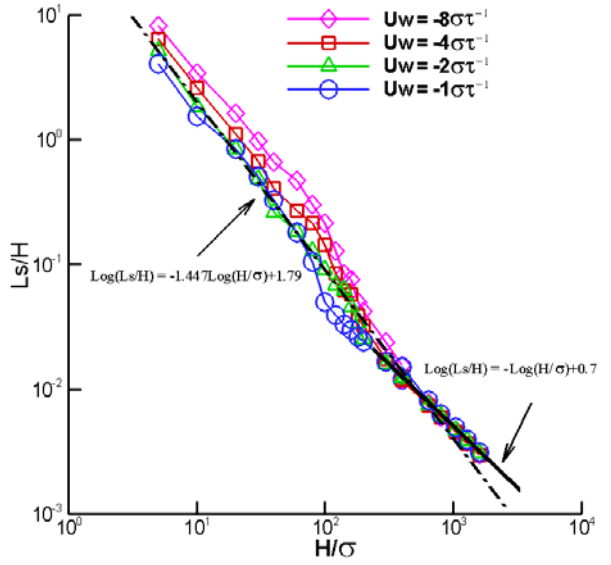


**(b)**

**Figure 4-13 Relative slip length ($L_s$ / $H$) for different moving velocities by using pure MD simulation and the hybrid scheme: (a) $L_s$ / $H$ versus $H/\sigma$; (b) Log ($L_s/H$) versus Log ($H/\sigma$).**

With the fact that the results of a relatively wide range of shear rate and channel scale that all collapse to the same logarithmic curve, it is apparent that the two coefficients in the logarithmic relation (for small channels; for large channel, only one) are dependent on the material properties of the fluid and the solid wall. While seeking specific relations between these coefficients and the material properties is beyond the scope of the current study, the simple linear relation in Eq. (4.12) can be used as a guide for them to be determined by only a few data points, from either simulation or measurement with just a limited number of variations of channel heights, velocities, or shear rates.

It should be noted that in the high shear limit, Martini et al. (2008b) showed that MD simulations must account for heat transfer to the solid wall whereas the solid wall is considered a flexible wall with the thermostat also applied to the wall molecules. The MD simulation presented in this study is limited to rigid walls only. The applicability of the hybrid method with heat transfer deserves future research.

### 4.2.4 Summary of the Slip Behavior Study

In Section 4.2, we used both pure molecular dynamics simulation and a hybrid molecular-continuum computation method to analyze the surface properties in a Couette flow. The numerical schemes for both methods are proved to be accurate by comparing the simulation results with the analytical solutions and the literature data. The simulated results provide evidences that the continuum theory can only be used in macro-scale systems (several micrometers and larger), though in general the size and shape of fluid molecules can significantly affect their surface behavior and thus the limit at which the fluid can be treated as a continuum. As the scale goes down to the nano-scale, the MD simulation has to be involved. The advantage of the hybrid molecular-continuum scheme is its efficiency to provide comparable

results to those of pure MD while reducing much computational time. Under different magnitudes of moving velocities and channel heights, the relative slip length changes following an exponential function of the channel height. The coefficients of the function depend on the fluid and wall materials. For large channels (greater than hundreds of $\sigma$), the no-slip assumption is valid on the solid surface because the slip length effect is negligible. For small channels, especially for heights less than tens of $\sigma$, the slip property has to be considered.

## 4.3 Surface Diffusion

The surface diffusion, related to both the fluid and solid material properties and the flow rate, can be used as a parameter for estimating the adsorbing capacity of a porous nano-material. Consequently, our study attempted to determine how much the flow could penetrate the fluid/porous interfaces through the nano-pores. The transport of fluids through porous materials, especially, occurs mainly by diffusion. In this section, a molecular-continuum hybrid scheme is again used for the study of the diffusion in the representative Couette flow problem. The difference between the current diffusion investigation and the previous slip behaviors study is that there are several nano-pores constructed in the solid walls of the channel. From the results of the simulation, both the self diffusivities and the transport diffusivities were estimated. Also the macroscopic transport properties, such as pressure and mass flux, were calculated. By varying the velocity of the moving-solid wall, we investigated the effect of the shearing condition on the mass flux going through the pores. The relationship of the physical mechanisms and the transport phenomena (e.g. Fick's law) were then linked among the different length scales.

### 4.3.1 Introduction

Fluid transport with diffusion through micro-/nano- channels is found to be useful in many natural phenomena and industrial processes, including fluid transport or diffusion through nano-materials, molecular/atomistic transfer across nuclear pores or in the MEMS devices among other applications. Currently, nano-science/technology has been of fundamental and practical interest. And those nano-pores can be treated as nano-channels in the thin layers of the membranes. The transport phenomena of fluid in such small confined channels, usually in the size of ten molecular diameters or less, differs significantly from its bulk behaviors, which can be described with continuum theory. In this case, molecular dynamics (MD) simulation, rather than continuum methods, is better suited to study the phenomena. Activated carbon with its high surface area has been emerging as a promising candidate for an adsorbent due to not only its stable thermodynamic and mechanical properties but also its homogenous and isotropic porous distribution and relatively even pore size. In this section, we mainly focus on the characteristics of the permeation and the adsorption process between different gases and the carbon substrate under various shearing conditions. The investigation of the diffusion process of fluids through the pores of the nano-materials has become an interesting topic in recent decades. This investigation has been divided into two major areas: 1) the diffusivity estimation and 2) the transient diffusion rate.

Two different pure-fluid diffusivities have been measured/calculated in experiments and simulations: self-diffusivity ( $D_s$ ) and transport diffusivity ( $D_t$ ). Self-diffusivity is the diffusion from the molecules into the bulk fluid. The transport diffusivity counts the transport from one phase to another and is related to concentration. The self-diffusion coefficient can be determined experimentally or by using MD simulations, which records the trajectories of the molecules. The

Stokes-Einstein relation can be used to obtain $D_s$, which is shown in Section 4.3.2. The transport diffusivity is defined by Fick's law of diffusion, which relates the flux to the concentration gradient. The numerical way to obtain $D_t$ is not as straightforward as the other. Basically, there are two methods for computing: non-equilibrium molecular dynamics (NEMD) techniques and equilibrium molecular dynamics (EMD) methods. A review of using molecular simulations to reach the macroscopic properties can be found in Sholl (2006). Other literature include Rowley and Painter (1997), who calculates the diffusion for Lennard-Jones fluid, and Ackerman et al. (2003), who estimated the diffusivities of Ar and Ne in carbon nanotubes. In the current study, we will not concentrate on calculating the value of the diffusivities but focus on the transient diffusion process. However, calculating the self-diffusivity could be used as a validation case to check the motion of the pure fluid molecules, which is explained later.

Many recent molecular simulation studies have been carried out on the adsorption and transport of some fluids or their mixtures into various solid substrates or membranes. The macroscopic properties and mechanisms, such as pressure, temperature, diffusion model, and others, have been explored in an atomistic point of view. Generally, grand canonical Monte Carlo (GCMC) simulation is often adopted to simulate the equilibrium diffusion (Duran et al., 2002), while molecular dynamics simulation (MD) is more preferable to study the non-equilibrium transport properties. Also, some non-equilibrium molecular dynamics (NEMD) methods have recently been developed. These include the grand canonical molecular dynamics (GCMD) method, and especially the so-called dual-volume GCMD technique (DCV-GCMD) (Ford and Heffelfinger, 1998 a, b; Martin et al. 2001; Duran et al. 2002; Newsome and Sholl, 2005, 2008; Huang et al. 2006, 2007; Want et al. 2006 a, b; Wu et al. 2008). And Huang et al. (2007) compared the results from the small scale discrete model to the continuum model solved

with Navier-Stokes equations and achieved promising results, which proved the accuracy of applying such molecular schemes to the diffusion problem. The previous work provides valuable insight into the transport of the fluids through a porous medium.

In this work, we apply a hybrid scheme to a model problem of various gases transport through a carbon substrate with several pores in a channel flow under different shear rates. Instead of inserting and deleting particles from the control volumes used in the DCV-GCMD method, we kept the number of particles in the simulation system constant. The interactions between fluid/fluid, fluid/solid and solid/solid were all assumed to be under Lennard-Jones potentials, which made modeling relatively simple. The same as in the slip behavior study, the Couette flow using the hybrid scheme is still applied here. The only difference is that by constructing those nano-pores, we allowed the fluids to go through the substrate. Hence, the transient diffusion rate (flux) could be captured.

The organization of the presentation is as follows: in Section 4.3.2, we introduce the numerical model and method. Since the hybrid scheme was validated in Section 4.2, it was directly applied to the new diffusion model; in Section 4.3.3, we first explain the natural diffusion by calculating the self-diffusivity of liquid argon and its structural distribution in the equilibrium bulk state and comparing it to experimental measurements. Then we present and discuss the surface diffusion including the mass flux calculation, the transport diffusivity estimation and the influence of the nano-scale simulation to the macroscopic transport theories. Finally, in Section 4.3.4, we present our conclusions.

### 4.3.2 Numerical Scheme

The physical model used in this study was based on a channel flow problem with a multi-layer carbon substrate as the solid wall that contained several nano-pores (Fig. 4-14). As defined in the Couette flow, the fluid was driven by the motion of the walls with defined speed. Because the hybrid scheme was used, the MD simulation performed on just the thin layer near the solid wall while the continuum linear theoretical solution was used in the bulk flow. Details about the Couette flow and the hybrid scheme are discussed in Section 4.2. In the slip behavior study, the slip length provides a boundary condition, which is needed for the macroscopic momentum transport. While in the diffusion simulation, the mass transport problem also requires a boundary condition, which is one of the objectives of the molecular dynamics simulation. The macroscopic mass transport equation is in the following form:

$$\frac{\partial C}{\partial t}+\frac{\partial (u_j C)}{\partial x_j}=\frac{\partial}{\partial x_j}\left(D_s \frac{\partial C}{\partial x_j}\right), \tag{4.15}$$

where $C$ is the concentration, $u_j$ is the velocity component that can be obtained from momentum transport, and, $D_s$ is the diffusivity, which can be determined both experimentally and numerically. In the current simulation, we assume that the flow is steady-state and that the concentration change only occurs in the vertical direction. Thus Eq. (4.15) can be simplified and the concentration can be expressed after integration in the vertical direction as:

$$C(z)=\frac{J}{D_s}z+b. \tag{4.16}$$

where $J$ is the mass flux and $b$ is a constant that requires a boundary condition , which is surface-property dependent and supplied by the molecular dynamics simulation.

In the molecular dynamics simulation, since the periodic boundary condition is also applied in the vertical direction, the loss of the molecules entering those nano-pores is compensated by inserting the same amount back to the MD region, which is the C → P interface (see the purple arrow in Fig. 4-14). And this loss is exactly how much adsorption by the solid substrate through the diffusion process. The constant *b* is thus obtained from this loss, which is the concentration boundary condition for the continuum simulation though it is a thin layer away from the real fluid/solid interface at a location of the P → C layer. Hence, the relationship of the mass transport between the nano-scale and the other two scales is established. Also, the nano-scale diffusion simulation can provide more interface transport information, which is explained later.

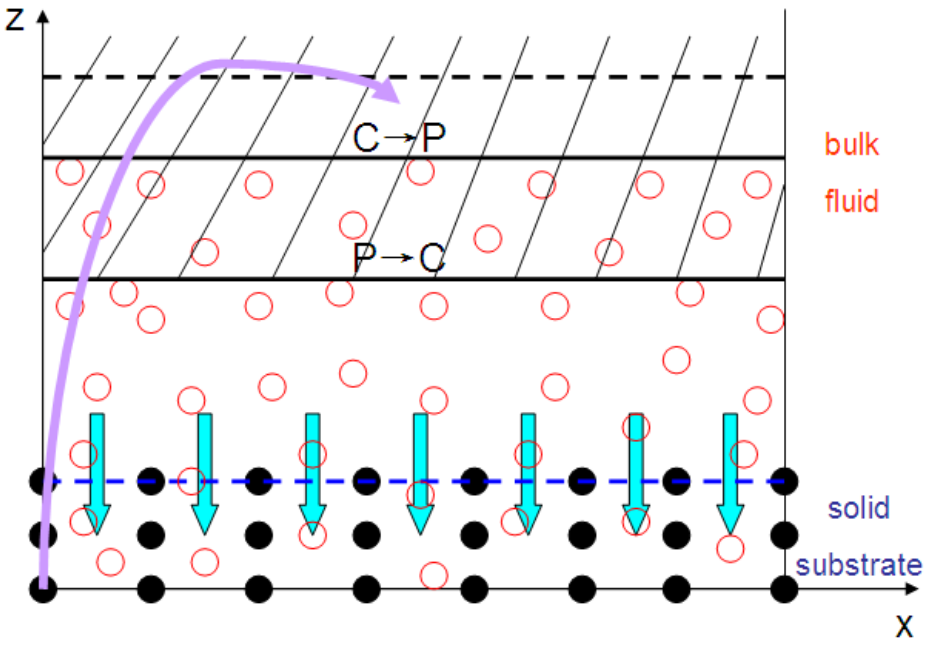


**Figure 4-14 The concept of the diffusion model.**

The interactions between fluid/fluid and fluid/solid molecules are modeled with the standard Lennard-Jones potential:

$$\phi(r_{ij}) = 4\varepsilon_{ij}\left[\left(\frac{\sigma_{ij}}{r_{ij}}\right)^{12} - \left(\frac{\sigma_{ij}}{r_{ij}}\right)^{6}\right], \tag{4.17}$$

where the values of $r_{ij}$ (inter-molecule distance), $\sigma_{ij}$ (characteristic length scale)and $\varepsilon_{ij}$ (characteristic energy scale) are listed for different types of gases/materials (Wu et al. 2008) in Table 4-1. The reduced cut-off length is $2.2\sigma$. And Lorentz-Berthelot mixing rules (Allen and Tildesley, 1987) are used to obtain the fluid/solid interactions as:

$$\sigma_{ij} = \frac{\sigma_{ii} + \sigma_{jj}}{2}, \tag{4.18}$$

and

$$\varepsilon_{ij} = 2\sqrt{\varepsilon_{ii}\varepsilon_{jj}}\ . \tag{4.19}$$

| | **Ar** | **$H_2$** | **CO** | **Carbon** |
|---|---|---|---|---|
| **Characteristic length ($\sigma$, *nm*)** | 0.3542 | 0.296 | 0.376 | 0.34 |
| **Characteristic energy ($\varepsilon/\kappa$, *K*)** | 93.3 | 34.2 | 100.2 | 28 |

**Table 4-1 Lennard-Jones parameters for various gases/materials.**

For the diffusion model, the nano-pores in the solid substrate were modeled as aligned slits (small channels), which are illustrated in Fig. 4-15. The gas flow was isothermal and the thermo effect and the heat transfer between the flow and the solid due to the shear was neglected.

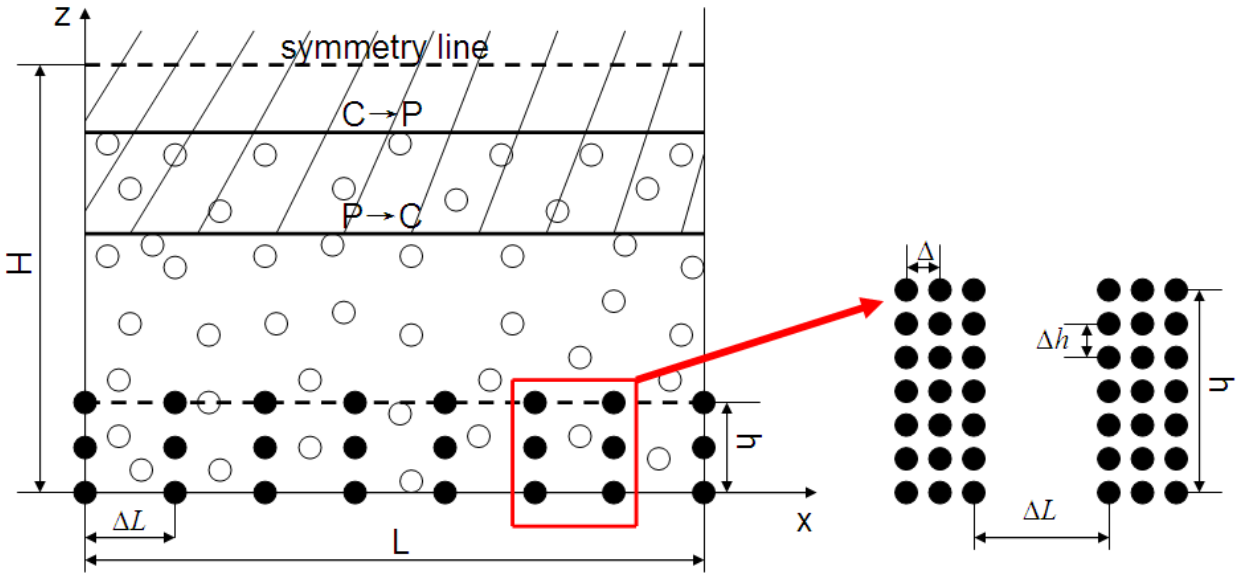


**Figure 4-15 Computational domain of the diffusion simulation.**

The computational domain of the diffusion simulation is similar to the one used in the hybrid scheme for slip behavior study (see Fig. 4-8). The only difference is that in the solid substrate is the existence of regular arrays of channel-like nano-pores through which the fluid molecules can pass. The solid wall was constructed with multi-layers of carbon molecules and the distance (pore width) between the two columns ( $\Delta L$ ) ranged from $2\sigma$ to $6\sigma$, which assured the fluid molecules could pass. The gaps between the two adjacent pore walls ( $\Delta$ ) and between pore layers ( $\Delta h$ ) were kept as $\sigma$. There were 16 layers for the solid substrate, which meant that the length of the pore ( $h$ ) was $15\sigma$. And in the current domain, eight slip pores were constructed.

The dimension of the domain ( $L \times W \times H$ ) was selected as $(8 \cdot \Delta L + 18\Delta) \times 10\sigma \times 40\sigma$ . Thus, the simulation was dimensionless and characterized only by the material properties. It should be noted that the value of $\sigma$ varies for different materials. Periodic boundary conditions were employed in all three directions. The same hybrid scheme was adapted in this diffusion problem for the coupling of the momentum of the fluid molecules. However, due to the diffusion into the nano-pores in the vertical direction (the fluid molecules could go through the channel-like pores), a number of molecules would be lost. This loss was compensated by inserting the same number of molecules back into the MD domain from the C → P interface. This procedure was carried out in a time period that varied from $100\tau$ to $400\tau$ , depending on the materials.

As mentioned in Section 4.3.1, the diffusivity estimation was one of the two important features that needed to be addressed in the diffusion study. By using the current hybrid scheme, we were able to estimate both self-diffusivity and transport diffusivity. We calculated the self-diffusivity using the Stokes-Einstein relation (Sholl, 2006) expressed as:

$$D_s = \frac{1}{6(t - t_0)} \left\langle \left| r_i(t) - r_i(t_0) \right|^2 \right\rangle, \tag{4.20}$$

where $t$ and $t_0$ are two instantaneous times, and, $r_i(t)$ and $r_i(t_0)$ are the trajectories of the molecules at those two moments. The transport diffusivity ( $D_t$ ) is defined as the proportionality constant relating a macroscopic mass flux to a spatial density gradient in Fick's law for mass transport. It relates the mass flux and the density change. The flux ( $J$ ) for gas diffusion through the nano-pores is given by

$$J = -D_t \frac{d\rho}{dz} = -\frac{D_t}{RT} \cdot \frac{\Delta p}{h}, \tag{4.21}$$

where $\rho$ is the density of gas, $\Delta p$ is the pressure gradient across each nano-pore, $R$ is the gas constant as $8.314 J \cdot mol^{-1} K^{-1}$, and, $T$ and $h$ are temperature and pore thickness respectively.

Rearranging Eq. (4.21), we determined the transport diffusivity as:

$$D_t = -\frac{J \cdot (RTh)}{\Delta p}, \tag{4.22}$$

where the mass flux $J$ and the pressure gradient $\Delta p$ need to be obtained numerically from the simulation and where they are in a linear relationship. The molecular flux is transient and was calculated by measuring the net number of the particles as:

$$J_i = \frac{N_i^H - N_i^L}{2A_{xy} \cdot n\delta t}, \tag{4.23}$$

where $N_i$ is the total number of molecules travelling across the nano-pore (the number difference between the two ends of the channel-like pore) in a certain time period $\Delta t = n \cdot \delta t$, $A_{xy}$ the surface area of the interface, $n$ the number of time steps in that period and $\delta t$ the MD simulation time step.

We obtained the pressure using the Virial pressure (Lu et al. 2002) as:

$$p = \frac{1}{3V}\left[ m\sum_{i=1}^{N}\left(u_i^2 + v_i^2 + w_i^2\right) + \sum\sum_{i \neq j}\left(r_j - r_i\right) f_{ij} \right], \tag{4.24}$$

where the three velocity components ($u_i, v_i$ and $w_i$) and the inter-molecular force ($f_{ij}$) are involved. Hence the pressure gradient $\Delta p$ is the difference between the two pressures calculated from the both ends of the pores.

### 4.3.3 Results and Discussion

The first result pertained to the natural diffusion model, for which the self-diffusivity and the radial distribution function were calculated statistically. Second, in the surface diffusion simulation, the transient mass flux through those nano-pores in the solid wall and the pressure gradient were calculated along with the transport diffusivity. These results enabled an analysis of the diffusion process.

#### *4.3.3.1 Natural Diffusion*

Before simulating the fluid transport through the nano-pores, we needed to validate the natural diffusion properties of the bulk fluid. To do this, a system (as a cube) consisting of pure liquid argon molecules was used to perform the pure MD simulation and the model shown in Fig. 4-14. The radial distribution function (RDF) was used as the parameter to verify the natural diffusion of the liquid argon fluid in the bulk flow, which is a structural correlation. It describes the spherically averaged local organization around any given molecule. The RDF is defined as:

$$g(r) = e^{-\phi(r)/\kappa T}, \tag{4.25}$$

where $\phi(r)$ is the potential function (LJ potential here, see Eq. 4.17), $\kappa$ is the Von Karman constant, and, $T$ is the cited temperature. In the simulation, the RDF was calculated discretely based on the inter-molecular potential function. The details can be found in Rapaport (2004).

For a certain density ( $\rho = 1.374 g/cm^3$ ) and temperature ( $T = 90K$ ), the calculated RDF was picked to compare it to experimental results. In these simulations, the length and energy scales for liquid argon were very close to the values listed in Table 4-1; the time step was $0.005\tau$, which is the same as the time step used in the slip behavior study. Figure 4-16 shows the comparison of the radial distribution functions from the MD prediction and the experimental

measurement of Eisenstein and Gingrich (1942). One sees that the MD simulation successfully captured the properties of molecular distribution with respect to distance and the agreement between simulation results and experimental data is fairly good.

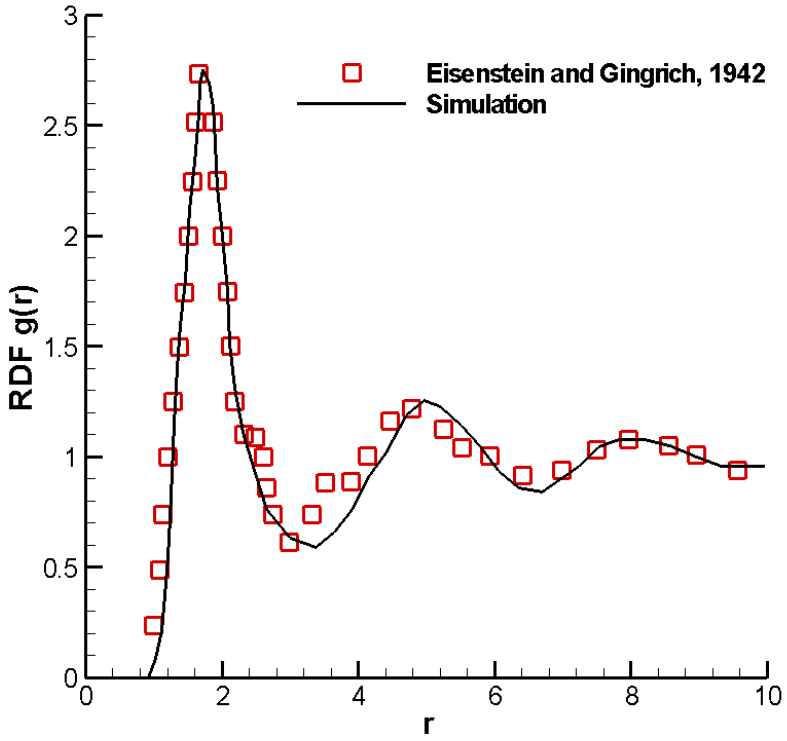


**Figure 4-16 Radial distribution function (RDF) of the pure liquid argon molecules.**

We calculated the self-diffusion constant using the Stokes-Einstein equation (Sholl, 2006). By using Eq. (4.20), we calculated that the self-diffusivity of liquid argon ($D_{s,Ar}$) in the current study is $2.35\times10^{-5} cm^2/s$. The experimental measurement is $2.43\times10^{-5} cm^2/s$. The difference between them is under 3%. These two validating tests show that the current scheme

works well and can be used to predict the liquid transport properties through a nano-pore in the solid substrate.

#### *4.3.3.2 Surface Diffusion*

In the current model, the solid wall is moving under a constant speed ($U_w = -1\sigma\tau^{-1}, -2\sigma\tau^{-1}$), which drives the gas molecules through the channel. The velocity magnitude profile along the channel height for the Couette flow is linear, even in the molecular level, which was validated in Section 4.2. The velocity magnitude profiles in the diffusion model are shown in Fig. 4-17.

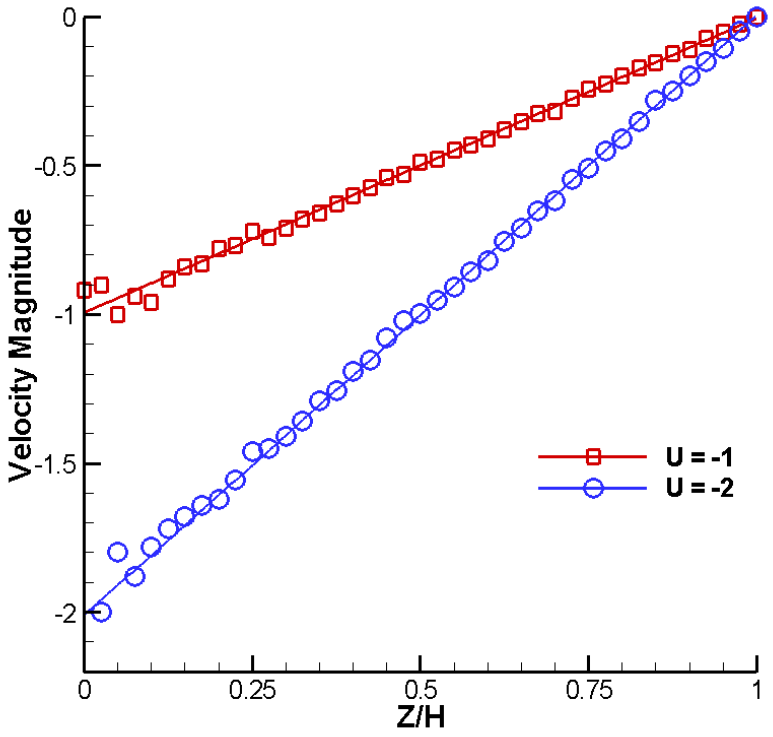


**Figure 4-17 The velocity magnitude profiles along the channel height in the diffusion model.**

In the diffusion model, due to the nano-pores in the solid wall, the flow penetrating the interface resulted in a certain amount of slip. However, the surface diffusion is a slow process and the velocity going into the pores is much smaller than the shear velocity. Thus the overall velocity magnitude profiles were not influenced much. Only some fluctuations near the wall region were detected.

Eight constructed nano-pores are used in the current diffusion model. We calculated the averaged pressures (in a time period and in each pore) at the fluid/solid interface using Eq. (4.24) and this distribution is shown in Fig. 4-18.

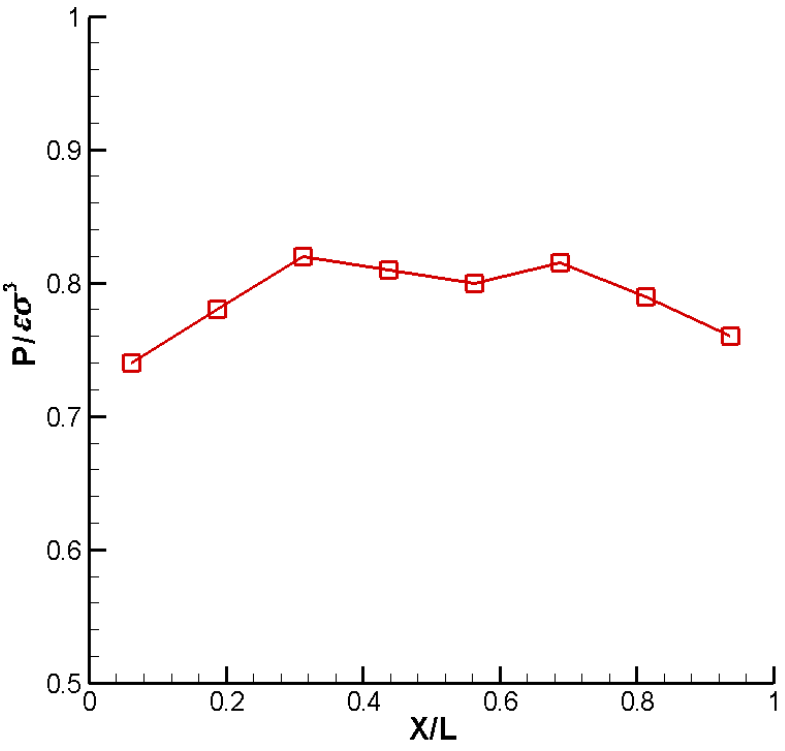


**Figure 4-18 The pressure calculated at the fluid/solid interface of each nano-pore.**

When the periodic boundary condition is used in the flow direction, the pressure value does not vary much from one to another, and varies a little bit for the two pores at both ends of the channel. This also suggests that the computation reaches a relatively stable state since those macroscopic properties do not change much.

After checking the process of the velocity and the pressure fields, we investigated the diffusion transport properties. As stated in Eq. (4.22), both the mass flux and the pressure need to be calculated before the transport diffusivity can be determined. This is required by the macroscopic transport theory but the value is difficult to be obtained for gas/nano-material adsorption. Figure 4-19 presents the linearly fitted results from Eq. (4.22) for $D_t$ of $H_2$ at two temperatures (273k and 300K). The pore width was chosen to be $3\sigma$.

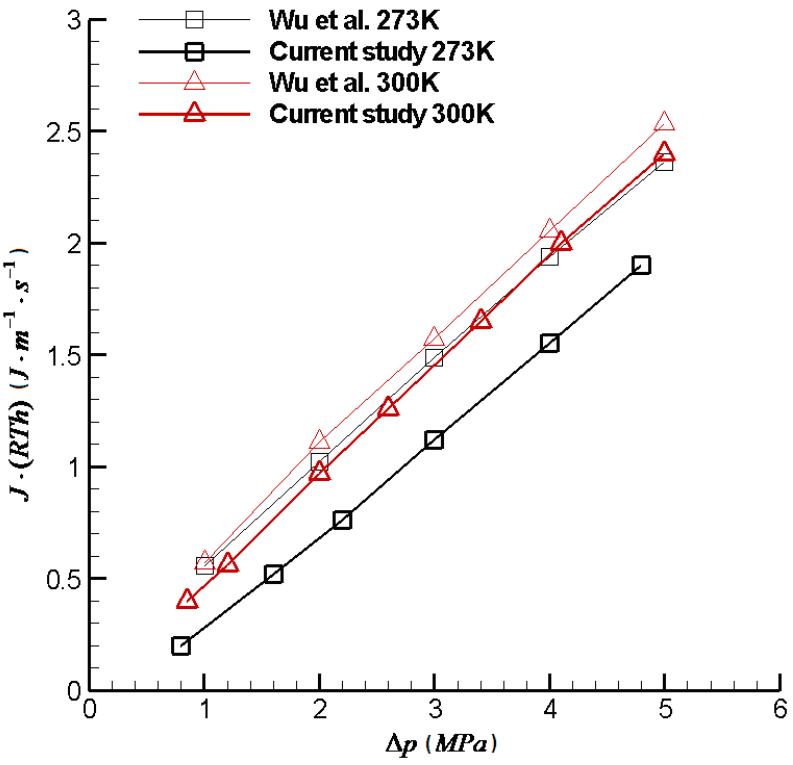


**Figure 4-19 Linearly fitted results for the transport diffusivities of hydrogen.**

By comparing our calculation to Wu et al. (2008) under similar circumstances, we found that the average (from 8 pores) and corrected mass flux $J \cdot (RTh)$ is linearly proportional to the average pressure gradient along the pore. And the slope of this relationship is the transport diffusivity, which is $4.6 \times 10^{-7} m^2 / s$ under 273K and $4.9 \times 10^{-7} m^2 / s$ under 300K. This indicates that the current simulation follows the Fick's law exactly. Similarly, for other gases (changing the characteristic length and energy in the LJ potential), the same linear relationships can also be obtained. Thus, the transport diffusivity for different material under various conditions can be calculated. These calculations are listed in Table 4-2. As Table 4-2 shows, the transport diffusivity increases with temperature.

| **Gas** | $D_t \times 10^7$ **(** $m^2 / s$ **)** | | | |
|---|---|---|---|---|
| | **273K** | | **300K** | |
| | **Current study** | **Wu** et al**., 2008** | **Current study** | **Wu** et al**., 2008** |
| $H_2$ | 4.6 | ---- | 4.9 | 4.92 |
| CO | 0.65 | ---- | 0.8 | 0.84 |
| Ar | 0.59 | ---- | 0.74 | ---- |

**Table 4-2 Transport diffusivities of various gases through the carbon substrate by diffusion at 273K and 300K.**

The mass fluxes of three gases and various pore widths were calculated. As shown in Fig. 4-20, they were all under 300K. Generally, with larger pores, the mass fluxes increase. However, among three gases, the increase of $H_2$ is much faster than the other two gases because of hydrogen's smaller molecular size. In another word, smaller molecules as $H_2$ have faster diffusion rates during the adsorption process.

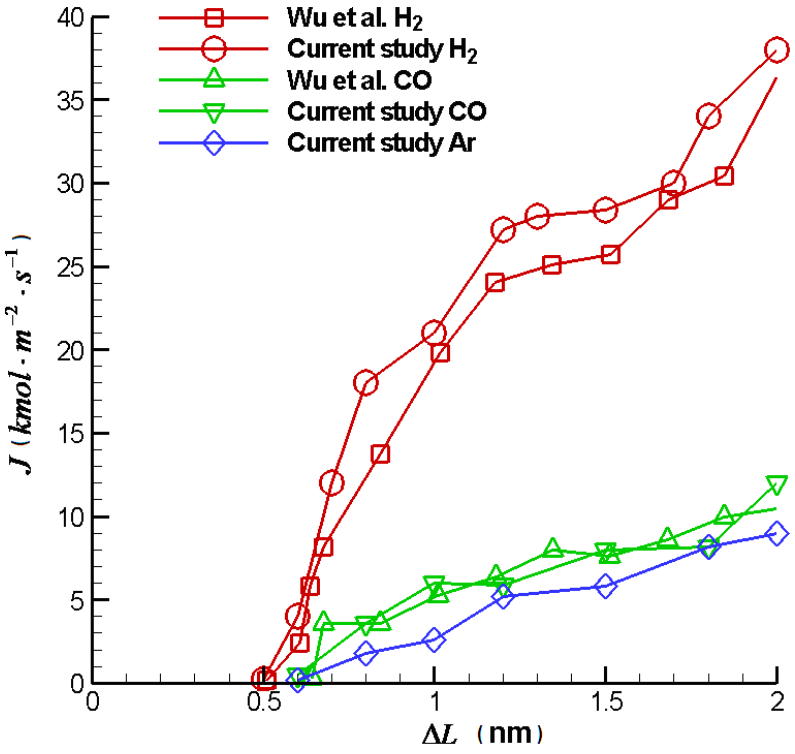


**Figure 4-20 Effect of pore width on diffusion flux of various gases.**

Equation (4.16) shows the linear concentration profile across the channel under the assumptions of the periodic flow used in the current simulations. Both the mass fluxes and the diffusivities either in the pores (near the interfaces) or in the bulk fluid can be determined using

the methods explained earlier. Thus, the coefficients required by Eq. (4.16) can be obtained. The concentration profiles for various gases and different pore size are presented in Fig. 4-21. In Fig. 4-21 (a), the pore size was fixed at $3\sigma$. And it is obvious that the concentration of $H_2$ changes the fastest in the channel, which also suggests the similar conclusion that we obtained previously – $H_2$ has largest diffusion rate. By using the same material ($H_2$) but varying the pore size, Fig. 4-21 (b) shows that wider pores allow more fluid molecules going through the solid substrate by having a larger flux (more steep concentration slope).

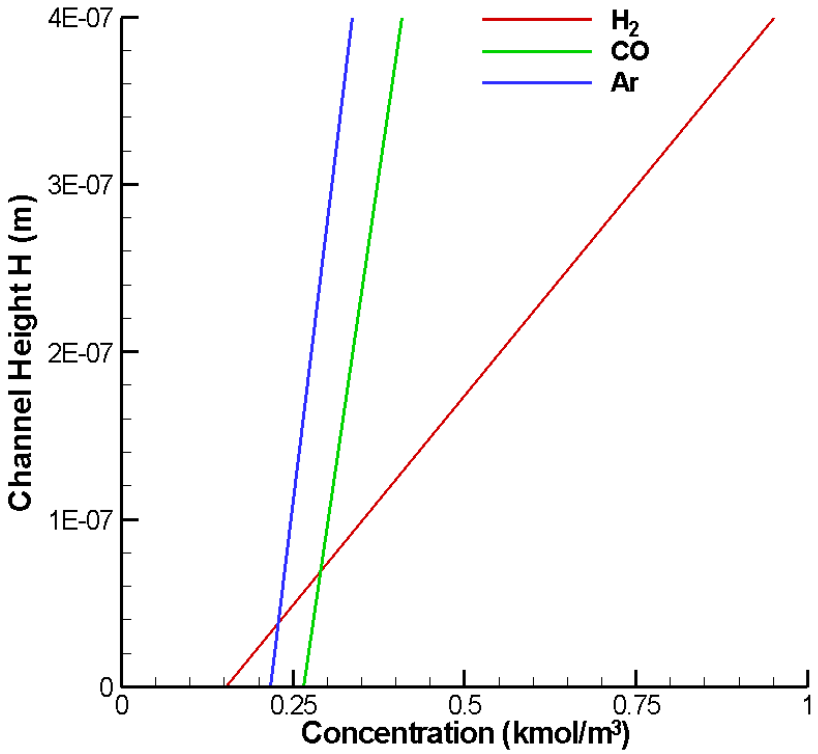


**(a)**

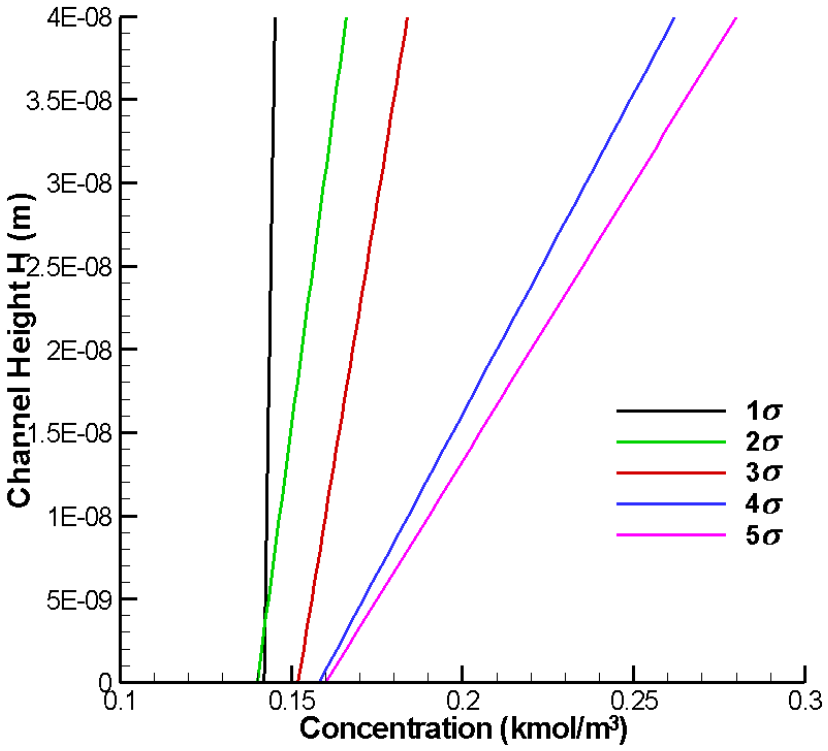


**(b)**

**Figure 4-21 Concentration profiles along the channel: (a) influence from various gases; (b) influence from the pore size for $H_2$.**

### 4.3.4 Summary of the Surface Diffusion Study

In Section 4.3, the hybrid scheme introduced in Section 4.2 was applied to a diffusion problem, in which various gases pass through a carbon substrate in a channel. The physical model was also a Couette flow, but it had several constructed nano-pores in the solid wall. Both natural diffusion and surface diffusion were investigated. The self-diffusivity and the radial distribution function were used to validate the natural diffusion of the liquid argon as their values agreed with those in the experimental data. In the surface diffusion simulation, we calculated the

mass fluxes across the fluid/solid interface and the average pressure. Thus, the transport diffusivities for different gases were determined from the linear relationship between the mass flux and the pressure, which were in agreement with the values cited in the literature. Also, the concentration profiles along the channel were obtained from the molecular level simulations. The influences of both the gas material property and the nano-pore size were studied.

## 4.4 Summary of the Nano-Scale Simulation

In the nano-scale simulation, the continuum theory-based simulations are no longer applicable. Thus, the atomistic models become more accurate and efficient for capturing the physical properties, especially the surface mechanisms in the molecular level. The molecular dynamics (MD) simulation and an innovative hybrid scheme have been used to simulate the slip behavior and the diffusion on the fluid/solid interfaces. The following conclusions can be reached with respect to both of these aspects:

- A model of the Couette flow problem was used to study the transport phenomena and the surface mechanisms in the nano-scale.
- The MD scheme and the hybrid scheme were validated when the velocity profiles were compared to those in the literature. The information exchange between the atomistic and the continuum regimes in the hybrid scheme was, therefore, successful.
- By changing the channel height and the moving velocity, we can calculate both the absolute and relative slip lengths. We found that the slip length becomes more important in smaller channels.

- We established a diffusion model for interactions between gases and carbon solid substrates. By constructing nano-pores in a carbon substrate, we captured the diffusion process from the fluid into the solid.
- Computational results of self-diffusivity and radial distribution function were used to validate the molecular diffusion model.
- Mass fluxes and pressure were calculated and used to determine the transport diffusivities for various gases, which agreed well with the values in the literature.
- The macroscopic concentration profiles were obtained from the molecular simulation.

# CHAPTER 5 - Conclusion

The conclusions for each scale of simulation have been summarized previously. In this chapter, the overall achievements of this thesis and their relations are illustrated in Fig. 5-1.

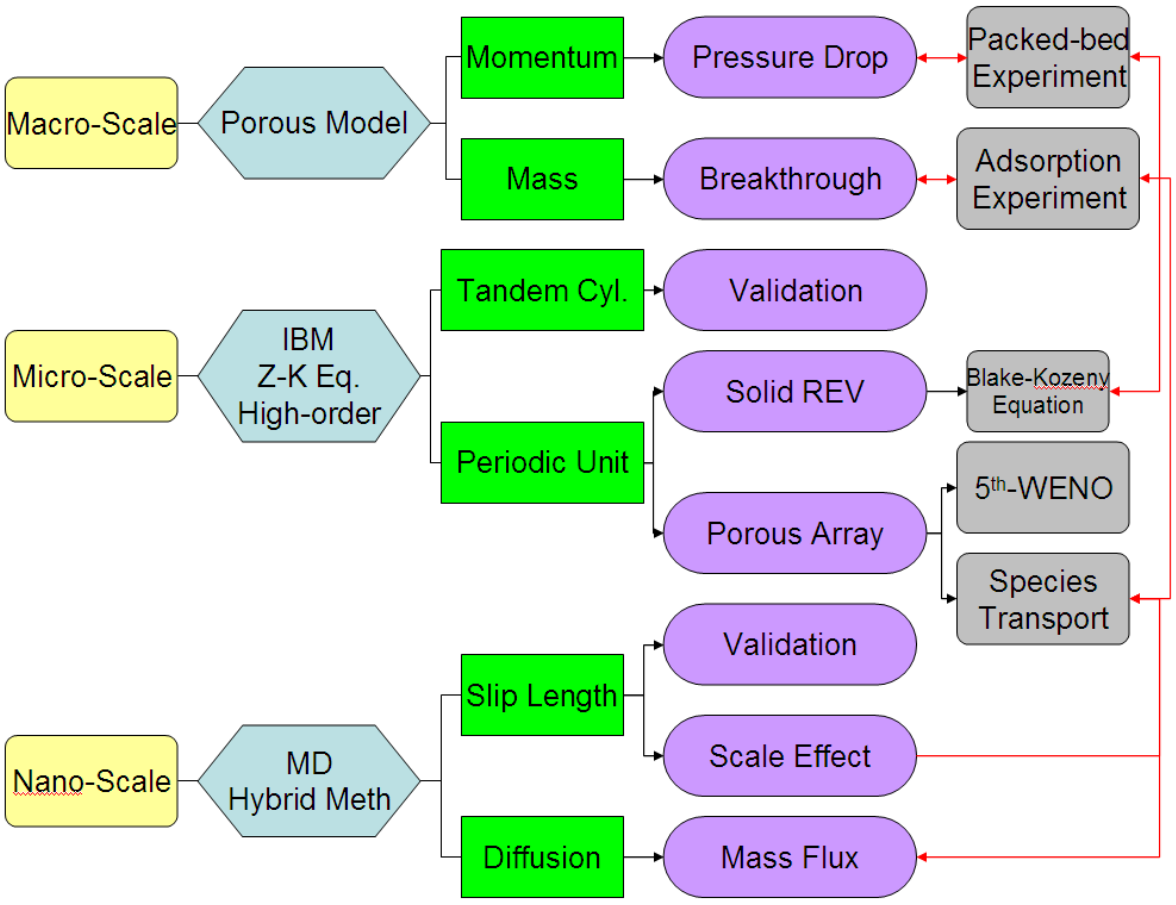


**Figure 5-1 Conclusions of the multi-scale simulation.**

In the macro-scale simulation, by using the porous models in the governing equations of the momentum and mass transport, we calculated the pressure drop and the breakthrough curves and compared them to those given for packed-bed and adsorption experiments. The agreement

we found among these data sets proves the capability and accuracy of the numerical model, which can, therefore, be used for future tests on various materials.

In the micro-scale simulation, a modified immersed-boundary method (IBM) with the Zwikker-Kosten (ZK) porous model and the high-order schemes was applied to simulate a periodic array of solid/porous cylinders. First a tandem impermeable cylinder system was tested to validate the IBM scheme. Second in the periodic unit, the solid case (treated as a Representative Elementary Volume, REV) was used to validate the high-order schemes by comparing it to results obtained with commercial CFD software. Also, the relationship between the pressure gradient and the porosity (Blake-Kozeny equation) could be determined from this level and fed back to the macro-scale simulation, which provided a link between two scales. The porous cylinders case was used to find the most accurate scheme, which is the $5^{th}$-order WENO scheme. And the flow fields in the porous medium have been studied. Based on this scheme, the species transport problem was also investigated with a porous model similar to the one used in the macro-scale. And the concentration change with different adsorption coefficient was not linear.

In the nano-scale simulation, the discrete molecular dynamics (MD) simulation and a coupled molecular-continuum scheme were applied to solve the momentum and the mass transport problems at the molecular level, a level for which the traditional continuum theory is no longer applicable. Both schemes have been verified from the surface slip behavior study when they are compared to what was found in the literature. Then the scale and the shear effect in the Coutte flow were investigated, showing that in the micro-/macroscopic investigations, the slip behavior could be neglected since it is only important in smaller scales. Later, the same hybrid scheme was applied to a diffusion model, which still used the same flow but had several nano-

pores constructed in the solid substrate. The interactions/adsorption between various gases and the carbon substrate were simulated. The mass fluxes cross the fluid/solid interfaces were counted and both self-diffusivity and transport diffusivity were estimated and compared to their respective values found in literature. Those transport properties are closely related to the species transport (Fick's law) in the macroscopic simulations. Finally, linear concentration profiles in the channel were obtained based on those transport properties for various gases going through different sizes of nano-pores.

Consequently, in the current study, we successfully built up a platform to study the nano-material filter device systematically from different scales of simulations. Various numerical methods and tools were tested and, were proved to be effective and efficient. The transport phenomena and the physical mechanisms were investigated and were shown to provide information that would be useful for the design of filtration devices and for understanding the behaviors of innovative nano-materials.

# References


Ackerman, D. M., Skoulidas, A. I., Sholl, D. S. and Johnson, J. K., 2003, "Diffusivities of Ar and Ne in Carbon Nanotubes," *Molecular Simulation*, Vol. 29, pp. 677-684.

Allen, M.P. and Tildesley, D.J., 1987, *Computer Simulation of Liquids*, Oxford University Press, New York.

Arturo, O. A., Facal L., Bernard P. A. and Shantanu R., 2002, "CFD Modeling and Simulation of Clogging in Packed Beds with Nonaqueous Media," *AIChE Journal*, Vol. 48, pp. 1596-1609.

Bhattacharyya, S., Dhinakaran, S., and Khalili, A., 2006, "Fluid Motion around and through a Porous Cylinder," *Chemical Engineering Science*, Vol. 61, pp. 4451-4461.

Bird, R. B., Stewart, W. E. and Lightfoot, E. N., 2002, *Transport Phenomena*, 2nd-edition, Wiley.

Chen, X. B., Yu, P., Winoto, S. H., and Low, H. T., 2008, "Numerical Analysis for the Flow past a Porous Square Cylinder based on the Stress-Jump Interfacial-Conditions," *International Journal of Numerical Methods for Heat & Fluid Flow*, Vol. 18, pp. 635-655.

Chen, X. B., Yu, P., Winoto, S. H., and Low, H. T., 2009, "Numerical Analysis for the Flow past a Porous Trapezoidal-Cylinder based on the Stress-Jump Interfacial-Conditions," *International Journal of Numerical Methods for Heat & Fluid Flow*, Vol. 19, pp. 223-241.

Cho, Y., Chopra, J., and Morris, P. J., 2007, "Immersed Boundary Method for Compressible High-Reynolds Number Viscous Flow around Moving Bodies," 45th AIAA Aerospace Sciences Meeting, January 9-11, 2007, Reno, NV.

Cieplak, M., Koplik, J., and Banavar, J. R., 2001, "Boundary Conditions at a Fluid-Solid Interface," *Physical Review Letters*, Vol. 86, pp. 803-806.

Cui, J., He, G. W., and Qi, D. W., 2006, "A Constrained Particle Dynamics for Continuum-Particle Hybrid Method in Micro- and Nano-Fluidics," *Acta Mechanica Sinica*, Vol. 22, pp. 503-508.

Darcy, H., 1856, *Les Fontaines Publiques de la Ville de Dijon* ("The Public Fountains of the Town of Dijon"), Dalmont, Paris.

Delgado-Buscalioni, R. and Coveney, P. V., 2003, "Continuum-Particle Hybrid Coupling for Mass, Momentum, and Energy Transfers in Unsteady Fluid Flow," *Physical Review E*, Vol. 67, 046704.

Deng, J., Ren, A. L., Zou, J. F., and Shao, X. M., 2006, "Three-Dimensional Flow around Two-Circular Cylinders in Tandem Arrangement," *Fluid Dynamics Research*, Vol. 38, pp. 386-404.

Duren, T., Keil, F. J. and Seaton, N. A., 2002, "Molecular Simulation of Adsorption and Transport Diffusion of Model Fluids in Carbon Nanotubes," *Molecular Physics*, Vol. 100, pp. 3741-3751.

Eisenstein, A. and Gingrich, N. S., 1942, "The Diffraction of X-Rays by Argon in the Liquid, Vapor, and Critical Regions," *Physical Review*, Vol. 62, pp. 261-270.

Ergun, S., 1952, "Fluid Flow through Packed Columns," *Chemical Engineering Progress*, Vol. 48, pp. 89-94.

Flekkoy, E. G., Wagner, G., and Feder, G., 2000, "Hybrid Model for Combined Particle and Continuum Dynamics," *Europhysics Letters*, Vol. 52, pp. 271-276.

FLUENT 6.3 Documents.

Ford, D. M. and Heffelfinger, G. S., 1998, "Massively Parallel Dual Control Volume Grand Canonical Molecular Dynamics with LADERA II. Gradient Driven Diffusion through Polymers," *Molecular Physics*, Vol. 94, pp. 673-683.

Frenkel, D. and Smit, B., 1996, *Understanding Molecular Simulation-from Algorithms to Applications*, Academic, New York.

Froment, G. F. and Bischoff, K. B., 1990, *Chemical Reactor Analysis and Design*, John Wiley & Sons, New York.

Gad-el-Hak, M., 2004, "Transport Phenomena in Microdevice," *ZAMM*, Vol. 84, pp.494-498.

Goyeau, B., Lhuillier, D., Gobin, D., and Velarde, M. G., 2003, "Momentum Transport at A Fluid-Porous Interface," *International Journal of Heat and Mass Transfer*, Vol. 46, pp. 4071-4081.

Guilmineau, E. Q. and Queutey, P., 2002, "A Numerical Simulation of Vortex Shedding from An Oscillating Circular Cylinder," *Journal of Fluids and Structures*, Vol. 16, pp. 773-794.

Hadjiconstantinou, N. G. and Patera, A. T., 1997, "Heterogeneous and Atomistic-Continuum Representations for Dense Fluid Systems," *International Journal of Modern Physics*, Vol. 8, pp. 967-976.

Harten, A., Engquist, B., Osher, S., and Chakravarthy, S. R., 1987, "Uniformly High-Order Accurate Essentially Nonoscillatory Schemes .3," *Journal of Computational Physics*, Vol. 71, pp. 231-303.

Heffelfinger, G. S. and Ford, D. M., 1998, "Massively Parallel Dual Control Volume Grand Canonical Molecular Dynamics with LADERA I. Gradient Driven Diffusion in Lennard-Jones Fluids," *Molecular Physics*, Vol. 94, pp. 659-671.

Herwig, H., 2002, "Flow and Heat Transfer in Micro Systems: Is Everything Different or Just Smaller?" *ZAMM*, Vol. 82, pp. 579-586.

Huang, C. K., Nandakumar, K., Choi, P. Y. K. and Kostiuk, L. W., 2006. "Molecular dynamics simulation of a pressure-driven liquid transport process in a cylindrical nanopore using two self-adjusting plates," *Journal of Chemical Physics*, Vol. 124, 234701.

Huang, C. K., Choi, P. Y. K., Nandakumar, K. and Kostiuk, L. W., 2007, "Comparative Study between Continuum and Atomistiv Approaches of Liquid Flow through a Finite Length Cylindrical Nanopore," *Journal of Chemical Physics*, Vol. 126, 224702.

Igarashi, T., 1981, "Characteristics of the Flow around Two Circular Cylinders of Different Diameters Arranged in Tandem," *Bulletin of JSME*, Vol. 24, pp. 323-331.

James, D. F. and Davis, A. M. J., 2001, "Flow at the Interface of a Model Fibrous Porous Medium," *Journal of Fluid Mechanics*, Vol. 426, pp. 47-72.

Jester, W. and Kallinderis, Y., 2003, "Numerical Study of Incompressible Flow about Fixed Cylinder Pairs,"*Journal of Fluids and Structures*, Vol. 17, pp. 561-577.

Jonas, L. A. and Rehrmann, J. A., 1973, "Predictive Equations in Gas Adsorption Kinetics," *Carbon*, Vol. 11, pp. 59-64.

Koplik, J. and Banavar, J. R., 1995, "Continuum Deductions from Molecular Hydrodynamics," *Journal of Computational Physics*, Vol. 27, pp. 257-292.

Koumoutsakos, P., 2005, "Multiscale Flow Simulation Using Particle," *Annual Review of Fluid Mechnics*, Vol. 37, pp. 457-487.

Krishnamoorthy, S., Price, S. J., and Paidoussis, M. P., 2001, "Cross-Flow past an Oscillating Circular Cylinder: Synchronization Phenomena in the Near Wake," *Journal of Fluids and Structures*, Vol. 15, pp. 955-980.

Kuwahara, F., Kameyama, Y., Yamaashita S., and Nakayama A., 1998, "Numerical Modeling of Turbulent Flow in Porous Media Using a Spatially Periodic Array," *Journal of Porous Media*, Vol. 1, pp. 47-55.

Kuwahara, F., Yamane, I., and Nakayama, A., 2006, "Large Eddy Simulation of Turbulent Flow in Porous Media," *International Communications in Heat and Mass Transfer*, Vol. 33, pp. 411-418.

Lee, J. W., Choi, D. Y., Kwak, D. H., Jung, H. J., Shim, W. G. and Moon, H., 2005, "Adsorption Dynamics of Water Vapor on Activated Carbon," *Adsorption-Journal of International Adsorption Society*, Vol. 11, pp. 437-441.

Li, J., Chambarel, A., Donneaud, M., and Martin, R., 1991, "Numerical Study of Laminar Flow past One and Two Circular Cylinders," *Computers and Fluids*, Vol. 19, pp. 155-170.

Li, J., Liao, D., and Yip, S., 1998, "Coupling Continuum to Molecular-Dynamics Simulation: Reflecting Particle Method and the Field Estimator," *Physical Review E*, Vol. 57, pp. 7259-7267.

Li, J., Sun, J. and Roux, B., 1992, "Numerical Study of an Oscillating Cylinder in Uniform Flow and in the Wake of an Upstream Cylinders," *Journal of Fluid Mechanics*, Vol. 237, pp. 457-478.

Liang, C. and Papadakis, G., 2007, "Large Eddy Simulation of Cross-Flow through a Staggered Tube Bundle at Subcritical Reynolds Number," *Journal of Fluids and Structures*, Vol. 23, pp. 1215-1230.

Lichter, S., Martini, A., Snurr, R. Q., and Wang, Q., 2007, "Liquid Slip in Nanoscale Channels as a Rate Process," *Physical Review Letters*, Vol. 98, pp. 4.

Lichter, S., Roxin, A., and Mandre, S., 2004, "Mechanisms for Liquid Slip at Solid Surfaces," *Physical Review Letters*, Vol. 93, pp. 4.

Lodewyckx, P., Wood, G. O. and Ryu, S. K., 2004, "The Wheeler-Jonas Equation: A Versatile Tool for the Prediction of Carbon Bed Breakthrough Times," *Carbon*, Vol. 42, pp. 1351-1355.

Long, X. L., Cheng, H., Xin, Z. L., Xiao, W. D., Li, W. and Yuan, W. K., 2008, "Adsorption of Ammonia on Activated Carbon from Aqueous Solutions," *Environmental Progress*, Vol. 27, pp. 225-233.

Lu, M. C., Hsieh, H. M., Tseng, F. G. and Chieng, C. C., 2002, "Molecular Dynamic Simulation of Nano-sized Channel Flow," Proceedings of IMECE2002 – 33775.

Mangun, C. L., Braatz, R. D., Economy, J. and Hall, A. J., 1999, "Fixed Bed Adsorption of Acetone and Ammonia onto Oxidized Activated Carbon Fibers," *Industrial & Engineering Chemical Research*, Vol. 38, pp. 3499-3504.

Martin, M. G., Thompson, A. P. and Nenoff, T. M., 2001, "Effect of Pressure, Membrane Thickness, and Placement of Control Volumes on the Flux of Methane through Thin Silicalite Membranes: A Dual Control Volume Grand Canonical Molecular Dynamics Study," *Journal of Chemical Physics*, Vol. 114, pp. 7174-7181.

Martini, A., Roxin, A., Snurr, R. Q., Wang, Q., and Lichter, S., 2008, "Molecular Mechanisms of Liquid Slip," *Journal of Fluid Mechanics*, Vol. 600, pp. 257-269.

Martini, A., Hsu, H., Patankar, N. A., and Lichter, S., 2008, "Slip at High Shear Rates," *Physical Review Letters*, Vol. 100, pp. 206001.

Mittal, R., Dong, H., Bozkurttas, M., Najjar, F. M., Vargas A., and von Loebbecke, A., 2008, "A Versatile Sharp Interface Immersed Boundary Method for Incompressible Flows with Complex Boundaries," *Journal of Computational Physics*, Vol. 227, pp. 4825-4852.

Mittal, R. and Iaccarino, G., 2005, "Immersed Boundary Method," *Annual Review of Fluid Mechanics*, Vol. 37, pp. 239-261.

Mohd-Yusof, J., 1996, *Interaction of Massive Particles with Turbulence,* Ph.D. Dissertation, Dept. of Mechanical and Aerospace Engineering, Cornell University.

Moulinec, C., Pourquie, M., Boersma, B. J., Buchal, T., and Nieuwstadt, F. T. M., 2004, "Direct Numerical Simulation on a Cartesian Mesh of the Flow through a Tube Bundle," *International Journal of Computational Fluid Dynamics*, Vol. 18, pp. 1-14.

Nakayama, A., Kuwahara, F., and Hayashi, T., 2004, "Numerical Modelling for Three-Dimensional Heat and Fluid Flow through a Bank of Cylinders in Yaw," *Journal of Fluid Mechanics*, Vol. 498, pp. 139-159.

Newsome, D. A. and Sholl, D. S., 2005, "Predictive Assessment of Surface Resistances in Zeolite Membranes Using Atomically Detailed Models," *Journal of Physical Chemistry* B, Vol. 109, pp. 7237-7244.

Newsome, D. A. and Sholl, D. S., 2008, "Atomically Detailed Simulations of Surface Resistances to Transport of $CH_4$, $CF_4$, and $C_2H_6$ through Silicalite Membranes," *Microporous and Mesoporous Materials*, Vol. 107, pp. 286-295.

Nie, X. B., Chen, S. Y., and Robbins, M. O., 2004, "A Continuum and Molecular Dynamics Hybrid Method for Micro- and Nano-Fluid Flow," *Journal of Fluid Mechanics*, Vol. 500, pp. 55-64.

Nijemeisland, M. and Dixon, A. G., 2001, "Comparison of CFD Simulations to Experiment for Convective Heat Transfer in a Gas-solid Fixed Bed," *Chemical Engineering Journal*, Vol. 82, pp. 231-246.

Nijemeisland, M. and Dixon, A. G., 2004, "CFD Study of Fluid Flow and Wall Heat Transfer in a Fixed Bed of Spheres," *AIChE Journal*, Vol. 50, pp. 906-921.

Ochoa-Tapia, J. A. and Whitaker, S., 1995, "Momentum Transfer at the Boundary between a Porous Medium and a Homogeneous Fluid 1: Theoretical Development," *International Journal of Heat and Mass Transfer*, Vol. 38, pp. 2635-2646.

Ochoa-Tapia, J. A. and Whitaker, S., 1995, "Momentum Transfer at the Boundary between a Porous Medium and a Homogeneous Fluid 2: Comparison with Experiment," *International Journal of Heat and Mass Transfer*, Vol. 38, pp. 2647-2655.

O'Connell, S. T. and Thompson, P. A., 1995, "Molecular Dynamics-Continuum Hybrid Computations: a Tool for Studying Complex Fluid Flows," *Physical Review E*, Vol. 52, pp. 5792-5795.

Ongoren, A. and Rockwell, D., 1988, "Flow Structure from an Oscillating Cylinder. Part 1. Mechanisms of Phase Shift and Recovery in the Near Wake," *Journal of Fluid Mechanics*, Vol. 191, pp. 197-223.

Papaioannou, G. V., Yue, D. K. P., Triantafyllou, M. S., and Karniadakis, G. E., 2006, "Three-Dimensionality Effects in Flow around Two Tandem Cylinders," *Journal of Fluid Mechanics*, Vol. 558, pp. 387-413.

Papaioannou, G. V., Yue, D. K. P., Triantafyllou, M. S., and Karniadakis, G. E., 2008, "On the Effect of Spacing on the Vortex-Induced Vibrations of Two Tandem Cylinders," *Journal of Fluids and Structures*, Vol. 24, pp. 833-854.

Park, S. J. and Kim, B. J., 2005, "Ammonia Removal of Activated Carbon Fibers Produced by Oxyfluorination," *Journal of Colloid and Interface Science*, Vol. 291, pp. 597-599.

Patankar, S. V., Liu, C. H., and Sparrow, E. M., 1977, "Fully Developed Flow and Heat-Transfer in Ducts Having Streamwise-Periodic Variations of Cross-Sectional Area," *Journal of Heat Transfer-Transactions of the ASME*, Vol. 99, pp. 180-186.

Pedras, M. H. J. and De Lemos, M. J. S., 2001, "Simulation of Turbulent Flow in Porous Media Using a Spatially Periodic Array and a Low Re Two-Equation Closure," *Numerical Heat Transfer Part a-Applications*, Vol. 39, pp. 35-59.

Perry, R. H. and Green D. W., 1997, *Perry's Chemical Engineers' Handbook: 7$^{th}$-edition*. McGraw-Hill, New York.

Peskin, C. S., 1972, "Flow Patterns around Heart Valves: A Numerical Method," *Journal of Computational Physics,* Vol. 10, pp. 252-271.

Qi, N., Appel, W. S., LeVan, M. D. and Finn, J. E., 2006. "Adsorption Dynamics of Organic Compounds and Water Vapor in Activated Carbon Beds," *Industrial & Engineering Chemical Research*, Vol. 45, pp. 2303-2314.

Rapaport, D. C., 2004, *The Art of Molecular Dynamics Simulation*, Cambridge University Press, Cambridge, UK.

Ren, W. and E, W., 2005, "Heterogeneous Multiscale Method for the Modeling of Complex Fluids and Micro-Fluidics," *Journal of Computational Physics*, Vol. 204, pp. 1-26.

Ribeiro, A. M., Sauer, T. P., Grande, C. A., Moreira, R., Loureiro, J. M. and Rodrigues, A. E., 2008, "Adsorption Equilibrium and Kinetics of Water Vapor on Different Adsorbents," *Industrial & Engineering Chemical Research*, Vol. 47, pp. 7019-7026.

Rollet-Miet, P., Laurence, D., and Ferziger, J., 1999, "LES and RANS of Turbulent Flow in Tube Bundles," *International Journal of Heat and Fluid Flow*, Vol. 20, pp. 241-254.

Roychowdhury, D. G., Das, S. K., and Sundararajan, T., 2002, "Numerical Simulation of Laminar Flow and Heat Transfer over Banks of Staggered Cylinders," *International Journal for Numerical Methods in Fluids*, Vol. 39, pp. 23-40.

Saiki, E. M. and Biringen, S., 1996, "Numerical Simulation of a Cylinder in Uniform Flow: Application of a Virtual Boundary Method," *Journal of Computational Physics,* Vol. 123, pp. 450-465.

Savage, N. and Diallo, M. S., 2005, "Nanomaterials and Water Purification: Opportunities and Challenges," *Journal of Nanoparticle Research*, Vol. 7, pp. 331-342.

Sharman, B., Lien, F. S., Davidson, L., and Norberg, C., 2005, "Numerical Predictions of Low Reynolds Number Flows over Two Tandem Circular Cylinders," *International Journal for Numerical Methods in Fluids*, Vol. 47, pp. 423-447.

Sholl, D. S., 2006, "Understanding Macroscopic Diffusion of Adsorbed Molecules in Crystalline Nanoporous Materials via Atomistic Simulations," *Account of Chemical Research*, Vol. 39, pp. 403-411.

Shu, C. W. and Osher, S., 1988, "Efficient Implementation of Essentially Non-Oscillatory Shock-Capturing Schemes," *Journal of Computational Physics*, Vol. 77, pp. 439-471.

Shu, C. W. and Osher, S., 1989, "Efficient Implementation of Essentially Non-Oscillatory Shock-Capturing Schemes .2," *Journal of Computational Physics*, Vol. 83, pp. 32-78.

Squires, T. M. and Quake, S. R., 2005, "Microfluidics: Fluid Physics at the Nanoliter Scale," *Review of Modern Physics*, Vol. 77, pp. 977-1026.

Swarztrauber, P. N. and Sweet, R. A., 1979, "Algorithm 541: Efficient Fortran Subprograms for the Solution of Separable Elliptic Partial Differential Equations [D3]," *ACM Transaction in Mathematics Software*, Vol. 5, pp. 352-364.

Tanida, Y., Okajima, A., and Watanabe, Y., 1973, "Stability of a Circular Cylinder Oscillating in Uniform Flow or in a Wake," *Journal of Fluid Mechanics*, Vol. 61, pp. 769-784.

Teruel, F. E., 2007, *Macroscopic Turbulence Modeling and Simulation for Flow through Porous Media*, Ph.D. thesis, University of Illinois at Urbana-Champaign, Urbana-Champaign, IL.

Teruel, F. E. and Rizwan, U., 2009, "A New Turbulence Model for Porous Media Flows. Part I: Constitutive Equations and Model Closure," *International Journal of Heat and Mass Transfer*, Vol. 52, pp. 4264-4272.

Teruel, F. E. and Rizwan, U., 2009, "A New Turbulence Model for Porous Media Flows. Part I: Analysis and Validation Using Microscopic Simulations," *International Journal of Heat and Mass Transfer*, Vol. 52, pp. 5193-5203.

Teruel, F. E. and Rizwan, U., 2009, "Characterization of a Porous Medium Employing Numerical Tools: Permeability and Pressure-Drop from Darcy to Turbulence," *International Journal of Heat and Mass Transfer*, Vol. 52, pp. 5878-5888.

Thompson, P. A. and Robbins, M. O., 1990, "Shear-Flow near Solids – Epitaxial Order and Flow Boundary Conditions," *Physical Review A*, Vol. 41, pp. 6830-6837.

Thompson, P. A and Troian, S. M., 1997, "A General Boundary Condition for Liquid Flow at Solid Surface," *Nature*, Vol. 389, pp. 360-362.

Tung K. L., Chang Y. L., Lai J. Y., Chang C. H., Chuang C. J., 2004, "A CFD Study of the Deep Bed Filtration Mechanism for Submicron/Nano-Particle Suspension," *Water Science and Technology*, Vol. 50, pp. 255-264.

Wakao, N. and Smith, J., 1964, "Diffusion and Reaction in Porous Catalysts," *Industrial and Engineering Chemistry Fundamentals*, Vol. 3, pp. 123-127.

Wang, S. M., Yu, Y. X. and Gao, G. H., 2006, "Grand Canonical Monte Carlo and Non-Equilibrium Molecular Dynamics Simulation Study on the Selective Adsorption and Fluxes of Oxygen/Nitrogen Gas Mixtures through Carbon Membranes," *Journal of Membrane Science*, Vol. 271, pp. 140-150.

Wang, S. M., Yu, Y. X. and Gao, G. H., 2006, "Non-Equilibrium Molecular Dynamics Simulation on Pure Gas Permeability through Carbon Membranes," *Chinese Journal of Chemical Engineering*, Vol. 14, pp. 164-170.

Wang, Y. C. and He, G. W., 2007, "A Dynamic Coupling Model for Hybrid Atomistic-Continuum Computations," *Chemical Engineering Science*, Vol. 62, pp. 3574-3579.

Werder, T., Walther, J. H., and Koumoutsakos, P., 2005, "Hybrid Atomistic-Continuum Method for the Simulation of Dense Fluid Flows," *Journal of Computational Physics*, Vol. 205, pp. 373-390.

Wilke, C. R. and Lee, C. Y., 1955, "Estimation of Diffusion Coefficients for Gases and Vapors," *Industrial and Engineering Chemistry*, Vol. 47, pp. 1253-1257.

Williamson, C. H. K., 1988, "Defining a Universal and Continuous Strouhal-Reynolds Number Relationship for the Laminar Vortex Shedding of a Circular Cylinder," *Physics of Fluids*, Vol. 31, pp. 2742-2744.

Williamson, C. H. K., 1996, "Vortex Dynamics in the Cylinder Wake," *Annual Review of Fluid Mechanics*, Vol. 28, pp. 477-539.

Wilson, D. K., Collier, S. L., Ostashev, V. E., Aldridge, D. F., Symon, N. P., and Marlin, D. H., 2006, "Time-Domain Modeling of the Acoustic Impedance of Porous Surfaces," *Acta Acustica United with Acustica*, Vol. 92, pp. 965-975.

Wilson, D. K., Ostashev, V. E., Collier, S. L., Symons, N. P., Aldridge, D. F., and Marlin, D. H., 2007, "Time-Domain Calculations of Sound Interactions with Outdoor Ground Surfaces," *Applied Acoustics*, Vol. 68, pp. 173-200.

Wu, Z., Liu, Z., Wang, W., Fan, Y., and Xu, N., 2008, "Diffusion of $H_2$, CO, $N_2$, $O_2$ and $CH_4$ through Nanoporous Carbon Membranes," *Chinese Journal of Chemical Engineering*, Vol. 16, pp. 709-714.

Xu, J. L. and Li, Y. X., 2007, "Boundary Conditions at the Solid-Liquid Surface over the Multiscale Channel Size from Nanometer to Micron," *International Journal of Heat and Mass Transfer*, Vol. 50, pp. 2571-2581.

Xu, Y., Zheng, Z. C., and Wilson, D. K., 2010, "Simulation of Turbulent Wind Noise Reduction by Porous Windscreens Using High-order Schemes," *Journal of Computational Acoustics*, accepted for publication.

Yang, J. and Balaras, E., 2006, "An Embedded-Boundary Formulation for Large-Eddy Simulation of Turbulent Flows Interacting with Moving Boundaries," *Journal of Computational Physics*, Vol. 215, pp. 12-40.

Yang, X. and Zheng, Z. C., 2010, "Nonlinear Spacing and Frequency Effects of an Oscillating Cylinder in the Wake of a Stationary Cylinder," *Physics of Fluids*, Vol. 22, 043601.

Yang, X., Zheng, Z. C., 2010, "Effects of Channel Scale on Slip Length of Flow in Micro/Nano-Channels," *Journal of Fluids Engineering*, Vol. 132, 061201.

Yen, T., Soong, C., and Tzeng, P., 2007, “Hybrid Molecular Dynamics-Continuum Simulation for Nano/Mesoscale Channel Flows,” *Microfluidics Nanofluidics*, Vol. 3, pp. 665-675.

Zhang, N. and Zheng, Z. C., 2007, “An Improved Direct-Forcing Immersed-Boundary Method for Finite Difference Applications,” *Journal of Computational Physics*, Vol. 221, pp. 250-268.

Zheng, Z. C. and Zhang, N., 2008, “Frequency Effects on Lift and Drag for Flow past an Oscillating Cylinder,” *Journal of Fluids and Structures*, Vol. 24, pp. 382-399.

Zdravkovich, M. M., 1985, “Flow-Induced Oscillations of Two Interfering Circular Cylinders," *Journal of Sound and Vibration*, Vol. 101, pp. 511-521.

Zdravkovich, M. M., 1997, *Flow around Circular Cylinders*, Oxford University Press.

Zwikker, C. and Kosten, C. W., 1949, *Sound Absorbing Materials*, Elsevier, New York.